STUDY OF NATIVE PROTEIN COMPLEXES USING GAS-PHASE ION/ION REACTIONS VIA MASS SPECTROMETRY

by

Abdirahman Abdillahi

A Dissertation

Submitted to the Faculty of Purdue University

In Partial Fulfillment of the Requirements for the degree of

Doctor of Philosophy

Department of Chemistry

West Lafayette, Indiana

December 2021

THE PURDUE UNIVERSITY GRADUATE SCHOOL

STATEMENT OF COMMITTEE APPROVAL

Dr. Scott McLuckey, Chair

Department of Chemistry

Dr. Mary Wirth

Department of Chemistry

Dr. Corey Thompson

Department of Chemistry

Dr. Jean Chmielewski

Department of Chemistry

Approved by:

Dr. Christine Hrycyna

Dedicated to my parents Fardowsa and Mohamed, and my siblings Faisa, Omar, Ahmed, Amina, Shukri and Warfa – for their unwavering support

ACKNOWLEDGMENTS

I would like to begin this section by first giving thanks and acknowledgment to Allah (SWT).

The culmination of my higher education career began well over a decade ago. I would like to thank the Posse Foundation for their support system during my undergraduate studies at Denison University, and the support of their impressive network of alumni for the years that followed. I would like to thank my Posse advisor and dear friend of fourteen years, Dr. Charles Sokolik. I would like to thank Dr. Kevin Owens for his advice during my studies at Drexel University. My initial foray into mass spectrometry is thanks to him.

At Purdue University, I would like to thank my research advisor Dr. Scott McLuckey who is the true embodiment of a scientist. Entering an unfamiliar field and interacting with someone as accomplished as Scott can be unnerving. However, his down-to-earth demeanor and general willingness to help quickly abates those feelings. I would like to also thank my committee members Dr. Mary Wirth, Dr. Jean Chmielewski, Dr. Corey Thompson, and Dr. Garth Simpson, for their support during my graduate school career. I would like to recognize the support from Dr. Vicki Wysocki, at the Ohio State University and her group for advice in conducting native mass spectrometry experiments. I would also like to recognize SCIEX for their willingness to modify our instruments to help improve our native MS experiments.

I would like to acknowledge, both the current and former, members of my research group. They created an environment that fostered stimulating conversations about science and about life. I would like to thank Fei Fei, Nan, Mack, Dave, Josh J, Josh F, John, Kenny, and Caitlin who each demonstrated the intangibles needed for success in graduate school. I would like to thank Elissia, Chris, and Anthony, who have been essential in demonstrating that you fun can be had in graduate school, even as you burn the midnight oil. I would like to thank my current colleagues Hsi-Chun, Jay, Ian, De'Shovon, Kim, Nicole, Sarah, Alex, Nick, Zach, Angelique, and Sam for their support during my studies. De'Shovon has been very supportive to me during my time here in many ways, but especially through her culinary skillset.

My Purdue support system outside of lab involved four of my closest friends. Hsi-Chun who was mentioned previously, but insisted he receive his own separate sentence in my acknowledgment section, is a one-of-a-kind supportive person who always looks out for those

around him. Denilson, who had tremendous confidence and had a habit of showing me a figure and asking me, “Do you know what this is?” to which I replied, “a paper”. Andres who is a natural comedian, in his own respect, with a penchant for creating his own jargon mid-conversation. Lastly, Sebastian who plays basketball like he spent a stint at the Euro Leagues but was/is my favorite point guard to play alongside. I’d like to thank these gentlemen for their support during my time at Purdue.

TABLE OF CONTENTS

LIST OF FIGURES

ABBREVIATIONS

AC	Alternating Current
BT-CID	Beam-type CID
CEM	Chain Ejection Model
CDMS	Charge detection mass spectrometry
CID	Collision Induced Dissociation
CRM	Charge Residue Model
CSD	Charge State Distribution
DC	Direct Current
DDC	Dipolar Direct Current
DTIMS	Drift Tube Ion Mobility Spectrometry
ESI	Electrospray Ionization
GC	Gas Chromatography
HPLC	High Performance Liquid Chromatography
IEM	Ion Evaporation Model
LC	Liquid Chromatography
LQIT	Linear Quadrupole Ion Trap
MWCO	Molecular Weight Cut Off
nESI	Nanoelectrospray Ionization
nMS	Native Mass Spectrometry
PFO	2,2,3,3,4,4,5,5,6,6,7,7,8,8,8-Pentadecafluoro-1-Octanol
PTR	Proton Transfer Reaction
RF	Radio Frequency
SID	Surface-induced dissociation
QTOF	Quadrupole Time Of Flight
TOF	Time Of Flight

ABSTRACT

The advent of electrospray ionization enabled the study of intact protein complexes via MS. For example, in the mid-1990s, the observation that viruses can survive after entering the gas-phase and still retain activity was shown. Advances in sample preparation methodologies, mainly native MS, allowed for the preservation of large non-covalently bound complexes, which led to structural characterization studies that were previously unachievable. However, native MS suffers from complications arising from inherent heterogeneity and severe salt adduction. Consequently, the spectra can consist of broad and overlapping peaks that may even preclude the ability to obtain a mass measurement. This dissertation will focus on a gas-phase technique to address highly complex native MS scenarios that give rise to poorly resolved signals using the *E. coli* ribosome as one model system. Moreover, brief discussion of improvements made on our QToF platform (SCIEX 5600) will be compared with other state-of-the-art instruments. Lastly, other applications to our ion/ion reaction workflow will be explored.

CHAPTER 1. INTRODUCTION TO NATIVE MASS SPECTROMETRY AND GAS-PHASE ION/ION CHEMISTRIES

The early pioneers of mass spectrometry J.J. Thompson and Francis Aston (1,2) would be astounded by its growth as an abundantly utilized tool. The impact of MS ranges from drug testing (3) to the petroleum industry (4), with many other sectors across a wide range of fields. In the strictest sense, MS is the analytical measurement of the molecular weight, which aids in the identification of the analyte. There have been many advancements since its inception, which will be discussed in this chapter.

1.1 Ionization techniques

MS is a gas-phase technique, wherein ions are generated, and their motions controlled to traverse through the instrument via ion optics to eventually reach the detector. Consequently, the initial analytes that were amenable to MS were small and volatile molecules. The early ionization techniques involved the bombardment of high energy electrons, referred to as electron impact (5-6). The high energy used to generate ions led to severe fragmentation and frequently precluded the observation of the molecular ion. Moreover, this technique was not useful in studying proteins because of the low volatility of proteins precludes their vaporization via conventional methods.

1.1.1 Electrospray ionization

A technique that couples well with the study of large and fragile biomolecules was developed in the late 1980s by John Fenn (7), although the first use of electrospray ionization with MS was reported in the late 1960s (8). This methodology is referred to as a soft ionization technique due to the observation of intact non-covalently bound complexes. During Fenn's Nobel speech, he referred to this method as "wings for molecular elephants" (9). Consequently, this technique has allowed for the study of large systems that were previously inaccessible. The schematic of ESI can be seen in **Figure 1.1**. The process of ESI begins with filling the sample inside the spraying nozzle. An electric field is generated between the end of the nozzle and the MS interface. This creates what is referred to as a Taylor cone (10) which emits droplets from the tip of the cone. These droplets contain the analyte molecule with charges on the surface of the droplet. The droplet

undergoes solvent evaporation until the Rayleigh limit is reached (11), wherein the repulsive force is greater than the surface tension of the droplet. The solvent evaporation and coulombic fission process repeat until the charge is deposited onto the analyte. Another iteration is referred to as nano-ESI (**Figure 1.2**) where the sample is placed in a glass capillary that is approximately 1-3 μM wide at the tip, referred to originally as micro-ESI. It is important to note that there is another soft-ionization technique called Matrix Assisted Laser Desorption Ionization (MALDI) that was also developed in the 1990s (12). Both MALDI and ESI can generate $[M + nH]^{n+}$. It is very common for MALDI to form singly charged peaks. This prevents the ability to study large ions, because the *m/z* may not be accessible to most mass analyzers. Furthermore, the process of embedding the analyte into a matrix is often not conducive to the preservation of non-covalent complexes. Consequently, the focus of this dissertation was the ESI technique because of the ability to form multiply-charged ions and the ability for charge-state manipulation.

1.1.2 Evaporation models

There are competing evaporation models for ESI (**Figure 1.3**), where the analyte can undergo any single or combinatory path (13). The size of the analyte molecule indicates the most likely path of the ions. For small molecules, the ion evaporation model is the most probable pathway. Moreover, analyte molecules with a high surface affinity also tend to undergo the ion-evaporation pathway. For large globular proteins, the droplet undergoes evaporation until the charge is deposited across the surface of the analyte. This is referred to as the charged residue mechanism (CRM). Lastly, proteins that have unfolded, which is achieved by utilizing denaturing conditions, tend to result in the chain ejection model (CEM), where a portion of the analyte is extruded through the surface of the droplet and undergoes a charge equilibrium. The difference between CRM and CEM is key to understanding the structural difference between a native vs denatured MS (14). The spectra of both can be seen in **Figure 1.4**.

1.2 Native MS

Native MS (spraying under non-denaturing conditions) is a technique that allows the protein complex to maintain its fully intact tertiary structure (15-17). The term ‘native MS’ was mentioned in 2004 (18), but evidence of the presence of folded proteins were seen as early as 1991

(**Figure 1.5**), where using a slightly higher pH revealed holo-myoglobin ions, which retain the non-covalently bound heme group. This early data showed that the proteins can remain in a folded state as they enter the gas-phase. Another early example was demonstrated with viral ions (**Figure 1.6**), where the tobacco mosaic viral ions were generated and retained both the supramolecular structure and the viral viability, which was shown by inoculating tobacco leaves (19). A truly fascinating experiment that initiated the study of viral ions, which were previously unattainable.

The "native MS" sample preparation methodology nomenclature has varied over the years, such as the terms non-denaturing, macromolecular or supramolecular MS (16). Recently, clearly defining the term "native" has gained consensus. The term "native" is meant to describe the proteins solution condition, which should resemble the physiological state the protein experiences. Factors that are important here include the pH and salt concentrations. MS is a gas-phase technique. Consequently, if the sample solution being analyzed is devoid of organics (methanol, acetonitrile etc.) and the pH is within an appropriate range (pH ~7), the sample is considered to be native. However, in some cases, additions to the solution, such as magnesium ions, may also be required to form and preserve a specific non-covalent complex.

This sample methodology, coupled with instrumentation capable of analyzing ions of high *m/z*, has allowed for the study of supramolecular compounds, such as viruses (20-21), ribosomes (22-24) and membrane proteins (25). Prior to the maturation of native MS, obtaining structural information and subunit stoichiometry presented challenges. The typical analytical techniques used for studying protein complexes are nuclear magnetic resonance and X-ray crystallography, each with limitations such as needing high concentrations and needing to be crystallized (which can be difficult). Native MS methodology has developed and improved over the last 20 years and is now a complementary technique to these biophysical methods, as it addresses, to some degree, their respective shortcomings and provides mass information.

1.2.1 Differences in spectra between native and denatured MS

The main differences between native and denatured MS can be observed in **Figure 1.4.** The immediate observation is the lower charge states of the native MS peaks compared to the charge states of peaks generated from denatured proteins. This is due to the difference in evaporation model each sample preparation method leads toward. For denatured samples, the protein unfolds, which reveals more solvent-accessible surface area to obtain more charge. During

the extrusion of the analyte from the droplet, the analyte abstracts more charge before being fully ejected. In contrast, the protein is folded for the native sample and thus does not have as much solvent-accessible surface area for protonation leading to a lower charge state. The width of the charge-state distribution (CSD) is also different between the two methods. For the denatured the CSD is much wider and has over 20 peaks, while the native CSD is 4 peaks wide.

1.3 Key factors for native MS experiments

The native MS experiment can be separated into 3 different sections. The first being the sample preparation method, the second being the instrumentation utilized and the last being the data analysis section. An introduction to these can be seen below. Our instrument platform, and its improvements will be mentioned in a later chapter.

1.3.1 Sample Preparation

The sample preparation varies for each analyte, but there is a general trend to follow. For small molecule analysis, the sample conditions are 1:1 with water: methanol/acetonitrile and ~1% acetic acid (or ammonium hydroxide for negative mode MS). This causes the denaturation and unfolding of the sample, which will preclude the preservation of non-covalent bonds. For native MS, the use of aqueous conditions with a physiological pH range is required. Most common buffers used for the storage of the protein complexes contain non-volatile salts, such as NaCl, which are not ideal for MS experiments. There is severe signal suppression when incorporating these non-volatile buffers, as well as severe adduction which complicates the spectral interpretation. Consequently, native MS experiments utilize a “MS-friendly” buffer – the most common buffer is ammonium acetate. The use of volatiles buffers allows for the removal of these salt adducts through collisions with bath gas in the MS. This preparation is done by using a spin column with molecular weight cut-off that is approximately 1/3rd of the mass of the target analyte. Initially, the storage sample is buffer exchanged in this spin column and in some cases, this repeated cycle of spin, remove flow-through, add new buffer is done several times (23,26). Low concentration of sample, such as 1–20 μM, is required for native MS analysis. The use of conventional ESI, is not ideal for native MS workflow. The higher flow-rate required by conventional ESI limits the analysis of low-volume samples and the larger droplet size generated

by ESI causes saltier charge states (27). Consequently, nano-ESI is utilized for native MS experiments, where both of those limitations are addressed. Typically, a 10 µL solution is placed in the capillary and the voltage is generated by a metal emitter wire (or the capillary is gold coated). All the experiments in this dissertation were done using a platinum emitter, as opposed to steel, which can generate redox reactions in the solution after the voltage is applied and affect the native structure of the protein.

1.3.2 MS instrumentation for native MS

The MS instrumentation for native MS is crucial in being able to measure *m/z* values. Native MS samples utilize aqueous solvents at neutral pH and the ions have less charge, relative to ions generated using the denatured sample preparation approach. Therefore, the charge state envelope appears at higher *m/z*. The maximum charge state of the analyte can be approximated using the Z_R (Rayleigh charge) and increases with higher mass. An example would be that ions appearing at 4,000 and 20,000 *m/z*, their respective masses would be 100 and 2,400 kDa (16). This necessitates the use of an instrument capable of wide *m/z* range and a high upper *m/z* limit for native MS experiments. Most of the early research was with time-of-flight mass analyzers, which satisfy these requirements and was used in the measurement of large viruses (20,21). As instrumentation has rapidly developed for studying these large native complexes, the Orbitrap™ has pushed the current capabilities. Charge detection mass spectrometry (CDMS), a single particle technique where the masses of individual ions are determined by the measurement of the *m/z* and the charge, has measured multiple-MDa systems (28). The Q-Exactive ultra-high mass range (UHMR) is an Orbitrap™-based instrument designed to take into consideration the transmission, resolution, upper *m/z* of large native complexes and has pushed the boundaries for commercialized instrumentation (29). Recently, the Q-Exactive UHMR underwent alterations, such as the use lower frequencies for all ion-routing elements to improve ion transmission of large *m/z* ions.

A separate aspect of the native MS workflow is the need for higher pressure regions to facilitate transmission of large ions. MS analyzers and the detector suffer when pressures are too high, which is why the analyzer region is under low-pressure for MS instruments. The transmission of ions, however, benefits from having a higher-pressure region near the interface of the instrument. This is most evident with larger ions (30). The ions entering the MS need to be radially focused to pass through the aperture and along the rest of the ion optics. This can be done by altering the

frequency, as done by the Q-Exactive UHMR, or by altering the initial region's pressure. The effect of the latter can be seen in (**Figure 1.7**). The 20S proteasome is approximately 690 kDa and under low pressure in Q0, the initial quadrupole, the analyte signal was very low. As the pressure continued to increase, the analyte signal became much more prominent. The higher pressure enabled the ions to focus/collapse to the center of the quadrupole, and therefore transmit more efficiently towards the subsequent ion-optics by a process known as collisional cooling. There was a point where any further increase of pressure did not improve the signal (after 30 mTorr). This an early version of the SCIEX QTOF platforms. A separate quadrupole, referred to as QJet, was recently introduced as a higher-pressure region preceding the Q0 quadrupole.

A major benefit to native MS experiments is the ability to study the connectivity of complexes which can be done by employing separate fragmentation techniques. The gold standard for fragmentation in MS experiments is collision induced dissociation (CID). The most common use of CID is in the generation of vast libraries that aid in the identification of unknown analytes (31-32). This technique is affected by accelerating the ions across the instrument into a high-pressure collision cell, referred to as beam-type or high-energy CID. The other form is referred to as ion-trap CID, where the ions are first trapped in the collision cell and a voltage applied at their secular frequency to position the ions out of the center of the trap by resonance excitation (33-34). As the ions get closer to the rods on the quadrupole, they are exposed to higher electric fields that result in energetic collisions with the gas in the trap until enough internal energy is deposited to induce fragmentation.

The vast majority of native MS CID studies have employed the high-energy methodology. There are other fragmentation methods that have proven to be very useful for studying non-covalent complexes. The creative use of a metal surface, which is much larger than the mass of the commonly used N_2 bath gas, has shown great promise in uncovering the connectivity of protein complexes (35). This method is referred to as surface induced dissociation (SID), and its major benefit lies in its fast activation capability. The commonly observed signal for non-covalently bound complex CID experiments is the monomer and the (n-1)mer. For example, if the complex is made by 14 monomers (14-mer) then the fragmentation will be a monomer and a 13-mer. One of the most commonly studied system in native MS is GroEL, which is an example of a 14-mer complex. The SID spectrum of GroEL generates a variety of products up to heptamers and CID generates only the products mentioned above (36). The new generation of SID devices are

minimally invasive to conventional ion paths and have been introduced into different MS platforms (37-38). The other methods used for fragmenting ions are spectroscopic (39-40) and electron transfer/capture dissociation techniques (41).

The mass measurement is the most important aspect of an MS experiment. The narrow CSD of native MS ions can lead to erroneous mass measurements, as the more independent *m/z* measurements the probability of correctly assigning the charge states is increased. If the native MS ions contain a heterogeneous mixture, or are severely adducted, the charge states may overlap leading to a "blob". Our lab has addressed both limitations to native MS ions by employing gas-phase ion/ion reactions (24).

1.4 Ion/ion reactions

The advent of ESI, which tend to lead to multiple charging of large analytes, has allowed for the exploration of gas-phase ion/ion reactions. This is a technique that can be used to manipulate analyte charge states and, in some cases probe their structures, with demonstrated utility for lipids, proteins, and carbohydrates (42-44). The kinetics of ion/ion reactions are different from those of ion/molecule reactions. The kinetics are driven by the attractive potential of the oppositely charged ions for ion/ion reactions, and the ion/dipole-induced dipole interaction for ion/molecule reactions. Another important consideration is the cross section of ion/ion reaction process which can be approximated by the following equation [45].

$$\sigma_{orbit} \approx \frac{Z_1^2 Z_2^2 e^4}{4\pi \varepsilon_0 (\mu v^2)^2} \quad (1)$$

Z_1 and Z_2 are related to the unit charges of the ions, e is the electron charge, ε_0 is the vacuum permittivity, v is the relative velocity and μ is the reduced mass. The ions can be positioned with a large enough distance to preclude the reaction. However, the dampening of the relative velocity of the ions via collisions, as well as "tidal" effects that arise from the effect of changing electric field as ions orbit each other, can be bring the ions close enough for chemical reactions (i.e., electron transfer, proton transfer, or complex formation). Consequently, the cross-section can be orders of magnitude greater with ion/ion reactions than with ion/molecule reactions. There are a variety of ion/ion reactions that can occur, such as proton transfer, multiply-charged ion attachment, electron transfer, metal transfer and covalent modification (44). The focus of this dissertation will be on proton transfer and multiply-charged ion attachment.

1.4.1 Ion/ion reaction experimental

The first step in performing an ion/ion reaction is to electrospray oppositely charged species. This can be accomplished by setting two emitters at the interface of the MS instrument. The dual emitters, which are typically nano-electrospray emitters, need to be alternatively pulsed to ensure there is adequate time for product ions to reach the detector (46). Once the initial ions are sprayed, they are accumulated and stored in q2. The first emitter is turned off and a voltage is applied to the second emitter that generates oppositely charged ions. During this step, the ion optics are switched to allow for the transmission of the oppositely charged ions. Once these ions reach q2, a supplemental alternating current (AC) is applied to the surrounding lenses (47) to allow for the mutual storage of both ion polarities. This reaction time is referred to as mutual storage, and the longer the mutual storage time the more extensive the reaction (i.e., greater depletion of reactants and greater likelihood for multi-step reactions). There are a few other modifications that will be mentioned in later chapters, but these are the only modifications needed to perform an ion/ion reaction.

1.4.2 Competing ion/ion reactions

The mutual storage of oppositely charged ions can lead to different products. Proton transfer reactions lead to product peaks that differ in mass by 1 Da and one charge and occurs when the reagent ion either abstracts or donates a proton to the analyte ion for positive-mode and negative-mode MS, respectively. Proton transfer can occur either via formation of and subsequent break-up of a long-lived complex or via proton transfer at a crossing-point on the energy surface without formation of a long-lived complex. Alternatively, a long-lived complex can be formed that survives detection. In this case, the mass of the complex is the sum of the masses and charges of the reactant ions. When the reagent ion is multiply-charged, the mass and charge of the product peak change by more than 1 Da in mass and more than a single charge. In the case of our native MS workflow, we refer to this complex formation technique as **m**ass **a**nalysis of **m**acro-molecular **a**nalytes via **m**ultiply-charged **i**on **a**ttachment or MAMA-MIA, which is illustrated in **Figure 1.7** (24). The equation for maximum distance a proton can hop (r_{PT}) can be estimated by equation 2 (45).

$$r_{PT} \approx \frac{z_1 z_2 e^2}{4\pi\varepsilon_0 \Delta H_{PT}} \qquad (2)$$

where ΔH_{PT} represents the enthalpy of the proton transfer reactions. For the MAMA-MIA application, it is desirable to avoid single proton transfer, as this can complicate the measurement. To maximize the formation of long-lived complex, it is therefore desirable that the cross-section for a physical collision is comparable to or larger than the cross-section for proton hopping (i.e., πr_{PT}^2). This is favored by the use of physically large reactant ions and ions of relatively low charge employing an appropriate reagent that has a large physical collisional cross-section and relatively low charge (45). For the reagents and analytes studied thus far, MAMA-MIA undergoes complex formation exclusively, which can be seen in later chapters.

1.5 Conclusions

The advent of ESI has allowed for the study of large ions, which was previously not possible with the existing ionization techniques. The study of large viral ions, and other molecular machines were observed shortly after the development of ESI. The scene was set for native MS to enter and improve the structural characterization of non-covalently bound complexes. Although there are many benefits to native MS, there are limitations that arise due to the narrow CSD and the adducted/desolvated ions that are commonly associated with such experiments, which can preclude the accurate mass assignment of the analyte. The use of ion/ion reaction techniques address these concerns, and thus bring value to the native MS field.

1.6 References

1. The Nobel Prize in Chemistry 1922 https://www.nobelprize.org/prizes/chemistry/1922/summary/

2. Thompson, J.J. Rays of Positive Electricity and Their Application to Chemical Analysis. Nature 92, 549–550 (1914).

3. Performing drug screening through high resolution mass spectrometry in the clinical laboratory: to implement or not? | AACC.org https://www.aacc.org/science-and-research/scientific-shorts/2017/validation-of-a-broad-spectrum-drug-screening-method

4. Lozano, D.; Gomez-Escudero, A.; Barrow, M. Chapter 32 | Mass Spectrometry in the Petroleum Industry. Fuels Lubr. Handb. Technol. Prop. Perform. Test. 2nd Ed. (2019).

5. Märk, T. D.; Dunn, G. H. Electron Impact Ionization; Springer Science & Business Media, (2013).

6. Dagam, S.; Amirav, A. Electron impact mass spectrometry of alkanes in supersonic molecular beams, J Am Soc Mass Spectrom. 6(2):120-31 (1995).

7. Electrospray Ionization for Mass Spectrometry of Large Biomolecules https://www.science.org/doi/abs/10.1126/science.2675315.

8. Dole, M.; Mack, L. L.; Hines, R. L.; Mobley, R. C.; Ferguson, L. D.; Alice, M. B. Molecular Beams of Macroions. J. Chem. Phys. 49(5), 2240–2249 (1968).

9. The Nobel Prize in Chemistry 2002 https://www.nobelprize.org/prizes/chemistry/2002/fenn/lecture/

10. Wilm, M. S.; Mann, M. Electrospray and Taylor-Cone Theory, Dole's Beam of Macromolecules at Last? Int. J. Mass Spectrom. Ion Process. 136 (2), 167–180 (1994).

11. Principles of Electrospray Ionization - Molecular & Cellular Proteomics https://www.mcponline.org/article/S1535-9476(20)30199-7/fulltext

12. Bahr, U.; Karas, M.; Hillenkamp, F. Analysis of Biopolymers by Matrix-Assisted Laser Desorption/Ionization (MALDI) Mass Spectrometry. Fresenius J. Anal. Chem. 348(12), 783–791 (1994).

13. Konermann, L.; Ahadi, E.; Rodriguez, A. D.; Vahidi, S. Unraveling the Mechanism of Electrospray Ionization. Anal. Chem. 85(1), 2–9 (2013).

14. Kafader, J. O.; Melani, R. D.; Schachner, L. F.; Ives, A. N.; Patrie, S. M.; Kelleher, N. L.; Compton, P. D. Native vs Denatured: An In-Depth Investigation of Charge State and Isotope Distributions. J. Am. Soc. Mass Spectrom. 31 (3), 574–581 (2020)

15. The Diverse and Expanding Role of Mass Spectrometry in Structural and Molecular Biology. EMBO J. 35(24), 2634–2657 (2016).

16. Leney, A. C.; Heck, A. J. R. Native Mass Spectrometry: What Is in the Name? J. Am. Soc. Mass Spectrom. 28(1), 5–13 (2017).

17. Boeri Erba, E.; Petosa, C. The Emerging Role of Native Mass Spectrometry in Characterizing the Structure and Dynamics of Macromolecular Complexes. Protein Sci. Publ. Protein Soc. 24(8), 1176–1192 (2015).

18. Native protein mass spectrometry: from intact oligomers to functional machineries - ScienceDirect https://www.sciencedirect.com/science/article/pii/S1367593104001048

19. Siuzdak, G.; Bothner, B.; Yeager, M.; Brugidou, C.; Fauquet, C. M.; Hoey, K.; Change, C.-M. Mass Spectrometry and Viral Analysis. Chem. Biol. 3(1), 45–48 (1996).

20. Tito, M. A.; Tars, K.; Valegard, K.; Hajdu, J.; Robinson, C. V. Electrospray Time-of-Flight Mass Spectrometry of the Intact MS2 Virus Capsid. J. Am. Chem. Soc., 122(14), 3550–3551 (2000).

21. Snijder, J.; Rose, R. J.; Veesler, D.; Johnson, J. E.; Heck, A. J. R., Studying 18 MDa Virus Assemblies with Native Mass Spectrometry. Angew. Chem. Int. Edit. 52, 4020-4023 (2013).

22. Rostom, A. A.; Fucini, P.; Benjamin, D. R.; Juenemann, R.; Nierhaus, K. H.; Hartl, F. U.; Dobson, C. M.; Robinson, C. V. Detection and Selective Dissociation of Intact Ribosomes in a Mass Spectrometer. Proc. Natl. Acad. Sci. U. S. A. 97(10), 5185–5190 (2000).

23. van de Waterbeemd, M.; Fort, K. L.; Boll, D.; Reinhardt-Szyba, M.; Routh, A.; Makarov, A.; Heck, A. J. R. High-Fidelity Mass Analysis Unveils Heterogeneity in Intact Ribosomal Particles. Nat. Methods 14(3), 283–286 (2017).

24. Abdillahi, A. M.; Lee, K. W.; McLuckey, S. A. Mass Analysis of Macro-Molecular Analytes via Multiply-Charged Ion Attachment. Anal. Chem. 92(24), 16301–16306 (2020).

25. Keener, J. E.; Zhang, G.; Marty, M. T. Native Mass Spectrometry of Membrane Proteins. Anal. Chem. 93 (1), 583–597 (2021).

26. Hernández, H.; Robinson, C. V. Determining the Stoichiometry and Interactions of Macromolecular Assemblies from Mass Spectrometry. Nat. Protoc. 2(3), 715–726 (2007).

27. Susa, A. C.; Xia, Z.; Williams, E. R. Small Emitter Tips for Native Mass Spectrometry of Proteins and Protein Complexes from Nonvolatile Buffers That Mimic the Intracellular Environment. Anal. Chem. 89(5), 3116–3122 (2017).

28. Todd, A. R.; Barnes, L. F.; Young, K.; Zlotnick, A.; Jarrold, M. F. Higher Resolution Charge Detection Mass Spectrometry. Anal. Chem. 92(16), 11357–11364 (2020).

29. L. Fort, K.; Waterbeemd, M. van de; Boll, D.; Reinhardt-Szyba, M.; E. Belov, M.; Sasaki, E.; Zschoche, R.; Hilvert, D.; A. Makarov, A.; R. Heck, A. J. Expanding the Structural Analysis Capabilities on an Orbitrap-Based Mass Spectrometer for Large Macromolecular Complexes. Analyst 143(1), 100–105 (2018).

30. Chernushevich, I. V.; Thomson, B. A. Collisional Cooling of Large Ions in Electrospray Mass Spectrometry. Anal. Chem. 76(6), 1754–1760 (2004).

31. Kienhuis, P. G. M.; Geerdink, R. B. A Mass Spectral Library Based on Chemical Ionization and Collision-Induced Dissociation. J. Chromatogr. A 974(1–2), 161–168 (2002).

32. Method To Compare Collision-Induced Dissociation Spectra of Peptides: Potential for Library Searching and Subtractive Analysis | Analytical Chemistry https://pubs.acs.org/doi/10.1021/ac980122y

33. Wells, J. M.; McLuckey, S. A. Collision-Induced Dissociation (CID) of Peptides and Proteins. Methods Enzymol. 402, 148–185 (2005)..

34. McLuckey, S. A. Principles of Collisional Activation in Analytical Mass Spectrometry. J. Am. Soc. Mass Spectrom. 3(6), 599–614 (1992).

35. Wysocki, V. H.; Joyce, K. E.; Jones, C. M.; Beardsley, R. L. Surface-Induced Dissociation of Small Molecules, Peptides, and Non-Covalent Protein Complexes. J. Am. Soc. Mass Spectrom. 19(2), 190–208 (2008).

36. Zhou, M.; Jones, C. M.; Wysocki, V. H. Dissecting the Large Noncovalent Protein Complex GroEL with Surface-Induced Dissociation and Ion Mobility-Mass Spectrometry. Anal. Chem. 85(17), 8262–8267 (2013).

37. Panczyk, E. M.; Snyder, D. T.; Ridgeway, M. E.; Somogyi, Á.; Park, M. A.; Wysocki, V. H. Surface-Induced Dissociation of Protein Complexes Selected by Trapped Ion Mobility Spectrometry. Anal. Chem. 93(13), 5513–5520 (2021).

38. VanAernum, Z. L.; Gilbert, J. D.; Belov, M. E.; Makarov, A. A.; Horning, S. R.; Wysocki, V. H. Surface-Induced Dissociation of Noncovalent Protein Complexes in an Extended Mass Range Orbitrap Mass Spectrometer. Anal. Chem. 91(5), 3611–3618 (2019).

39. Greisch, J.-F.; Tamara, S.; Scheltema, R. A.; Maxwell, H. W. R.; Fagerlund, R. D.; Fineran, P. C.; Tetter, S.; Hilvert, D.; Heck, A. J. R. Expanding the Mass Range for UVPD-Based Native Top-down Mass Spectrometry. Chem. Sci. 10(30), 7163–7171 (2019).

40. Lee, K. W.; Harrilal, C. P.; Fu, L.; Eakins, G. S.; McLuckey, S. A. Digital Ion Trap Mass Analysis of High Mass Protein Complexes Using IR Activation Coupled with Ion/Ion Reactions. Int. J. Mass Spectrom. 458, 116437 (2020).

41. Lermyte, F.; Konijnenberg, A.; Williams, J. P.; Brown, J. M.; Valkenborg, D.; Sobott, F. ETD Allows for Native Surface Mapping of a 150 KDa Noncovalent Complex on a Commercial Q-TWIMS-TOF Instrument. J. Am. Soc. Mass Spectrom. 25(3), 343–350 (2014).

42. Randolph, C. E.; Foreman, D. J.; Betancourt, S. K.; Blanksby, S. J.; McLuckey, S. A. Gas-Phase Ion/Ion Reactions Involving Tris-Phenanthroline Alkaline Earth Metal Complexes as Charge Inversion Reagents for the Identification of Fatty Acids. Anal. Chem. 90(21), 12861–12869 (2018).

43. Prentice, B. M.; McLuckey, S. A. Gas-Phase Ion/Ion Reactions of Peptides and Proteins: Acid/Base, Redox, and Covalent Chemistries. Chem. Commun. Camb. Engl. 49(10), 947–965 (2013).

44. Foreman, D. J.; McLuckey, S. A. Recent Developments in Gas-Phase Ion/Ion Reactions for Analytical Mass Spectrometry. Anal. Chem. 92 (1), 252–266 (2020).

45. McLuckey, S. A.; Huang, T.-Y. Ion/Ion Reactions: New Chemistry for Analytical MS. Anal. Chem. 81(21), 8669–8676 (2009)..

46. Xia, Y.; Liang, X.; McLuckey, S. A. Pulsed Dual Electrospray Ionization for Ion/Ion Reactions. J. Am. Soc. Mass Spectrom. 16(11), 1750–1756 (2005).

47. Xia, Y.; Chrisman, P. A.; Erickson, D. E.; Liu, J.; Liang, X.; Londry, F. A.; Yang, M. J.; McLuckey, S. A. Implementation of Ion/Ion Reactions in a Quadrupole/Time-of-Flight Tandem Mass Spectrometer. Anal. Chem. 78(12), 4146–4154 (2006).

1.7 Figures

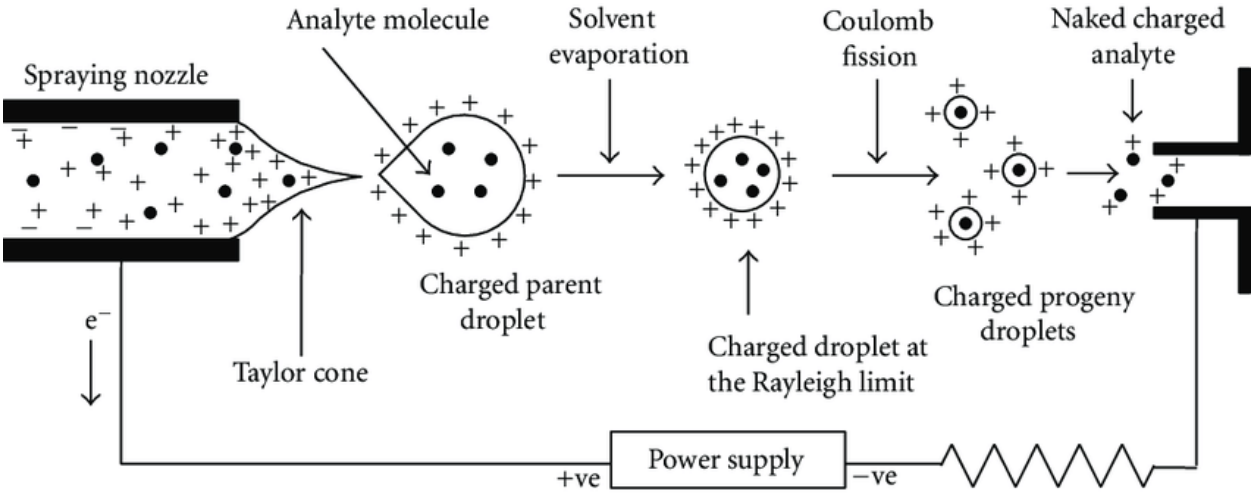

Figure 1.1. The schematic of electrospray ionization. Reproduced from Banerjee, S and Mazumdar, S. Int. J. of Anal. Chem., 2012(8), 1-40 (2012).

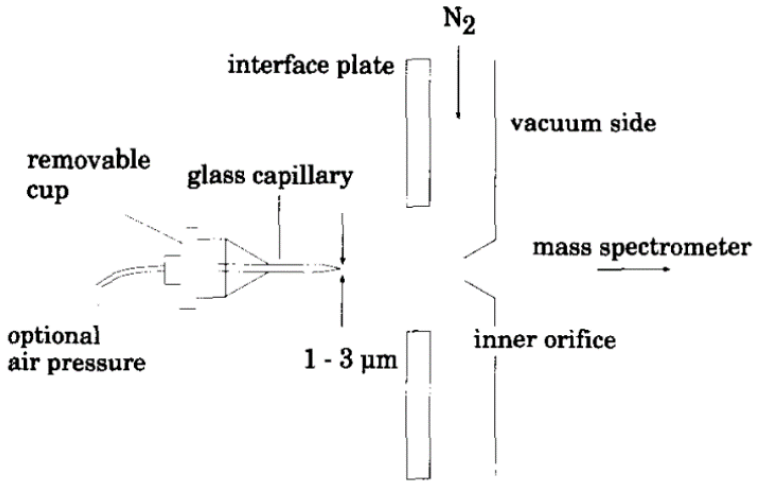

Figure 1.2. Micro(nano)-electrospray ionization which allowed for small volume (µL) MS analysis. Reproduced from Wilm, M.S. and Mann, M, Int. J. of Mass Spectrom. and Ion Process., 136(2), 167-180 (1994).

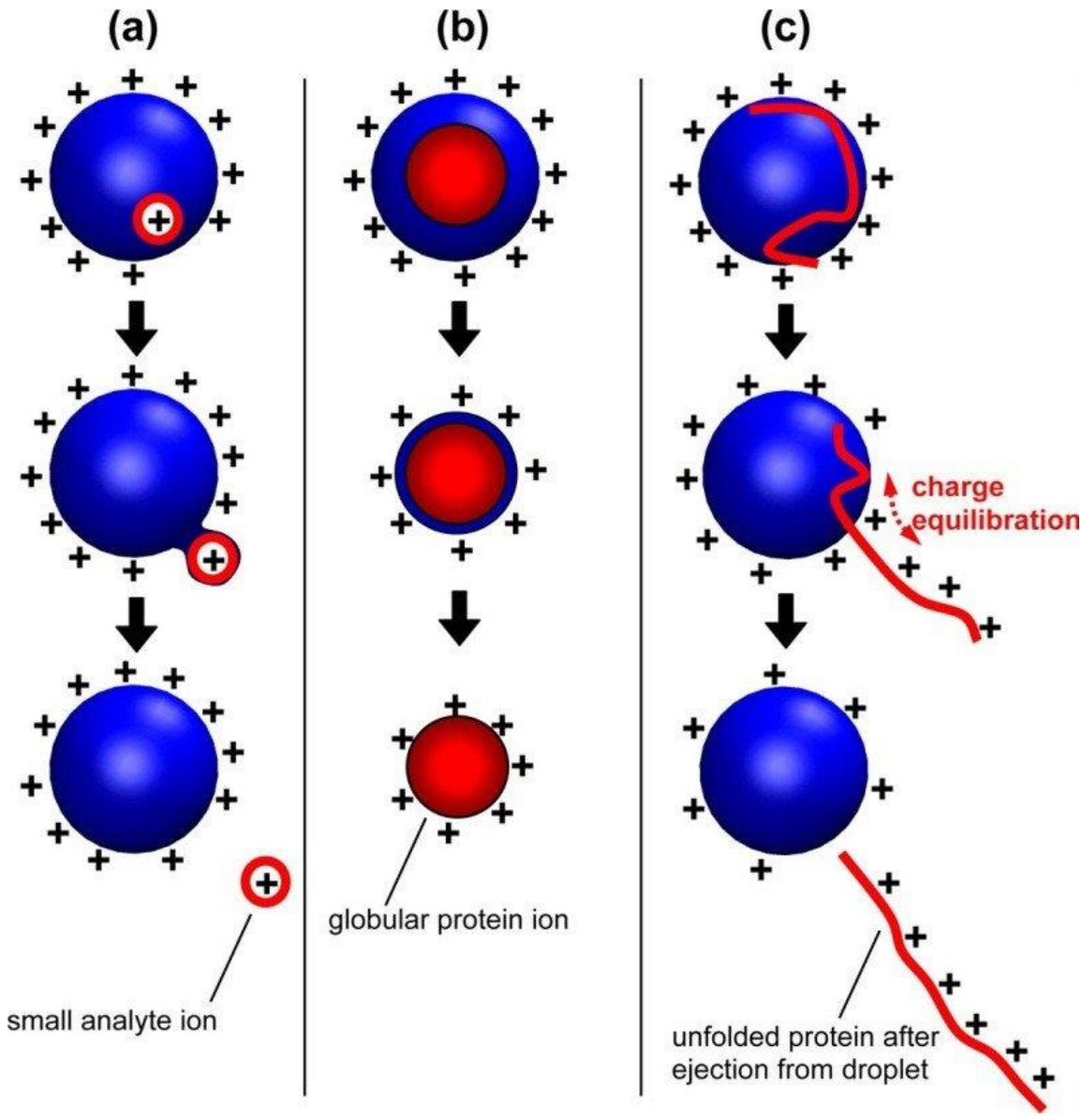

Figure 1.3. The schematic of the different evaporation models (a) ion evaporation, (b) charge residue model and (c) charge ejection model. Reproduced from Konermann, L.; Ahadi, E.; Rodriguez, A. D.; Vahidi, S. Anal. Chem. 85(1), 2–9 (2013).

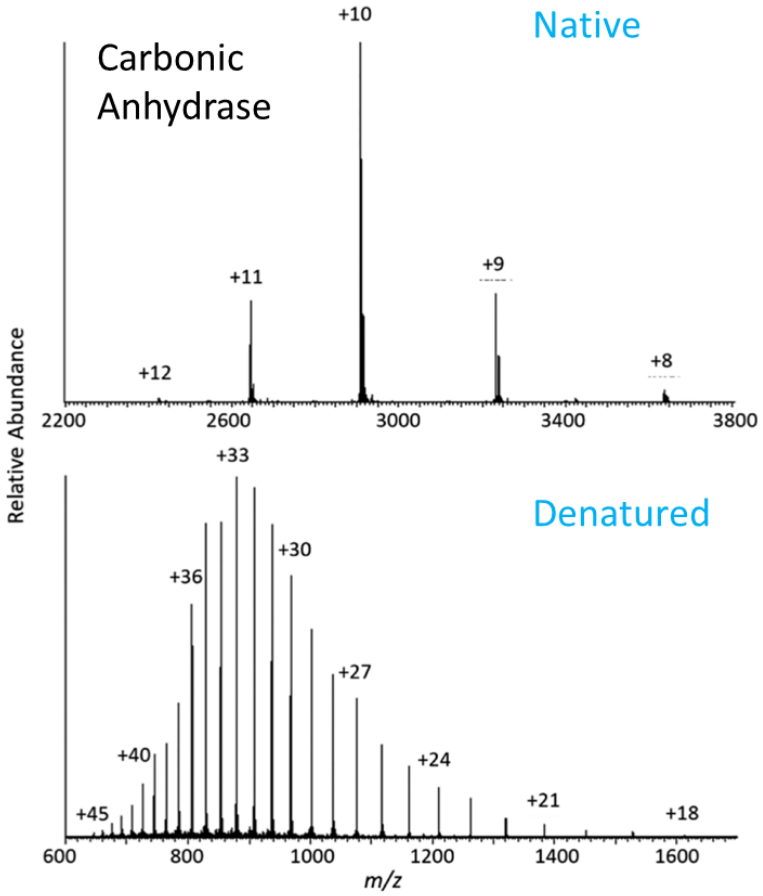

Figure 1.4. Carbonic anhydrase positive-mode ESI-MS with native (top) and denatured (bottom). Reproduced from Kafader, J. O.; Melani, R. D.; Schachner, L. F.; Ives, A. N.; Patrie, S. M.; Kelleher, N. L.; Compton, P. D., J. Am. Soc. Mass Spectrom. 31(3), 574–581 (2020).

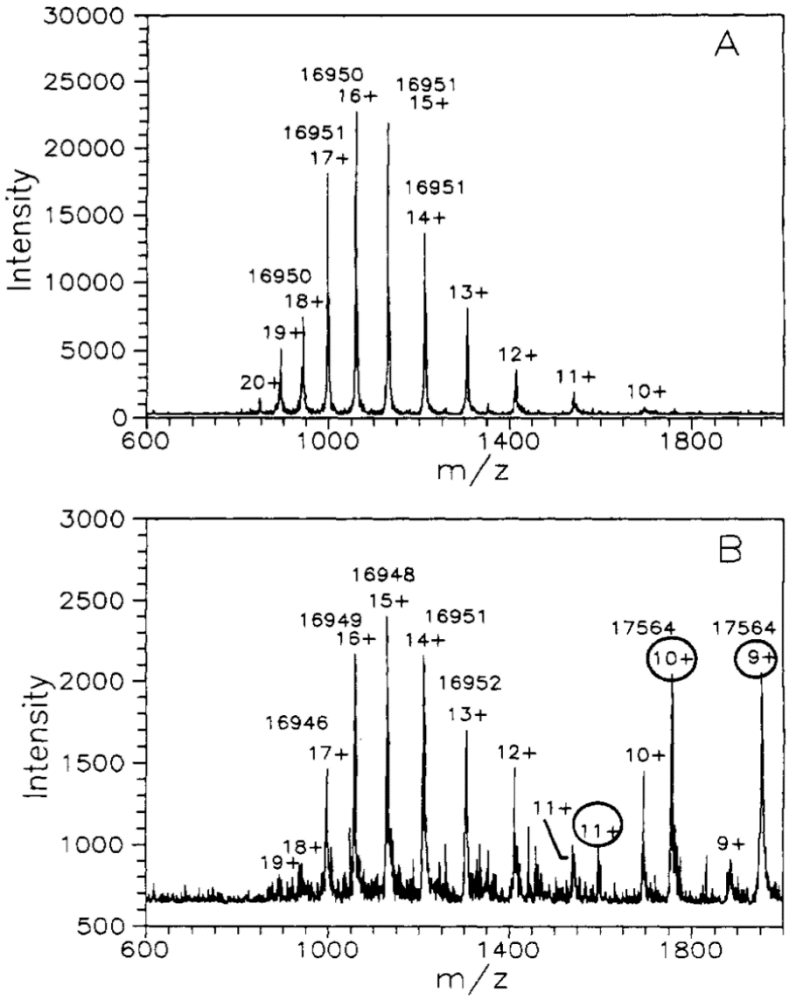

Figure 1.5. ESI-MS of myoglobin under pH 3.35 (top), and pH 3.90 (bottom). Reproduced from Katta, M. and Chait, B., JACS, 113(22), 8534-8535 (1991).

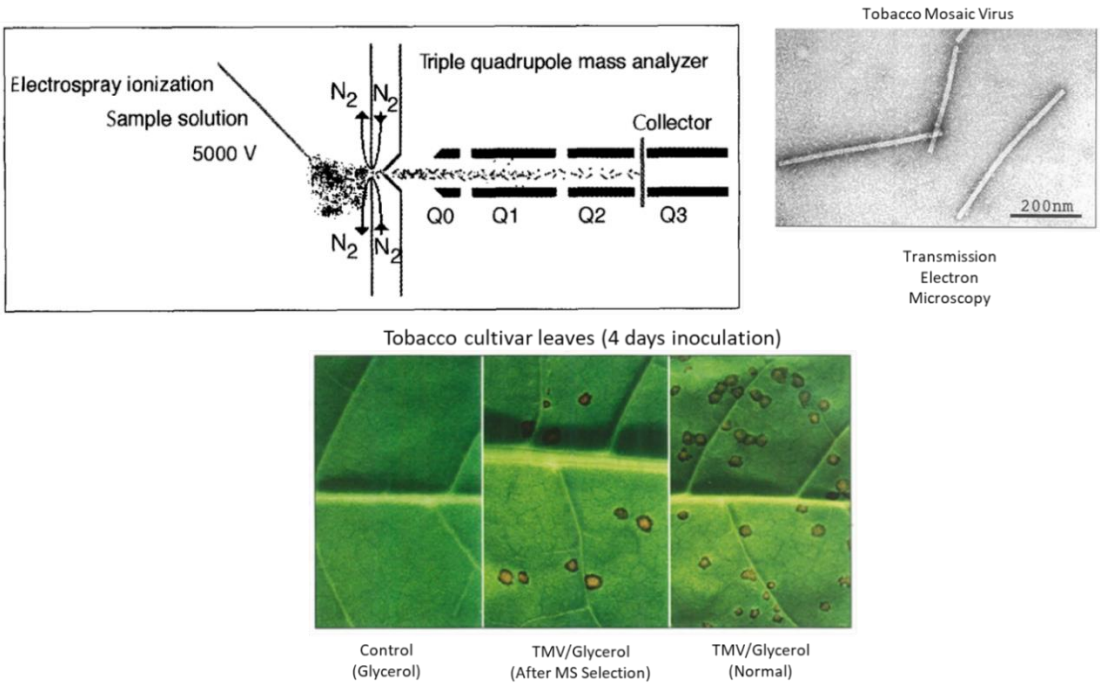

Figure 1.6. The ESI of tobacco mosaic virus ions. A collector plate is placed between Q2 and Q3 (top left). The transmission electron microscopy of the collected tobacco mosaic virus (top right). The inoculation of the collected viral ions on leaves (bottom). Reproduced from Siuzdak, G.; Bothner, B.; Yeager, M.; Brugidou, C.; Fauquet, C. M.; Hoey, K.; Change, C.-M., Chem. Biol. 3(1), 45–48 (1996).

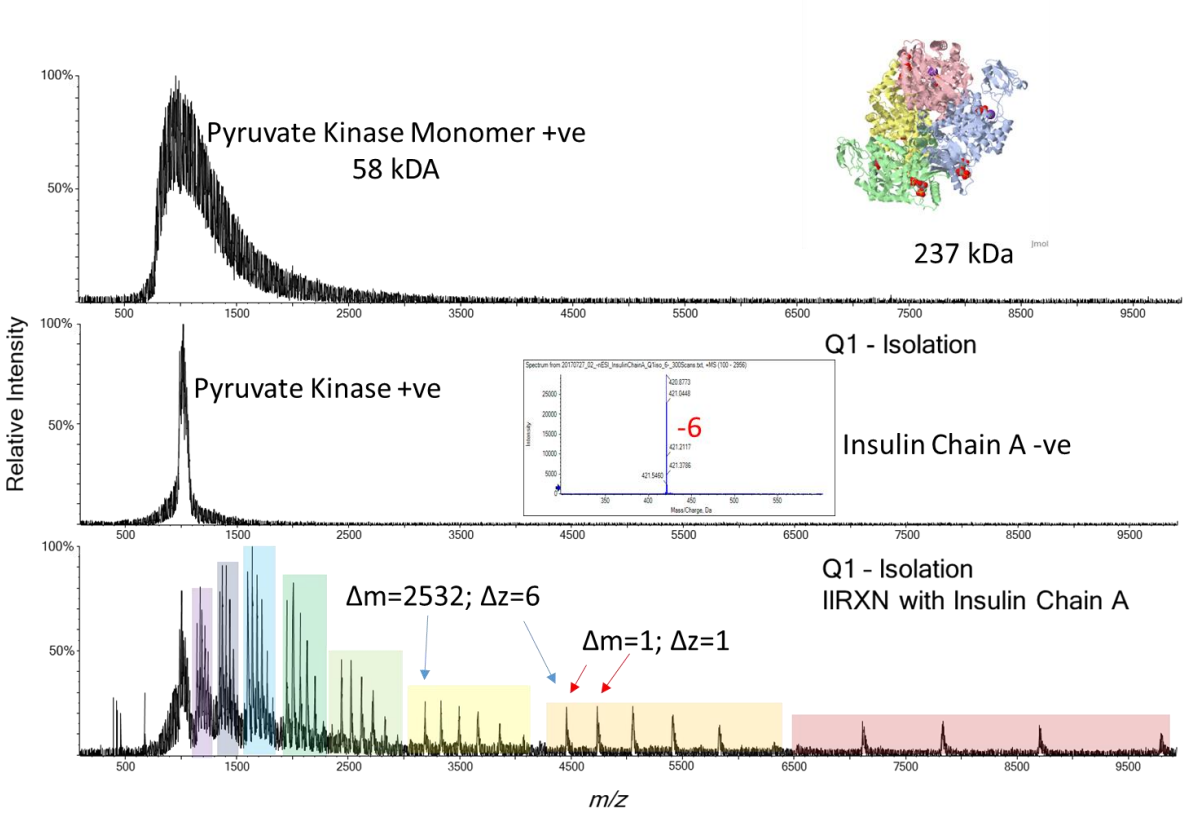

Figure 1.7. MAMA-MIA reaction with pyruvate kinase monomer sprayed under denaturing blobby conditions (top), an isolation of the blob and reacting with insulin chain A reagent (6-) charge state, and the ion/ion reaction (bottom).

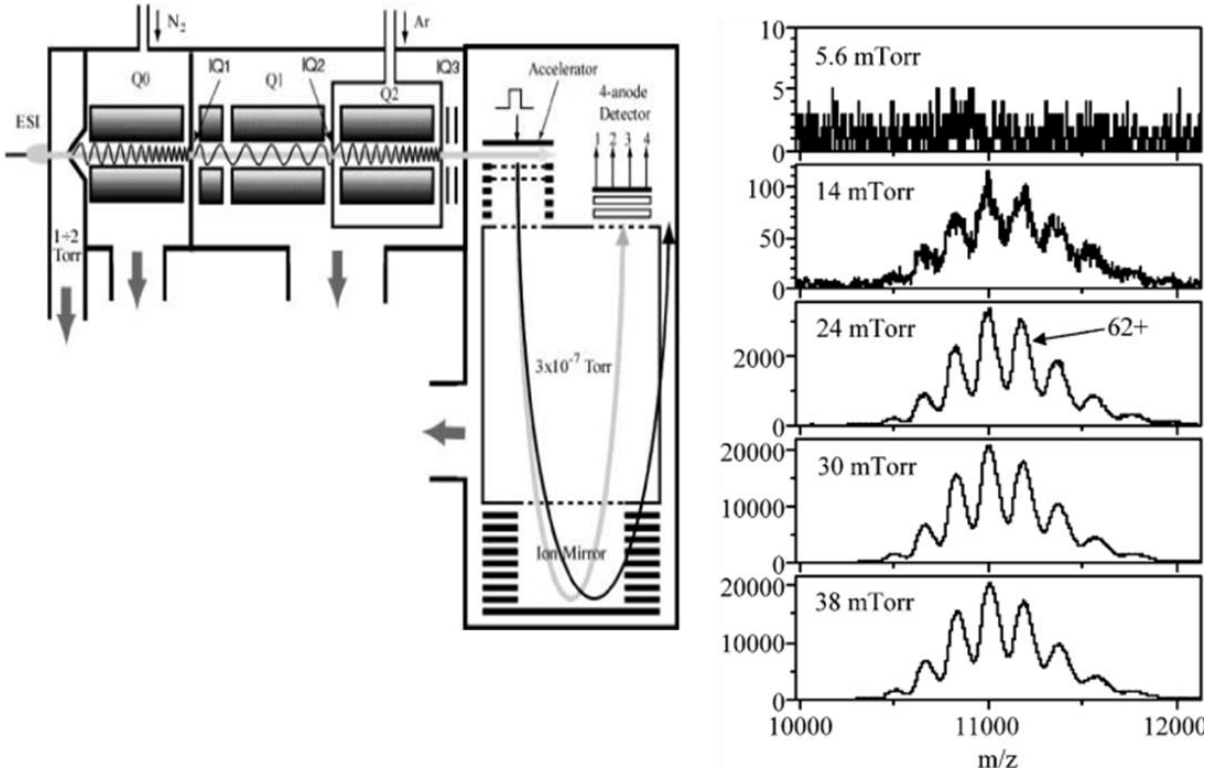

Figure 1.8. The schematic of a QToF (a), and the effect of pressure in Q0 and the ion signal for Proteasome 20S (b). Reproduced from Chernushevich, I. V. and Thomson, B. A., Anal. Chem. 76(6), 1754–1760 (2004).

CHAPTER 2. ION/ION REACTIONS ON THE SCIEX QTOF 5600 PLATFORM

The development of native MS was accelerated by improvements in sample preparation methods and the natural progression of MS instrumentation. However, native MS ions require specific instrumental upgrades, due to the transmission, the resolution, and the detection needed for high *m/z* ions. This chapter will illustrate the improvements made on our platform with focus on native MS ions.

2.1 Introduction

Native MS is aimed at the preservation of non-covalently bound complexes, stoichiometry, and composition of biomolecules (1,2). The main difficulties in measuring ions under native conditions can be categorized in two different ways. The first is when charge states overlap because of the inherent width of each peak, which widens with salt adduction, or because of population heterogeneity in the analyte (3–5). These complex sample analyses can lead to misassignment of the charge, which will lead to an erroneous mass measurement. The second difficulty lies in the narrow charge state distribution, which can also lead to misassignment of the charge state. Major improvements in native MS have attempted to deal with these limitations, leading to the ability for researchers to tackle complicated analytes, which was not possible during the initial years of native MS. These improvements can be categorized into deconvolution, instrumentation, and charge manipulation. The focus of this chapter will be on the two latter improvements.

The ESI measurement of large native MS ions appear at high *m/z*, which preclude the ability to utilize instruments with upper *m/z* limitations. Consequently, the initial ion detection used for native MS was the time-of-flight (TOF) mass analyzers, which detected large systems such as GroEL, viruses and ribosomes (6–8). An alternative approach to solve this is the simultaneous measurement of the *m/z* and the charge of the ion, which is the basic principle of charge detection mass spectrometry (CDMS). CDMS measures individual ions and bins these ions to generate a mass spectrum. This typically requires long acquisition times, with respect to TOF, but the usefulness of this experimental measurement has been demonstrated to outweigh this drawback (9). A separate instrument designed for the study of native MS ions is the Q-Exactive UHMR,

which is an Orbitrap™-based instrument that has gained attention over the last few years (10). This instrument has produced remarkable results with ribosome and viruses (5). However, there are certain shortcomings with utilizing an Orbitrap™. This chapter will illustrate the improvements made on our qTOF instrument, and how we utilize ion/ion reactions to address the two major issues with native MS ions – the overlap of charge states and the narrow charge state distribution, which may lead to erroneous mass measurements (11).

2.2 Experimental

2.2.1 Sample preparation for native mass spectrometry of bio-complexes

GroEL (Sigma Aldrich) lyophilized powder preparation was described before in detail (12). Briefly, the sample was buffer exchanged and underwent acetone precipitation. The buffer exchange occurred via centrifugation with a 150 mM ammonium acetate (Sigma Aldrich) buffer adjusted to pH 7 with ammonium hydroxide (Sigma Aldrich), using a 10 kilodalton (kDa) molecular weight cutoff (MWCO) Amicon Ultra 0.5 mL filter (Millipore Sigma). The final recovered sample (~15 µL) was diluted with the same buffer to achieve 1 µM concentration from the stock solution.

Rabbit pyruvate kinase was purchased from Sigma Aldrich. The lyophilized solid was reconstituted in water to create a stock solution at a concentration of 3 µM (calculated by using the mass of the tetramer). The sample underwent buffer exchange, via centrifugation, once with an ammonium acetate (Sigma Aldrich) buffer adjusted to pH 7 with ammonium hydroxide (Sigma Aldrich), using a 100 kilodalton (kDa) molecular weight cutoff (MWCO) Amicon Ultra 0.5 mL filter (Millipore Sigma). The recovered sample (15 µL) was diluted with the same buffer to achieve the same original concentration from the stock solution.

2.2.2 Sample preparation for the reagent anions

Our charge reducing reagent for proton transfer reactions is perfluoro-1-octonal (PFO), which was prepared as a 1 mg/mL stock solution in methanol. The working solution was diluted to 30 µM in methanol with 1% ammonium hydroxide to form the anion. The formation of singly deprotonated dimers, which were previously observed to be an effective reagent for proton transfer reactions, was isolated and used as our proton transfer reagent (13). For the multiply-charged ion

attachment reagent, we utilized oxidized insulin chain A (IcA) from bovine pancreas (average mass, free acid = 2531.66 Da) purchased from Sigma Aldrich. The lyophilized solid was reconstituted in water. The working solution was a 50:50 mixture of aqueous ammonium hydroxide (pH 11) and HPLC grade methanol (Sigma Aldrich) to give a final concentration of 25 µM. The most abundant charge states were $[IcA-5H]^{5-}$ and $[IcA-6H]^{6-}$. For negative mode nano-ESI analytes, our charge reducing reagent was bovine ubiquitin, which was prepared under similar denaturing conditions, except the use of 1% acetic acid. The charge state distribution and isolated peaks can be seen in **Figure 2.1**.

2.2.3 Ion-ion reactions in the mass spectrometer.

All experiments were performed using a QTOF 5600 (SCIEX), **Figure 2.2**, which was previously modified to allow for ion/ion reactions (14). The positive and negative ions were generated by utilizing an alternately pulsed nano-electrospray ionization source (nESI) (15). Mutual ion polarity trapping was enabled by applying a supplemental AC to the end plates of the linear ion trap reaction cell, q2. Multiply protonated protein cations and reagent anions were sequentially isolated before being stored in q2 to react over times of 50-100 ms. The reagent anions were isolated during Q1 transmission by conventional RF-DC apex isolation. The protein cations were too high in *m/z* to be isolated via conventional RF-DC apex isolation. Therefore, sequential resonance ejection ramps in q2 were used to eject ions of lower and higher *m/z* ratios that bordered the population of interest (16).

2.2.4 Native MS

Both analyte and reagent ions were generated via nESI from separately pulsed borosilicate glass emitters. The large bio-complexes were sprayed in both positive and negative mode with approximately ±1200 V applied to a platinum wire, which was in contact with the solution. The reagent anions were sprayed in negative or positive mode, respectively, with an applied voltage of approximately ±1400 V. The large complex ions were initially injected into the instrument and isolated (see above) and stored in q2. Subsequently, the reagent anions were injected and isolated during Q1 transmission before being accumulated and stored in q2. The mutual storage time can be controlled to determine the extent of the ion/ion reactions. Nitrogen gas was used in q2 at

pressures ranging from 6-8 mtorr. Due to the size of the large ions, the difference in DC offsets of Q0 and q2 were increased to as high as 50-70 V to collisionally activate the ions upon injection into q2 to drive off weakly-bound adduct species. A Q0-q2 voltage difference of 5-15 V was used for the reagent anions as minimal salt adduction was observed for these species. Mass calibration over a wide range was done in two stages, using primary and secondary calibrants. Cesium iodide, the primary calibrant, was used to calibrate the instrument over the range of *m/z* 1,000-10,000 (**Figure 2.3**). This allowed for an accurate mass determination of the pyruvate kinase tetramer, the secondary calibrant, from the mass spectrum derived under native conditions. Finally, the population of pyruvate kinase charge states was reacted with the oxidized insulin chain A, $[IcA-6H]^{6-}$ anions with product peaks spreading across a wide *m/z* with the final peak at *m/z* ~120,000.

2.3 Results and Discussions

2.3.1 Instrument

The platform we use for our native MS work is the quadrupole/time of flight (QTOF) 5600 instrument. This commercial instrument is comprised of four quadrupoles (**Figure 2.2**), which differs from the earlier rendition of the SCIEX instrument, the QStar instrument, which is comprised of three quadrupoles, Q0, Q1 and q2 (17). A reflectron TOF analyzer is used as the detector. The instrument is differentially pumped, and the pressure reduced, towards the TOF mass analyzer. The effect of increased pressure towards the initial segments of the instrument aids in the collisional cooling of the ions to the center of the ion path. This initial section under higher pressure is vital for the transmission of large native ions, such as proteasome 20S (~692 kDa), when increasing the Q0 pressure from 5 to 30 mTorr (18). Moreover, the overall signal of large ions with non-covalent interactions has shown to increase with higher pressures in the trapping region (19). The pressure in our initial ion guide, QJet in our schematic, is set to several orders of magnitude higher at 2 Torr to aid in the transmission of large ions. The frequency of our QJet was reduced and replaced with a 300 kHz coil box. It is known that reducing the frequency of the quadrupole aids in the transfer of large ions (10). Our group did not alter other quadrupole frequencies because doing so would inhibit the study of the small ions, which this platform is also used for. Lastly, we adjusted the gas inlet for q2, by placing a t-line with stoppage valves, to allow for the introduction of heavier bath gas. The introduction of larger bath gas will appear in the later

section of this dissertation. That is the extent of alterations made, in terms of physical hardware changes, on the 5600 platform. Our group utilizes SCIEX research grade software (ASD), which allows for the control of every ion optical element of the instrument. Consequently, we have a high degree of experimental flexibility.

The gradients and the relationships of the ion optics can be seen in the equations above **Figure 2.2**. A typical scan function involving ion/ion reactions can be seen in previous work done in our group (17). The schematic between spraying small and large *m/z* ions can be seen in **Figure 2.3**. The major difference is in the initial optics of the instrument, as that section has the largest impact on increasing analyte signal for large *m/z* ions. Typically, the spray voltage generates the ion which then travels through the MS in a steady gradient towards the detector. For large ions, the signal is increased if the orifice is set to a lower voltage than the QJet rod offset, while the curtain plate is set higher. This creates a voltage barrier that lowers the kinetic energy of the large *m/z* ions so their travel across QJet and Q0 has a longer duration, allowing for more collisional cooling of the ions. This technique discriminates against smaller *m/z* ions. Depending on the steepness of the voltage difference between the orifice and QJet rods, smaller ions may be prevented from passing through that barrier due to insufficient kinetic energy. As that voltage difference increases, the *m/z* of the measured ions increase.

2.3.2 Figures of Merit

During the advent of native MS experiments, most of the research was done using a TOF mass analyzer (8). However, improvements in MS that are directed towards the study of large biomolecules have made huge leaps over the last several years. In particular, the development of the Q-Exactive UHMR towards studying large complexes have pushed the limitations set by heterogenous mixtures (2,10). These improvements with instruments capable of much higher resolution has pushed research towards the direction of Orbitrap™ and FT-ICR instrumentation (1, 20). A TOF mass analyzer has certain benefits when employed for the detection of large ions. This section will address these benefits and compare them with the current state-of-the-art instrumentation for native MS.

2.3.3 Isolation

The isolation of ions is crucial when studying complex systems. Before fragmenting ions, simplifying the precursor by utilizing a homogeneous precursor ion population would aid in the mass spectral interpretation. Moreover, isolation is important for our ion/ion reaction experiments. If the precursor is extremely "blobby", where the ions have great overlap, performing charge reduction with proton transfer reactions can be difficult (see chapter 3). Our lab utilizes two different forms of isolation. Our RF/DC isolation, where the voltages are increased to position non-target ions out of the stable boundary conditions, can be done in Q1. However, there is an upper limit to that isolation type of *m/z* ~3000, which is not ideal for native ions.

For native MS studies, we utilized q2 RF ramping, where we use a fixed frequency and high amplitude to remove the borders of the target ion. Another form is stored-waveform isolation Fourier transform (SWIFT), which is a way to generate a tailored wave-form to isolate a region of interest (**Figure 2.5**).

2.3.4 Resolution

The large ions associated with native MS typically are formed with excess salt adduction and incomplete desolvation. The resolution required to resolve the isotopes with large *m/z* ions are prohibitive in most cases over 1 MDa. Our platform does not have better performance in that resolution measurement, but there is a benefit that is exclusive to TOF mass analyzer. The relationship between *m/z* and the various mass analyzers can be seen in **Figure 2.6** (21). The resolution of the orbitrap and FT-ICR are much higher at lower *m/z*. At high *m/z*, the resolution of those mass analyzers fall, due to their inverse relationship between *m/z* and resolution (21). The resolution is not related to the *m/z* for TOF mass analyzers. Moreover, for native MS experiments, the *m/z* position of the charge state distribution can be directly related to the molecular weight of the analyte (1). TOF mass analyzer are suitable for native MS studies because of their lack of dependence on *m/z* and resolution, while also having a theoretical unlimited upper *m/z* limit.

In our experiments, we performed an ion/ion reaction with GroEL and PFO (**Figure 2.7**). The initial precursor spectrum of GroEL, a 14mer that is ~800 kDa, is centered around *m/z* 11,000 under native MS positive-mode MS conditions. The reaction forms products across a wide *m/z* region. The overlaid spectra in different color traces indicate the injection conditions (Q0 – Q2)

for GroEL before the subsequent injection of the anions. Under small gradients, 10 V, the molecular weight of GroEL was ~807 kDa and for the highest gradient, 165 V, the molecular weight was ~801 kDa. The width of the peaks can visually be seen in the inset of **Figure 2.7**. The peaks shift to lower *m/z* as the gradient is increased, indicating a lower mass of the ions because each cluster of peaks is from similar charge states. The differences in mass are consistent with more extensive removal of excess salt as the energy of ion injection into q2 increases. A separate observation is the larger FWHM width of the 10 V gradient with respect to the 165 V gradient, where the high gradient narrows the FWHM of the peaks. This is also consistent with greater loss of excess salts at higher ion injection energies. The apparent resolution (i.e. FWHM of the mass of the peak profile) vs. the *m/z* of these ions are plotted in **Figure 2.8**. The resolution is doubled in the 165 V gradient. It is important to note that the resolution remains consistent across the *m/z* axis. This shows the strength of employing a TOF mass analyzer in the study of high *m/z* ions.

2.3.5 Upper m/z limits

A separate, but important, characteristic of the native MS instrumentation is the need for a sufficiently high *m/z* limit. This is the main reason for the early use of the TOF mass analyzer. For proteins under denaturing conditions, the *m/z* limit ranges from 500 – 2000 *m/z* (see **Figure 2.1**). However, large native ions are formed at much higher *m/z* values, beyond *m/z* 50,000 for viruses (3), for example. Theoretically, there is no upper *m/z* limit for TOF mass analyzer. The upper m/z in the present apparatus is limited by the initial ion optics, the ability to capture, cool to the center and transfer the ions, or detector response.

The ion/ion proton transfer reaction of GroEL with more PFO can be seen in **Figure 2.9**. To increase the amount of PFO in the reaction chamber, q2, the fill time segment, where a voltage is being applied to the PFO emitter, is increased. The ions were pushed ranging from *m/z* 40,000 to 400,000. The most abundant charge state was the 4+ in the bottom spectrum. There was a point at which any further increase of the PFO reagent would not increase the abundance of the 2+ charge state. Our explanation for this is the width of the ion cloud of those high *m/z* ions. If the q2RF voltage is not high enough to focus those clouds to the center of the trap before ejecting to the TOF mass analyzer, then a subsequent transfer across the narrow exit aperture may decrease the number of ions that reach the detector. We can see the effects of the q2RF on the abundance of high *m/z* ions in **Figure 2.10**. This voltage has a large effect, as increasing the q2RF from 200

to 400 V, the appearance of the *m/z* 400,000 ion becomes observable. However, the difference between 400 and 500 V is not immediately obvious as the abundance for that ion is roughly the same. Each experiment was averaged with 500 scans for a total acquisition time of about 5 mins. The use of a higher voltage may focus the ion clouds closer to the center and allow for an increase in the abundance of the 2+ charge state. We utilize the research grade software and can observe large mass ranges and high *m/z* ions on our platform because of the control we have for the pulsing of ions to the detector. There are certain limitations set in place for the commercial version, that we have learned to circumvent.

The pseudopotential well-depths of the ions generated from GroEL can be seen in **Figure 2.11**. The well-depth is the effective trapping potential of ions given certain storage conditions. Calculation of the well-depth requires the q value (22):

$$q = \frac{4zeV_{RF}}{mr_0^2\Omega_d^2} \quad (1)$$

where z is the charge of the ion, e is the electron charge, V_{RF} is the RF voltage amplitude (0-p), m is the mass of the ion, r is the radius of the quadrupoles and Ω is the drive frequency. From there, the well-depth can be approximated by (23):

$$D = \frac{qV}{8} \quad (2)$$

where D is the well-depth. The size of the trapped ion cloud is inversely related to the well-depth, meaning that a large *m/z* ion will have a shallower well-depth and thus less likely to be trapped (24). The well depth between the 4+ and the 2+ is not a large decrease, so the stability of these ions in the trap should be comparable. This agrees with our notion that the stability of ions do not cause the limit in the abundance of the 2+ charge state, but that, instead, the ion cloud is not narrow enough to pass through the exit aperture.

2.3.6 Fragmentation

In addition to mass information, mass spectrometry can also provide primary structural information via fragmentation. In the case of proteins, identification applications usually include the mass measurement of both precursor and product ions in a fragmentation experiment. There

are two general approaches for protein identification, referred to as the bottom-up and the top-down MS (25). The bottom-up approach starts by extracting the protein of interest from a cell or tissue. The protein is then digested, typically with trypsin, to form small peptides that undergo separate chromatographic separation before tandem mass spectrometry. Consequently, the mass information of the fully formed protein complex is not observed in bottom-up proteomics. However, there are many benefits to the bottom-up approach. For example, with the high resolution of low *m/z* ions, the location of post-translational modifications can be determined in the smaller peptides formed from the digestion step. This would be a difficult measurement with large native ions.

The top-down approach starts at the same step with protein purification; however, the protein is not digested to smaller peptides. Instead, the protein undergoes buffer exchange and then measured directly by the MS. The intact protein complex is then subjected to collisional activation techniques to induce fragmentation. The activation techniques were mentioned in the first chapter. Our platform is capable of beam-type (BT) CID, also referred to as high energy CID, and ion trap CID. The BT-CID of GroEL precursor can be observed in **Figure 2.12**. The typical fragmentation observed for native complexes, consisting of multiple monomers, is the release of a monomer and the residual N-1mer. In the case of GroEL, consisting of 14 monomers, the CID fragmentation would yield a monomer and a 13-mer. The ion-trap CID can be observed in **Figure 2.13**. The details of ion-trap CID can be found in chapter 1. Briefly, each *m/z* ion has a secular frequency that when applied come into resonance and move from the center of the trap. The maximum region that we can apply a "tickle", which is referred to when a particular ion observes its unique secular frequency, is *m/z* 46,000. The m/z of the ion is inversely related to the frequency. High *m/z* ions need lower frequency, and our current platform has a lower limit of 5 kHz for the frequency.

2.4 Conclusions

The rapid improvements for native MS instrumentation have enhanced the capabilities for studying large systems. Our QTOF platform has the capability needed to study large non-covalently bound complexes. Moreover, our platform is also equipped with ion/ion reaction capabilities which generate product peaks that spread across a very broad *m/z* region. The importance of this is that with more independent *m/z* measurements the associated error with the mass and charge assignment of the precursor peak is minimized (11, 26). The *m/z* region that we

have access to with our ion/ion reaction experiments is wide, and with that we can ensure an accurate mass measurement. Our current upper *m/z* limit is more than 3x the Q-Exactive UHMR, an instrument designed for ascertaining mass information from native ions. Moreover, the consistent resolution across a large *m/z* region makes this platform more suitable than the other leading instruments available for the study of large complexes.

2.5 References

1. Leney A.C., A.J.R. Heck: Native Mass Spectrometry: What is in the Name?: J. Am. Soc. Mass Spectrom. 28. 5–13 (2017).

2. Boeri Erba E., C. Petosa: The emerging role of native mass spectrometry in characterizing the structure and dynamics of macromolecular complexes.: Protein Sci. Publ. Protein Soc. 24. 1176–1192 (2015).

3. Snijder J. et al.: Studying 18 MDa Virus Assemblies with Native Mass Spectrometry.: Angew. Chem. Int. Ed. 52. 4020–4023 (2013).

4. Abdillahi A.M. et al.: Mass Analysis of Macro-molecular Analytes via Multiply-Charged Ion Attachment.: Anal. Chem. 92. 16301–16306 (2020).

5. van de Waterbeemd M. et al.: High-fidelity mass analysis unveils heterogeneity in intact ribosomal particles.: Nat. Methods 14. 283–286 (2017).

6. Rostom A.A., C.V. Robinson: Detection of the Intact GroEL Chaperonin Assembly by Mass Spectrometry.: J. Am. Chem. Soc. 121. 4718–4719 (1999).

7. Tito M.A. et al.: Electrospray Time-of-Flight Mass Spectrometry of the Intact MS2 Virus Capsid.: J. Am. Chem. Soc. 122. 3550–3551 (2000).

8. Rostom A.A. et al.: Detection and selective dissociation of intact ribosomes in a mass spectrometer.: Proc. Natl. Acad. Sci. U. S. A. 97. 5185–5190 (2000).

9. Todd A.R. et al.: Higher Resolution Charge Detection Mass Spectrometry.: Anal. Chem. 92. 11357–11364 (2020).

10. L. Fort K. et al.: Expanding the structural analysis capabilities on an Orbitrap-based mass spectrometer for large macromolecular complexes.: Analyst 143. 100–105 (2018).

11. Liepold L. et al.: Correct Charge State Assignment of Native Electrospray Spectra of Protein Complexes.: J. Am. Soc. Mass Spectrom. 20. 435–442 (2009).

12. Zhou M. et al.: Dissecting the large noncovalent protein complex GroEL with surface-induced dissociation and ion mobility-mass spectrometry.: Anal. Chem. 85. 8262–8267 (2013).

13. Xia Y. et al.: Pulsed Dual Electrospray Ionization for Ion/Ion Reactions.: J. Am. Soc. Mass Spectrom. 16. 1750–1756 (2005).

14. Xia Y. et al.: Mutual storage mode ion/ion reactions in a hybrid linear ion trap.: J. Am. Soc. Mass Spectrom. 16. 71–81 (2005).

15. Liang X. et al.: Alternately Pulsed Nanoelectrospray Ionization/Atmospheric Pressure Chemical Ionization for Ion/Ion Reactions in an Electrodynamic Ion Trap.: Anal. Chem. 78. 3208–3212 (2006).

16. McLuckey S.A. et al.: Selective ion isolation/rejection over a broad mass range in the quadrupole ion trap.: J. Am. Soc. Mass Spectrom. 2. 11–21 (1991).

17. Xia Y. et al.: Implementation of Ion/Ion Reactions in a Quadrupole/Time-of-Flight Tandem Mass Spectrometer.: Anal. Chem. 78. 4146–4154 (2006).

18. Chernushevich I.V., B.A. Thomson: Collisional Cooling of Large Ions in Electrospray Mass Spectrometry.: Anal. Chem. 76. 1754–1760 (2004).

19. Smith J.C. et al.: Collisional cooling enhances the ability to observe non-covalent interactions within the inducible nitric oxide synthase oxygenase domain: dimerization, complexation, and dissociation.: J. Am. Soc. Mass Spectrom. 15. 629–638 (2004).

20. Schachner L.F. et al.: Standard Proteoforms and Their Complexes for Native Mass Spectrometry.: J. Am. Soc. Mass Spectrom. 30. 1190–1198 (2019).

21. Lössl P. et al.: Boundaries of Mass Resolution in Native Mass Spectrometry.: J. Am. Soc. Mass Spectrom. 25. 906–917 (2014).

22. March R.E., J.F.J. Todd: Quadrupole ion trap mass spectrometry. 2nd ed. Hoboken, N.J. J. Wiley 2005.

23. Wuerker R.F. et al.: Electrodynamic Containment of Charged Particles.: J. Appl. Phys. 30. 342–349 (1959).

24. Lee K.W. et al.: Increasing the Upper Mass/Charge Limit of a Quadrupole Ion Trap for Ion/Ion Reaction Product Analysis via Waveform Switching.: J. Am. Soc. Mass Spectrom. 30. 1126–1132 (2019).

25. Gregorich Z.R. et al.: Proteomics in Heart Failure: Top-down or Bottom-up?: Pflugers Arch. 466. 1199–1209 (2014).

26. Laszlo K.J., M.F. Bush: Analysis of Native-Like Proteins and Protein Complexes Using Cation to Anion Proton Transfer Reactions (CAPTR).: J. Am. Soc. Mass Spectrom. 26. 2152–2161 (2015).

2.6 Figures

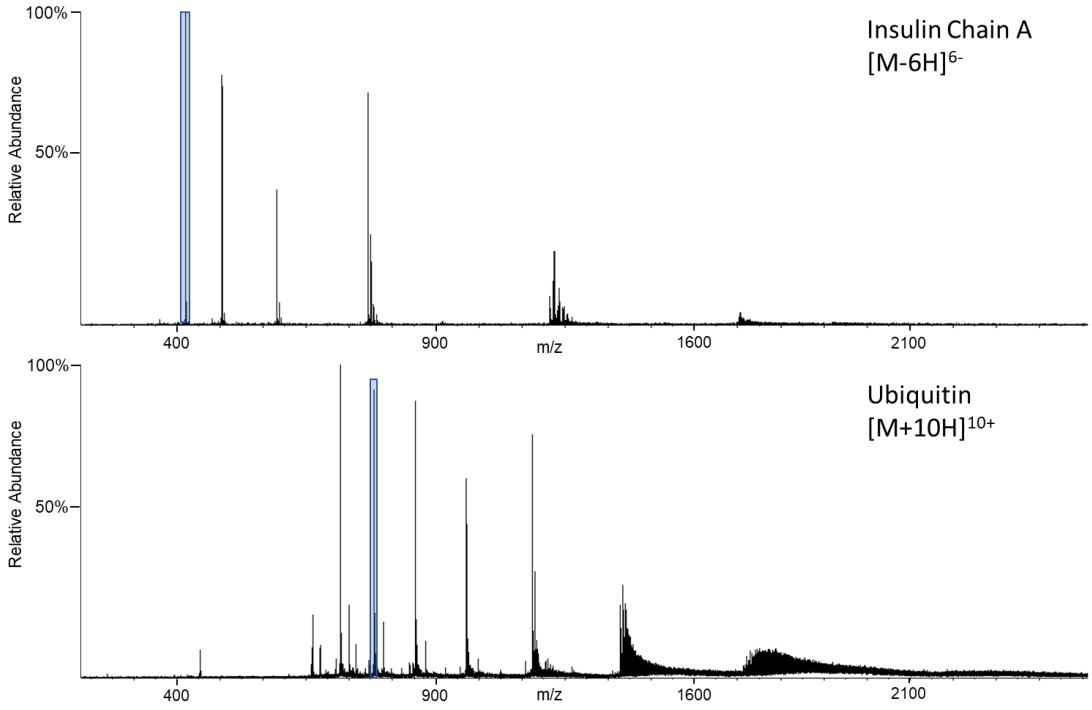

Figure 2.1. The reagents utilized for multiply-charged ion attachment experiments. When the analyte is in the positive mode, the insulin chain A is the reagent (top). When the analyte is in the negative mode, the ubiquitin is the reagent (bottom).

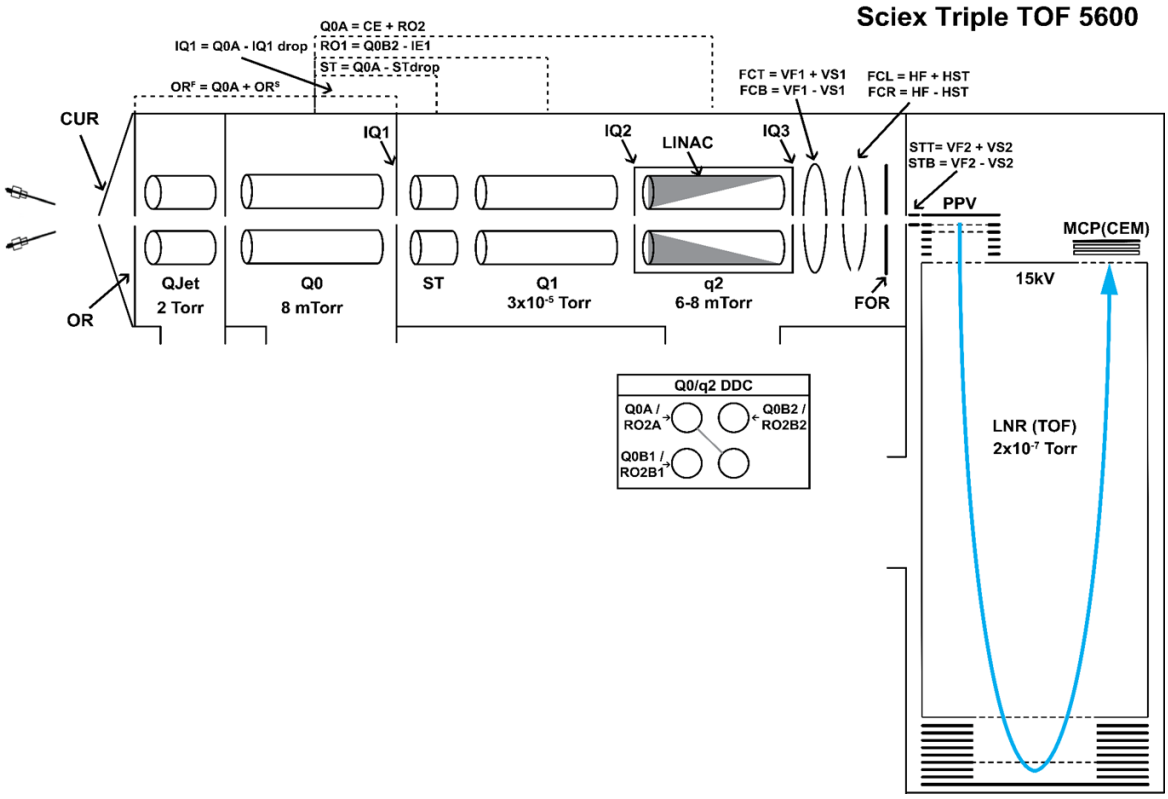

Figure 2.2. The instrument schematic for the SCIEX 5600. The dual emitter near the interface is pulsed to allow for each reagent to travel down the instrument. Supplemental AC is fixed on the the IQ2 and IQ3 lens to allow for mutual storage of the ions. Q0 and q2 DDC moves the ion off-axis.

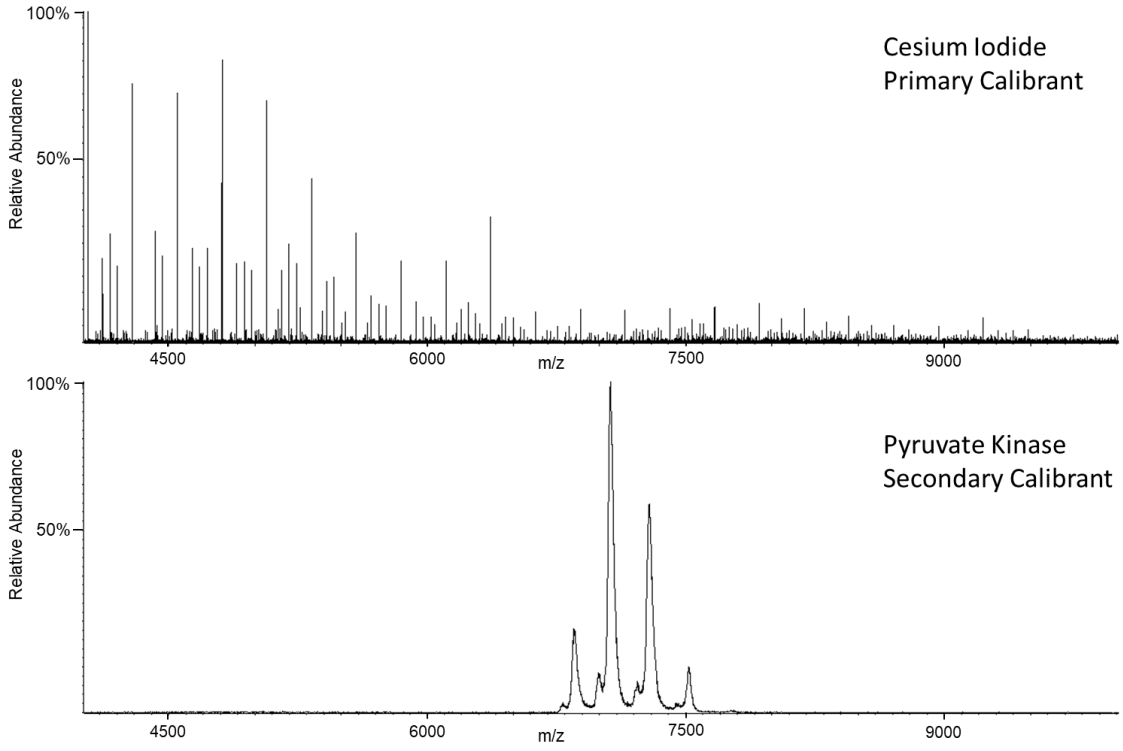

Figure 2.3. Cesium iodide clusters serve as the primary calibrant (top) to measure an accurate mass assignment of pyruvate kinase, the secondary calibrant (bottom)

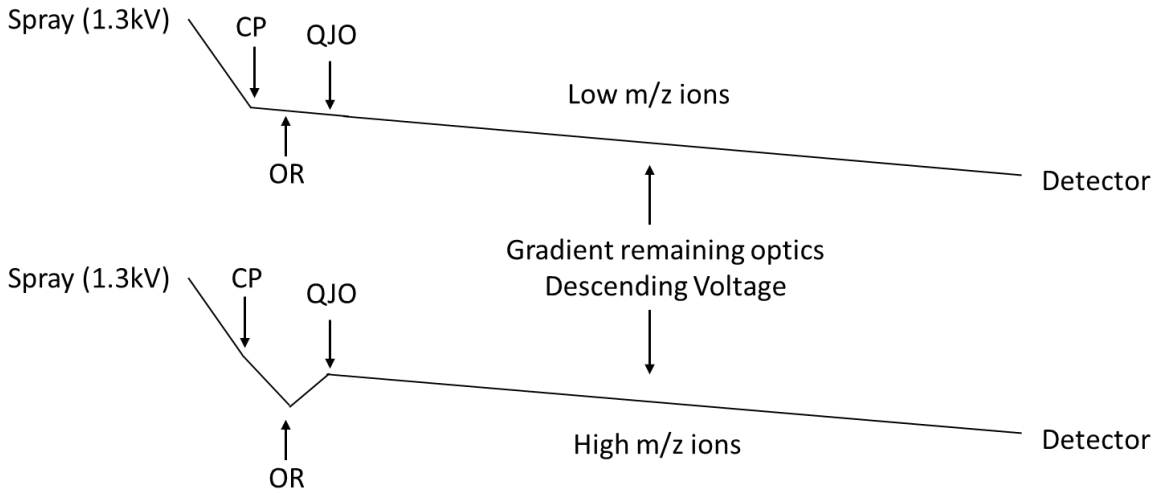

Figure 2.4. Schematic of the typical gradient for small m/z ions (top), and high m/z ions (bottom). CP = curtain plate, OR = orifice, QJO = rod offset for QJet.

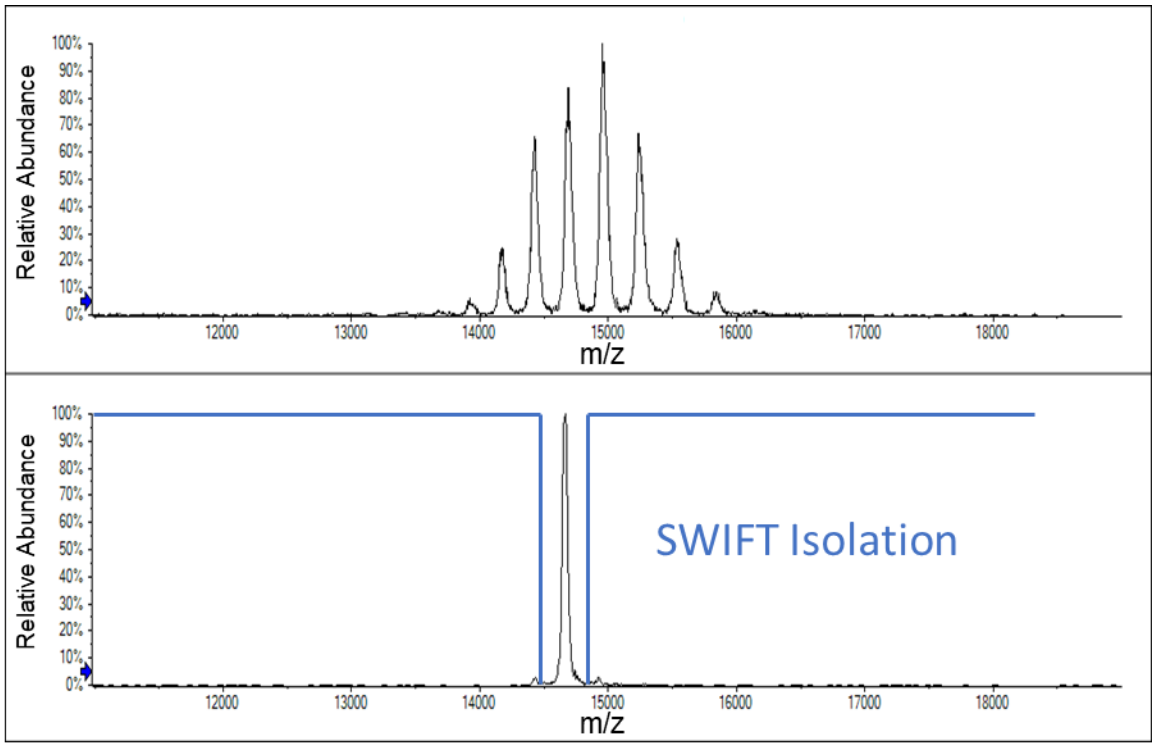

Figure 2.5. GroEL mass spectrum in the negative mode (top) and the isolation of GroEL by SWIFT.

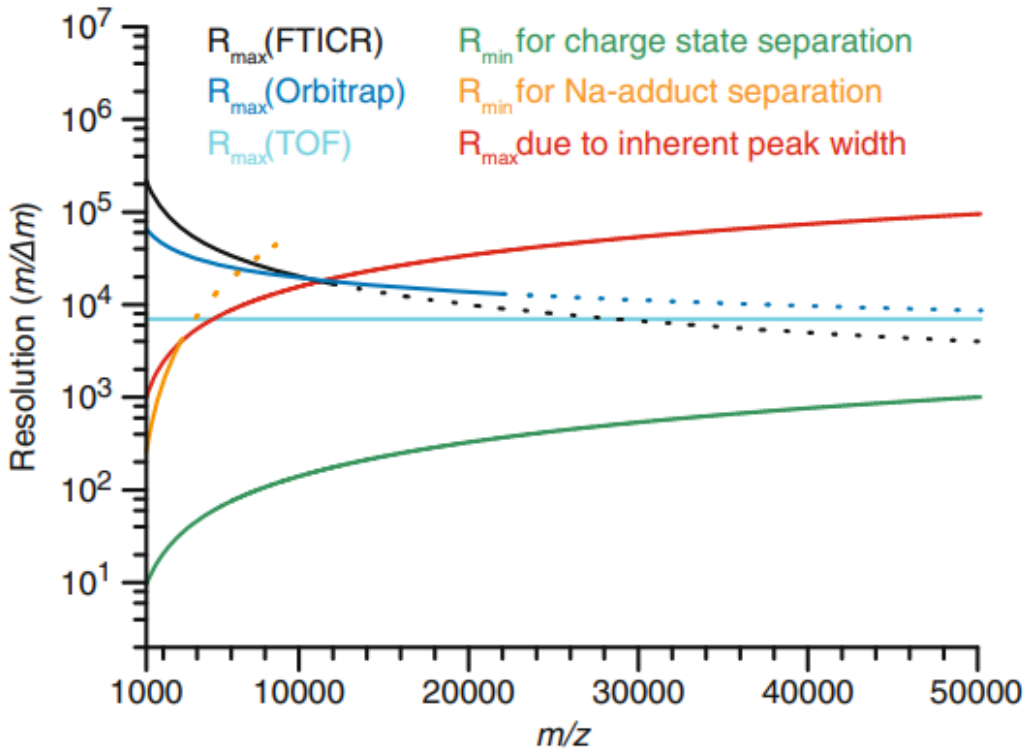

Figure 2.6. The relationship between the maximum resolution for the FTICR, Orbitrap, and TOF mass analyzer. The minimum resolution needed for charge state separation. Reproduced from Lössl P. et al., J. Am. Soc. Mass Spectrom. 25. 906–917 (2014).

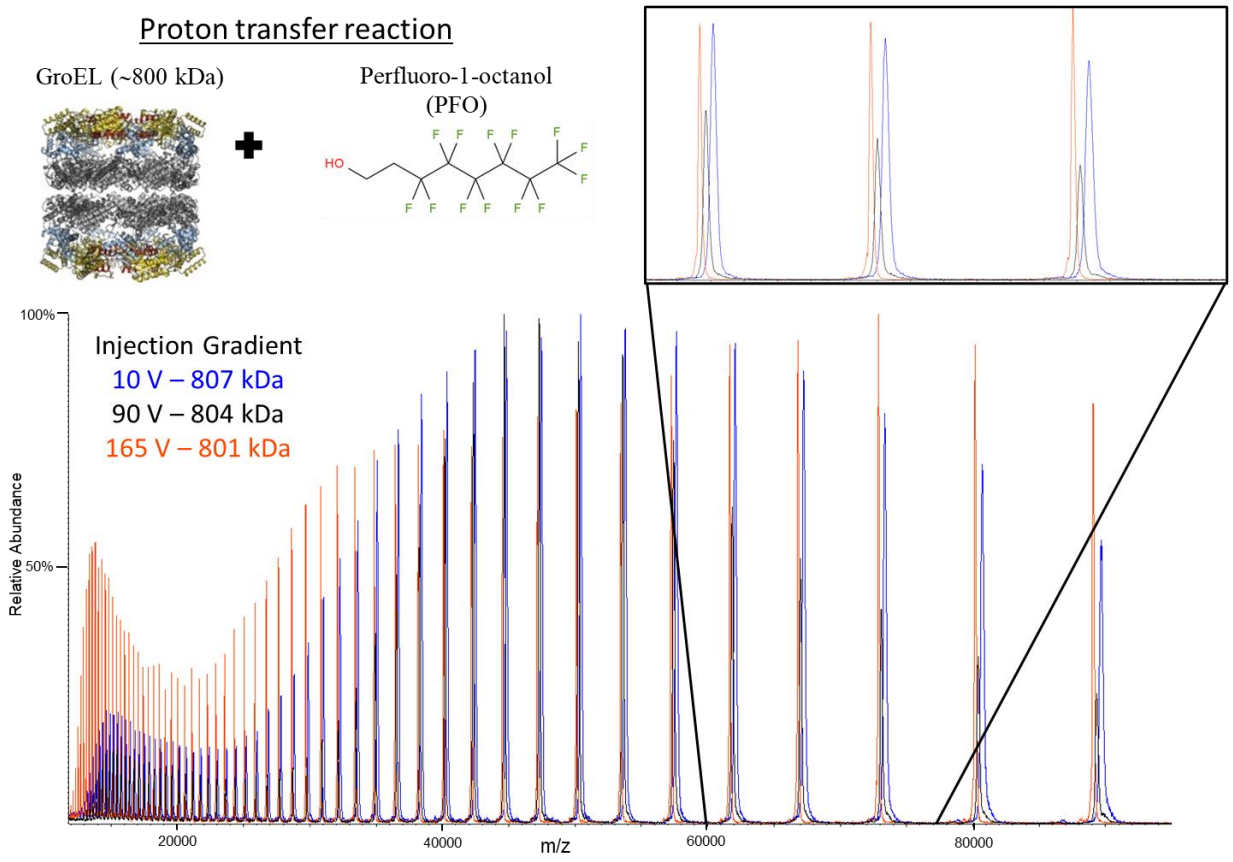

Figure 2.7. The ion/ion proton transfer reaction of GroEL and PFO, using different injection conditions for the GroEL prior to the reaction. The mass measurements next to the gradients were measured via zero-charge deconvolution. The inset is a section of the designated m/z.

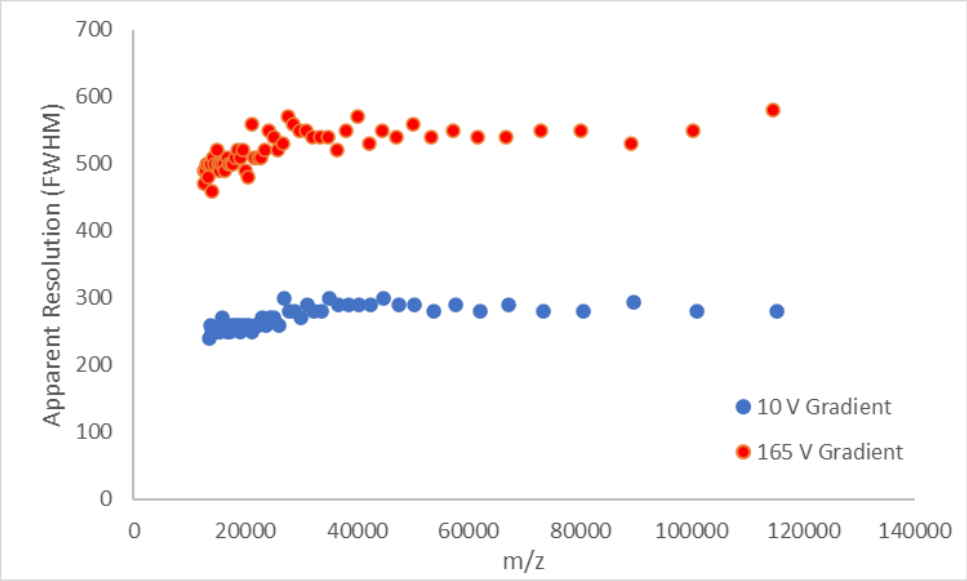

Figure 2.8. The apparent resolution vs the m/z of the GroEL/PFO proton transfer reaction for two ion optic gradients. The ion/ion reaction can be seen in the previous figure.

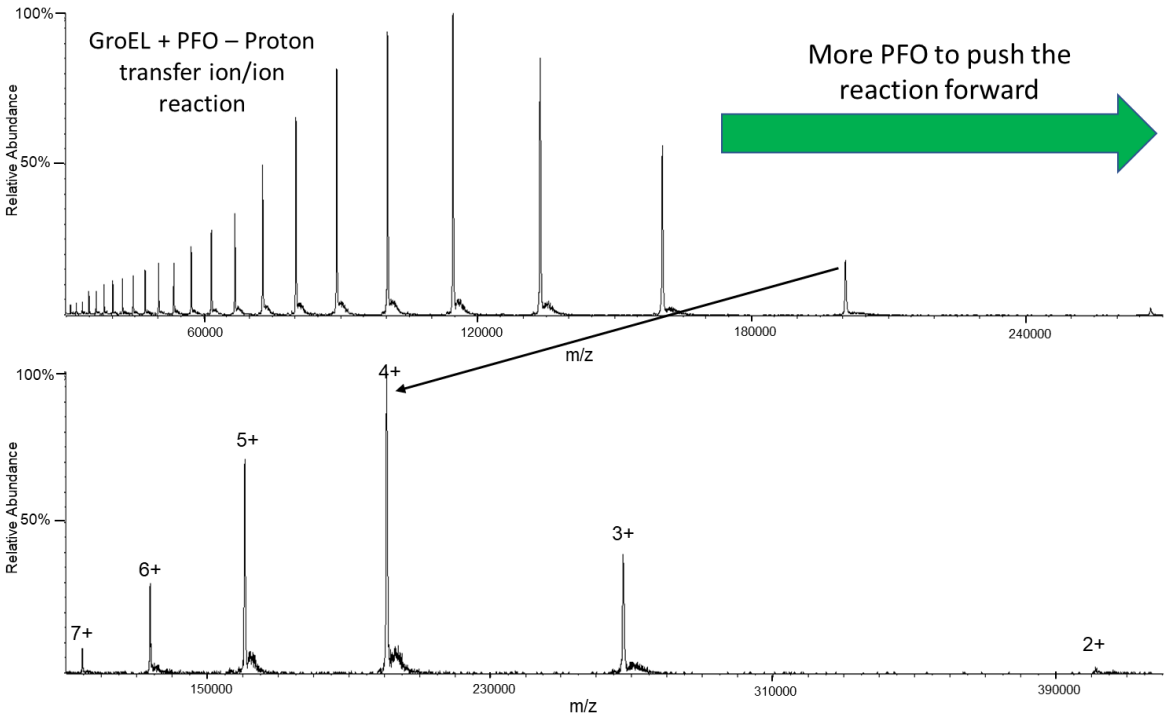

Figure 2.9. The proton transfer reaction of GroEL and PFO. The introduction of more PFO pushed the reaction forward so the most abundant charge state was the 4^+ regardless of any higher PFO fill times.

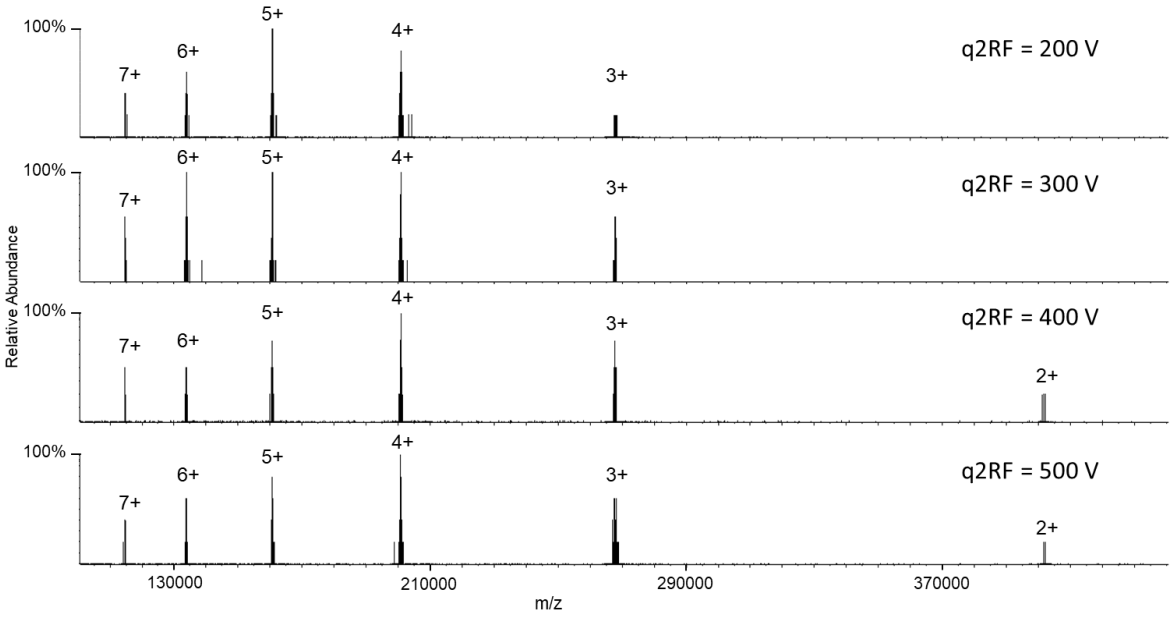

Figure 2.10. The effect of q2RF voltages on high m/z ions of GroEL with N_2 as the bath gas in the reaction chamber.

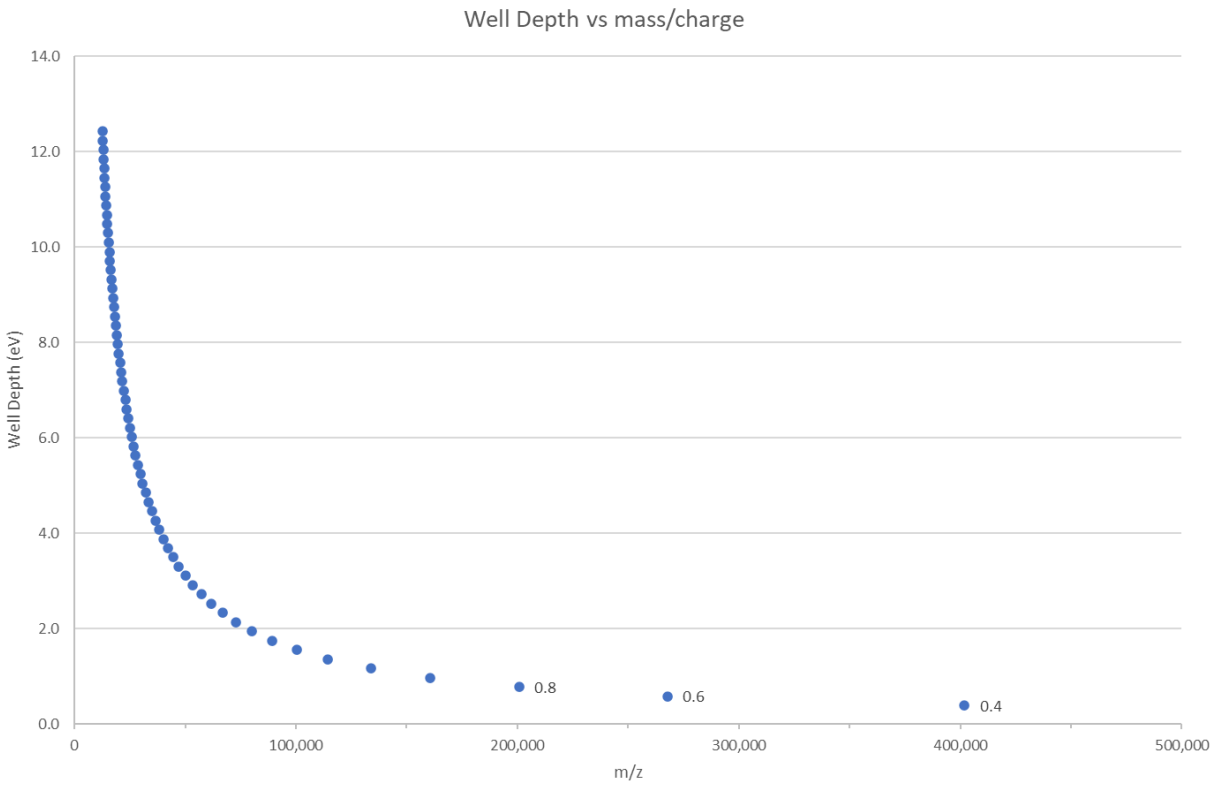

Figure 2.11. The well-depth vs the *m/z* of ions measured in the GroEL and PFO ion/ion proton transfer reactions.

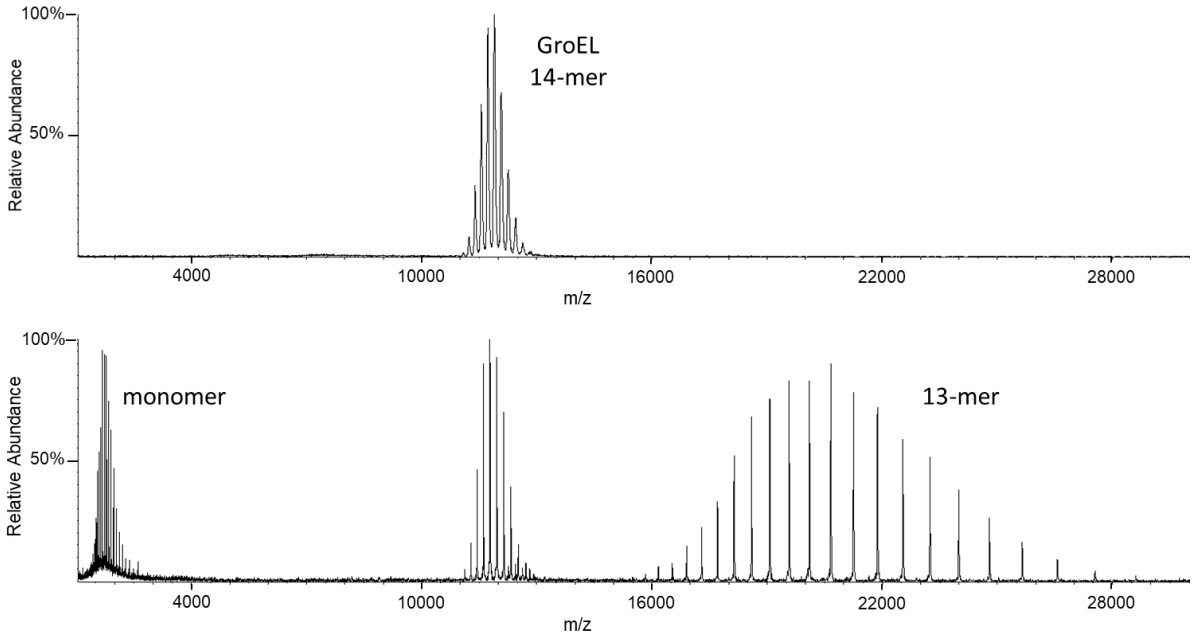

Figure 2.12. The GroEL precursor population (top) and the BT-CID activation of the precursor (bottom).

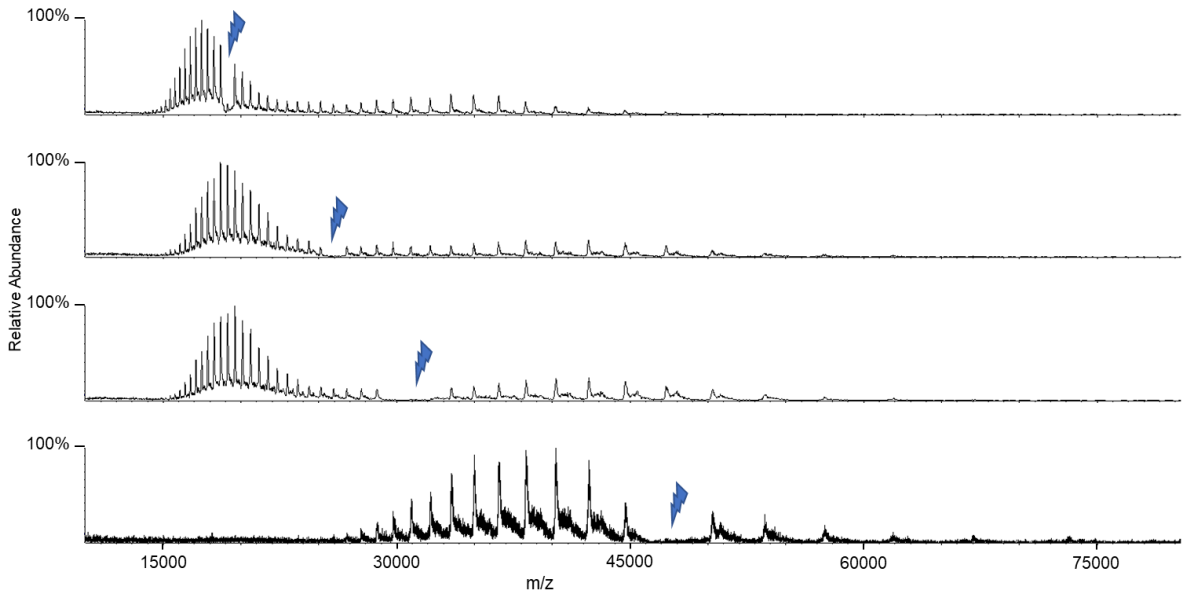

Figure 2.13. The ion/ion proton transfer reaction of GroEL and PFO. The thunderbolt is the location at which the ion is excited by using the secular frequency.

CHAPTER 3. MASS ANALYSIS OF MACRO-MOLECULAR ANALYTES VIA MULTIPLY-CHARGED ION ATTACHMENT

Adapted with permission from Abdillahi, A.M.; Lee, K. W.; McLuckey, S. A. Anal. Chem. 92(24), 16301–16306 (2020).

A novel gas-phase charge and mass manipulation approach is demonstrated to facilitate the mass measurement of high mass complexes within the context of native mass spectrometry. Electrospray ionization applied to solutions generated under native or near-native conditions has been demonstrated to be capable of preserving biologically relevant complexes into the gas phase as multiply-charged ions suitable for mass spectrometric analysis. However, charge state distributions tend to be narrow and extensive salt adduction, heterogeneity, etc. tend to lead to significantly broadened peaks. These issues can compromise mass measurement of high mass bio-complexes, particularly when charge states are not clearly resolved. In this work, we show that the attachment of high mass ions of known mass and charge to populations of ions of interest can lead to well-separated signals that can yield confident charge state and mass assignments from otherwise poorly resolved signals. The approach is demonstrated with the attachment of multiply-charged holo-myoglobin anions to cations generated from 30S, 50S, and 70S components of the *E. coli* ribosome.

3.1 Introduction

The observation of gaseous ions comprised of specific non-covalently bound components known to exist together in solution (1,2,3,4) was a remarkable development in electrospray ionization (ESI) mass spectrometry (MS). It indicates the possibility of generating gaseous ions from specific non-covalently bound protein-ligand, protein-protein, and protein-nucleic acid complexes for subsequent characterization by mass spectrometry and ancillary techniques. Since then, a branch of biological mass spectrometry, often referred to as 'Native MS', has emerged for the study of large non-covalent complexes (2,3,5,6,7,8). Native MS encompasses mass spectrometry, tandem mass spectrometry (9,10), and ion mobility measurements (11) applied to ions derived from complexes subjected to ESI under conditions designed to preserve the complexes of interest as gas-phase ions. Challenges associated with native MS include the fact that, despite the multiple charging associated with ESI, ions are of relatively high mass-to-charge

(*m/z*) ratios and are generated with relatively narrow charge state distributions, presumably due to their formation via the so-called 'charged residue mechanism (12,13,14). Therefore, technologies amenable to high *m/z* measurements, such as mass filters operated at low frequency for ion isolation and TOF or electrostatic traps for *m/z* measurement, are often employed (15,16). Ultimately, the complexity of the sample, which can arise from mixtures of counter-ions, salts and other adducts, and the native heterogeneity of the complex (e.g., post-translational modifications (PTMs), varying identities of components in the complex, etc.) can render the native MS uninterpretable due to an inability to resolve and/or identify charge states. One way to address this problem is to measure *m/z* and *z* simultaneously on an ion-by-ion basis, which is the approach taken by charge detection MS (17,18). We present an alternative approach to dealing with the heterogeneity problem that does not rely on single ion analysis/detection and that retains the potential for tandem mass spectrometry and ion mobility using platforms currently in use for native MS with relatively minor modification.

The underlying concept relies on simplifying the mixture of ions generated by ESI via mass-selection of a fraction of the broad distribution of *m/z* ratios present in the original ESI mass spectrum and subjecting this mixture to an ion attachment reaction that gives rise to a known Δm and Δz. This idea has been described for proton transfer ion/molecule (19) and ion/ion (20) reactions in which $\Delta m = 1$ Da and $\Delta z = 1$ unit charge. The idea has also been demonstrated with electron transfer ion/ion reaction reagents (21,22). Such small changes in mass and charge, however, can be difficult to resolve when they occur with highly charged high mass heterogeneous mixtures. We describe here ion attachment ion/ion reactions in which Δm and Δz are both much greater than 1 Da and 1 unit charge, respectively. This form of charge and mass manipulation leads to large *m/z* separations that are much more readily resolved than those associated with single proton or electron transfer.

3.2 Experimental

3.2.1 Sample preparation for native mass spectrometry of bio-complexes

Rabbit pyruvate kinase was purchased from Sigma Aldrich. The lyophilized solid was reconstituted in water to create a stock solution at a concentration of 3 μM (calculated by using the mass of the tetramer). The sample underwent buffer exchange, via centrifugation, once with

an ammonium acetate (Sigma Aldrich) buffer adjusted to pH 7 with ammonium hydroxide (Sigma Aldrich), using a 100 kilodalton (kDa) molecular weight cutoff (MWCO) Amicon Ultra 0.5 mL filter (Millipore Sigma). The recovered sample (15 µL) was diluted with the same buffer to achieve the same original concentration from the stock solution. Ferritin from equine spleen (Sigma Aldrich) lyophilized powder was prepared in a similar manner to pyruvate kinase. GroEL (Sigma Aldrich) lyophilized powder preparation was described before in detail (23). Briefly, the sample was buffer exchanged and underwent acetone precipitation.

E. coli 70S ribosome solution was purchased from New England Biolabs. The original sample, with an initial concentration of 13 µM, was constituted in a buffer containing 10 mM magnesium acetate, which is necessary for the 70S ribosome to be intact in the condensed phase. The sample preparation for the working solutions was described in detail previously (24) and modified accordingly. Briefly, the sample was buffer exchanged 8 times with 150 mM ammonium acetate and 10 mM magnesium acetate (Sigma Aldrich) with the same filter used in the aforementioned section. It is important to note a difference in the preparations. We utilized our reagent anion to perform the charge reduction of the protein in the gas phase, therefore we did not employ the use of the reducing agent, triethylammonium acetate, to the solution.

3.2.2 Sample preparation for the reagent anions

Oxidized insulin chain A (IcA) from bovine pancreas (average mass, free acid = 2531.66 Da) was purchased from Sigma Aldrich. The lyophilized solid was reconstituted in water. The working solution was a 50:50 mixture of aqueous ammonium hydroxide (pH 11) and HPLC grade methanol (Sigma Aldrich) to give a final concentration of 25 µM. The most abundant charge states were $[IcA\text{-}5H]^{5-}$ and $[IcA\text{-}6H]^{6-}$. In experiments where a larger charge reduction was required, we utilized myoglobin from equine skeletal muscle (Sigma Aldrich). Holo-myoglobin (hMb) (average mass=17,567 Da), which retains the heme group, was prepared with piperidine (Sigma Aldrich). We isolated and used the two different charge states in the experiments shown in this manuscript. The final solution was 20 µM holo-myoglobin and 50 mM piperidine in water.

3.2.3 Ion-ion reactions in the mass spectrometer.

All experiments were performed using a QTOF 5600 (SCIEX), which was previously modified to allow for ion/ion reactions (25). The positive and negative ions were generated by utilizing an alternately pulsed nano-electrospray ionization source (nESI) (26). Mutual ion polarity trapping was enabled by applying a supplemental AC to the end plates of the linear ion trap reaction cell, q2. Multiply protonated protein cations and reagent anions were sequentially isolated before being stored in q2 to react over times of 50-100 ms. The reagent anions were isolated during Q1 transmission by conventional RF-DC apex isolation. The protein cations were too high in *m/z* to be isolated via conventional RF-DC apex isolation. Therefore, sequential resonance ejection ramps in q2 were used to eject ions of lower and higher *m/z* ratios that bordered the population of interest (27).

3.2.4 Native MS

Both analyte and reagent ions were generated via nESI from separately pulsed borosilicate glass emitters (28). The large bio-complexes were sprayed in positive mode with approximately +1500 V applied to a platinum wire, which was in contact with the solution. The reagent anions were sprayed in negative mode with an applied voltage of approximately -1400 V. The large complex ions were initially injected into the instrument and isolated (see above) and stored in q2. Subsequently, the reagent anions were injected and isolated during Q1 transmission before being accumulated and stored in q2. The mutual storage time can be controlled to determine the number of sequential adductions. Nitrogen gas was used in q2 at pressures ranging from 6-8 mtorr. Due to the size of the ribosome particles, the difference in DC offsets of Q0 and q2 were increased to as high as 50-70 V to collisionally activate the ions upon injection into q2 to drive off weakly-bound adduct species. A Q0-q2 voltage difference of 5-15 V was used for the reagent anions as minimal salt adduction was observed for these species. Mass calibration over a wide range was done in two stages, using primary and secondary calibrants. Cesium iodide, the primary calibrant, was used to calibrate the instrument over the range of *m/z* 1,000-10,000. This allowed for an accurate mass determination of the pyruvate kinase tetramer, the secondary calibrant, from the mass spectrum derived under native conditions (see insert to **Figure 3.1a**). Finally, the population of pyruvate kinase charge states was reacted with the oxidized insulin chain A, $[IcA\text{-}6H]^{6-}$ anion

([IcA-6H]$^-$; Δm = 2526 Da) resulting in a series of peaks extending beyond m/z 100,000. This experiment allowed for the mass scale to be calibrated over the range of m/z 6,500-100,000.

3.2.5 Simulation of mass spectra

Predicted mass spectra of ion/ion reaction products were calculated and plotted using a R Shiny app developed in our lab (https://mcluckey-apps.shinyapps.io/iirxnspeccalc/). The analyte mass distribution is a normal distribution defined by a user defined mean and standard deviation. The user inputs a range of charge states for the analyte, and the relative intensities of the charge states are calculated from a user defined mean and standard deviation. The reagent ion can similarly be defined with a mass and charge distribution; however, for the experiments in this publication, the reagent ion is limited to one charge state. Additionally, the reagent ion has a number distribution which describes the extent of proton transfer or ion attachment. (Note that proton transfer is the same as ion attachment where the mass of the "attaching" reagent is −1 Da and the charge is −1.) The number distribution is also a normal distribution with a user defined mean and standard deviation. All possible masses and charges determined from the different number of reagent ions added to the analyte ion are calculated, and their ratios give the *m/z* values of the reaction products. The relative intensities of reaction products are given by multiplying the corresponding relative intensities from the charge distributions and the reagent ion number distribution. The widths of the product peaks are calculated by multiplying the variances (standard deviation squared) of the analyte and reagent ions that correspond to a particular reaction product and dividing it by the corresponding charge of that reaction product. The resulting product peaks are plotted individually and their intensities are summed to give the total predicted spectrum.

3.3 Results and Discussion

The concept is modeled in **Figure 3.1** for a cationic mixture of ions generated from a particle of average mass 2 MDa, width of 50 kDa (FWHM), charge state range of 70+ to 80+, and analyzer resolution of 10,000 FWHM (see Supplemental Information for a description of the model). Under these conditions, the ESI mass spectrum shows a large unresolved envelope (**Figure 3.1a**), which precludes a mass measurement due to a lack of information regarding charge. **Figure 3.1b** shows the simulated spectrum after an isolation step centered at the maximum of the

distribution with a FWHM width of 900 *m/z* units. **Figure 3.1c** shows the simulated spectrum following up to fifty single proton transfer steps, as might result from ion/ion reactions of the multiply-charged ions with singly charged anions of opposite polarity (20). **Figure 3.1d** shows the result after the attachment of up to 5 ions of mass 17,557 Da and unit charge of 10-. This Δm and Δz apply to the 10- charge of hMb, which is one of the reagents used for the data reported here (see below). After the isolation of ions in a selected region of the mass spectrum (**Figure 3.1b**), multiple single proton transfer reactions tend to spread the signal among many products (**Figure 3.1c**) without baseline resolution of adjacent peaks until close to 50 proton transfers. However, after the attachment of up to five high mass reagent anions of z = 10-, baseline-resolved peaks are apparent that can be used to determine the charge states of the ions that make up the centroids of the peaks without spreading the signal across much of the *m/z* range. After the fourth attachment, even the individual charge states within the initially selected ion population are beginning to separate sufficiently to be resolved.

The determination of charge states associated with the peak centroids in **Figure 3.1d**, which involves the attachment of reagent ions of known mass and charge to the high mass complex ions, requires a generalization of the relationships originally provided by Mann et al. (29) for the determination of charges from the *m/z* values of adjacent charge states in an electrospray mass spectrum. For positively charged complexes, the *m/z* value for a given charge state is given by:

$$m/z_1 = \frac{M+nx}{n} \quad (1)$$

where M is the mass of the neutral molecule, n is the charge state, and X is the average mass of the cationizing agent (e.g., an excess proton). The m/z value of the product generated by the attachment of a single reagent of mass = Δm and charge = Δz is given by:

$$m/z_2 = \frac{M+nx+\Delta m}{n-\Delta z} \quad (2)$$

The magnitude of the charge on the initial analyte ion, n, is given by:

$$n = \frac{\Delta z(m/z_1)-\Delta m}{(m/z_2-m/z_1)} \quad (3)$$

The same relationship applies for any two adjacent attachment products such that M, the mass of the original complex represented by peak apex, can be determined from any of the attachment products via:

$$M = \left(m/z_{(N+1)}\right)(n - N\Delta z) - nX - N\Delta m \qquad (4)$$

where N is the number of attached reagent anions.

It has been previously noted for relatively small proteins that reactions of oppositely charged proteins can result in the formation of a long-lived complex along with proton transfer products (30,31). When the hard-sphere cross-sections are large (i.e., when the reactants are physically large) and when the *m/z* ratios are large (i.e. the charge densities within the reactant ions are relatively low), the formation of long-lived complexes (i.e., the attachment of an ion to a cation), becomes the exclusive product (32). In the cases of the very large complexes encountered in native MS, ion attachment is essentially the exclusive ion/ion reaction process, provided the charge density of the reagent ion is not too high. This is illustrated in **Figure 3.2** with ions derived from the tetrameric pyruvate kinase complex (approximately 232 kDa) in reactions with two different anionic reagents. The insert in **Figure 3.2a** shows the charge state distribution generated via positive ion nESI of pyruvate kinase under native MS conditions. The shaded charge state was selected for subsequent ion/ion reactions with a) the $[IcA\text{-}6H]^{6-}$ anion (average Δm = 2525.7 Da) and b) the $[hMb\text{-}13H]^{13-}$ anion (Δm = 17,554 Da). The attachment of up to three reagent anions is observed in the case of $[IcA\text{-}6H]^{6-}$ (**Figure 3.2a**) and up to two reagent anions in the case of $[hMb\text{-}13H]^{13-}$ (**Figure 3.2b**). (Note that the addition of three anions in the case of $[hMb\text{-}13H]^{13-}$ would result in the generation of a negatively-charged complex.) The tabular insert in **Figure 3.2b** summarizes the measured *m/z* values and calculated charges and masses arising from the two experiments using the relationships listed above. The experiment of **Figure 3.2a** yielded an average mass of 231,969±2 Da and the experiment of **Figure 3.2b** yielded an average mass of 232,134±12 Da. Key observations from this proof-of-principle example are that multiply-charged reagent anions can give rise to exclusive ion attachment (i.e., no proton transfer is observed for either reagent) and that there is a high degree of flexibility in choosing reagents over wide ranges of Δm and Δz, which provides for the 'tunability' of the *m/z* spacings between successive ion attachments. It is also noteworthy that no loss of the non-covalently-bound heme group in hMb is observed in these experiments, which indicates that ion attachment to large complexes results in

little or no dissociation of the complex. Results of analogous experiments using the $[M-6H]^{6-}$ IcA anion in reactions with cations derived from ferritin (480 kDa) and GroEL (804 kDa) are provided in **Figures 3.3** and **3.4**, respectively. In all cases, exclusive ion attachment is observed, thereby reinforcing the generality of the observations noted in **Figure 3.2**.

The *E. coli* ribosome constitutes an example of a complex that is inherently heterogeneous (33). The protein complement can vary in stoichiometry, identities of proteins, and PTMs of proteins. There is also heterogeneity in ribosomal RNA that includes both alternative RNA and modifications of RNA. These sources of heterogeneity add to the usual mixture of counter ions, salts, etc. associated with any large bio-complex ion generated under native conditions via ESI (34). The *E. coli* ribosome is comprised of two components, the smaller 30S and larger 50S subunits, that associate to form the intact 70S ribosome. The presence of magnesium ions is important for the association of the two subunits and the appearance of the mass spectrum can be highly influenced by magnesium ion concentration (3). **Figure 3.5** shows mass spectra collected at concentrations of 0.5 mM Mg^{2+} (**Figure 3.5a**) and 10 mM Mg^{2+} (**Figure 3.5b**). Consistent with previous reports (3,24), at high Mg^{2+} concentrations (10 mM, in this case) ions associated with the 30S and 50S subunits are present in addition to ions associated with the 70S complex, the latter of which centered at roughly *m/z* 29,000 (**Figure 3.5b**). At 0.5 mM Mg^{2+} (**Figure 3.5a**), the 70S signals are largely absent and the ions from the 30S and 50S subunits show somewhat narrower peaks than do the subunits with higher magnesium concentrations, presumably due to extra adduction from counter ions, and non-specific adduction of magnesium (24). In all cases, overlapping charge state distributions are evident, indicating that a mixture of species is present for each of the 30S, 50S, and 70S-related complexes. We note that there is sufficient separation between peaks in the spectra of **Figure 3.5** to estimate the charges of the components via deconvolution. However, the limited numbers of charge states and peak overlap leads to significant uncertainty in charge state assignments (20,35).

Figure 3.6 summarizes the results from $[hMb-10H]^{10-}$ ion attachment experiments for the 30S (**Figure 3.6**) and 50S (**Figure 3.6**) species observed from nESI of the 10 mM Mg^{2+} solution. The mass spectrum is shown as an insert in **Figure 3.6** (see also **Figure 3.5b**) and the ions selected for subsequent ion attachment are indicated within a blue box (30S) or red box (50S). The ion attachment experiment for the 30S component (**Figure 3.6a**) revealed two major components (863.2 kDa (purple dots) and 802.0 kDa (green dots), respectively) that differ in mass by that of

the S1 stalk protein. The stalk protein, RS1 (61.2 kDa), is a labile component that has been observed to dissociate when the 30S ribosome is activated (3,23). The masses indicated above are roughly 1.8% greater than those expected for the intact 30S component (847.5 kDa) and 30S-S1 (786.3 kDa). The difference might be attributed to either non-specific magnesium adduction (24) and/or incomplete desolvation commonly seen on TOF platforms, which typically requires higher amounts of collisional cooling (16,36) or the presence of an additional roughly 15 kDa component, or the combination of both. We note that at a concentration of 0.5 mM Mg^{2+}, the average masses for the two components noted above were 861.8 kDa and 799.8 kDa, respectively, and a third major component (772.7 kDa) was observed following the ion attachment experiment which was consistent with the largest component minus both the S1 and S2 (26.7 kDa) (24) stalk proteins (see **Figure 3.7** for a summary of the ion attachment experiment associated with the 30S related ions at 0.5 mM Mg^{2+}).

For the 50S subunit (**Figure 3.6b**), we detected three major components of masses 1,479.7±0.2 kDa (blue line), 1,413±2 kDa (green line), and 1,399.4±0.6 kDa (red line). The mass difference between the two larger components is consistent with that of the stalk complex [L10(L7/L12)$_4$] (66.5 kDa) (37) and the mass difference between the two smaller components is consistent with that of the L11 ribosomal protein (14.9 kDa) (24). The stalk complex for the 50S subunit is believed to contain multiple dimers (L7/L12)$_4$ (38,39). The dimers are bound to the L10 ribosomal protein, which is also bound to the L11 protein. Consequently, the loss of these components is plausible. The 1,479.7 kDa component is roughly 1.7% higher in mass than the nominal mass of the 50S component (24), which could be due to the presence of additional protein component(s), salts, etc. These components were not well separated after the first two attachments but were resolved in the 3rd and 4th attachments. An expanded region highlighting the 4th [hMb-10H]$^{10-}$ attachment is provided as an insert in **Figure 3.6b**. Ion attachment data for the 50S-related ions generated at a concentration of 0.5 mM Mg^{2+} is provided in **Figure 3.8**. No evidence for the two larger intact components noted in **Figure 3.6b** was noted at lower Mg^{2+} concentration. Rather, a fourth component (1,389.5 kDa) was found to be most abundant along with the 1399.7 kDa component (see **Figure 3.8**). A prominent signal for a 50S component at relatively low Mg^{2+} concentration of 1,389.6 kDa has been noted previously and was ascribed to (50S-L10(RL7/12)$_4$) (24). The fact that we see this component as well as larger components might suggest that one or more additional components may be associated with the 50S particle at high Mg^{2+} concentrations.

Both examples illustrated in **Figure 3.6** involve the presence of mixtures of complexes. A complication in native MS is the fact that multiple combinations of mass and charge can give rise to similar *m/z* ratios over the narrow charge state ranges typically generated under native MS conditions. This can complicate charge state assignment as well as the identification that mixtures are present. However, ions of significantly different mass will not overlap over wide ranges of charge. The ion attachment approach described here allows for a very wide range of charge to be accessed, thereby resulting the separation of components somewhere along the *m/z* scale. Regions of significant overlap of the mixture components identified for both the 30S and 50S examples were observed prior to and after one or more ion attachments. However, in both cases, one or more attachments (e.g., attachments 3 and 4) showed separation of the components. A similar situation prevails for the 70S-related ions.

The extent of heterogeneity for both the 30S and 50S subunits can propagate to the 70S-related ions, so there is little surprise that overlapping mixture components appear to be present in the 70S region of the mass spectrum shown in the insert of **Figure 3.6a**. A similar result was found in both the *E. coli* (24) and *Thermus thermophilus* (40) ribosomes. In our 70S ribosome ion attachment mass spectrum (**Figure 3.9**), greater separation was noted for every successive attachment reaction. Nevertheless, a significant extent of overlap is observed even after four attachment reactions. We found at least three distinct populations. There are almost certainly more than three but the three we report here are the most abundant. We did not observe a clearly resolvable component with a molecular weight larger than the expected mass of the intact ribosome (2,302 kDa). The masses of the three assigned components were 2,271±2 kDa, 2,223±1kDa, and 2,209±1 kDa. The difference in mass between the largest and smallest components is consistent with the 30S S1 protein and the difference in mass between the two smaller components is consistent with the 50S L11 protein mentioned above. If the largest component corresponds to the loss of the large subunit stalk complex (70S-[L10(L7/L12)$_4$]), the mass measurement is roughly 1.5% high relative to the predicted value (2,236 kDa), which is consistent with the errors noted above for the 30S and 50S subunits ionized with 10 mM Mg^{2+}. We note that, given the widths of the peaks observed here, that a 70S-S1 (predicted value of 2,241 kDa) product could also be present.

3.4 Conclusions

Electrospray ionization applied to solutions that mimic physiological conditions has enabled the development of native MS. Such conditions, however, lead to relatively narrow charge state distributions and, broadened signals due to extensive salt adduction. These consequences can complicate mass measurement due to uncertainties in charge state assignment and/or extensive signal overlap that precludes the resolution of individual charge states. The situation is exacerbated for inherently heterogeneous complexes that generate mixtures with overlapping charge state distributions. A strategy introduced here to address these problems and demonstrated with ions generated from the *E. coli* ribosome, relies on the isolation of a sub-population of ions of interest and the attachment of a large highly-charged ion of opposite polarity of known mass and charge. The large defined change in mass and charge in a single step allows for the separation of ions of initially similar mass-to-charge ratios but different masses and charges. The charges of the selected ions can be determined via measurement of the m/z values of the successive ion attachment peaks. Charge state assignment accuracy is enhanced by the generation of related ions via successive reagent ion attachments over wide ranges of mass-to-charge. The net result is improved ability to determine the masses of high-mass heterogeneous complexes in native mass spectrometry.

3.5 References

1. Katta, V.; Chait, B. T., Observation of the heme-globin complex in native myoglobin by electrospray-ionization mass spectrometry. J. Am. Chem. Soc. 113, 8534-8535 (1991).

2. Rostom, A. A.; Robinson, C. V., Detection of the Intact GroEL Chaperonin Assembly by Mass Spectrometry. J. Am. Chem. Soc. 121, 4718-4719 (1999).

3. Rostom, A. A.; Fucini, P.; Benjamin, D. R.; Juenemann, R.; Nierhaus, K. H.; Hartl, F. U.; Dobson, C. M.; Robinson, C. V., Detection and selective dissociation of intact ribosomes in a mass spectrometer. Proc. Nat. Acad. Sci. USA 97, 5185-5190 (2000).

4. Forsberg, E.; Fang, M.; Siuzdak, G., Staying Alive: Measuring Intact Viable Microbes with Electrospray Ionization Mass Spectrometry. J. Am. Soc. Mass Spectrom. 28, 14-20 (2017).

5. Leney, A. C.; Heck, A. J. R., Native Mass Spectrometry: What is in the Name? J. Am. Soc. Mass Spectrom. 28, 5-13 (2017).

6. Heck, A. J. R., Native mass spectrometry: a bridge between interactomics and structural biology. Nat. Methods 5, 927 (2008).

7. Hernández, H.; Robinson, C.V., Determining the stoichiometry and interactions of macromolecular assemblies from mass spectrometry. Nat. Protoc. 2, 715 (2007).

8. Schachner, L. F.; Ives, A. N.; McGee, J. P.; Melani, R. D.; Kafader, J. O.; Compton, P. D.; Patrie, S. M.; Kelleher, N. L., Standard Proteoforms and Their Complexes for Native Mass Spectrometry. J. Am. Soc. Mass Spectrom. 30, 1190-1198 (2019).

9. Belov, M. E.; Damoc, E.; Denisov, E.; Compton, P. D.; Horning, S.; Makarov, A. A.; Kelleher, N. L., From Protein Complexes to Subunit Backbone Fragments: A Multi-stage Approach to Native Mass Spectrometry. Anal. Chem. 85, 11163-11173 (2013).

10. Li, H.; Nguyen, H. H.; Ogorzalek Loo, R. R.; Campuzano, I. D. G.; Loo, J. A., An integrated native mass spectrometry and top-down proteomics method that connects sequence to structure and function of macromolecular complexes. Nat. Chem. 10, 139 (2018).

11. Konijnenberg, A.; Butterer, A.; Sobott, F., Native ion mobility-mass spectrometry and related methods in structural biology. (2013) BBA - Proteins Proteom. 1834, 1239-1256 (2013).

12. Konermann, L.; Ahadi, E.; Rodriguez, A. D.; Vahidi, S., Unraveling the Mechanism of Electrospray Ionization. Anal. Chem. 85, 2-9 (2013).

13. Kebarle, P.; Verkerk, U. H., Electrospray: From ions in solution to ions in the gas phase, what we know now. Mass Spectrom. Rev. 28, 898-917 (2009).

14. Fernandez de la Mora, J. Electrospray ionization of large multiply charged species proceeds via Dole's charged residue mechanism. Anal. Chim. Acta 406, 93-104 (2000).

15. Fort, K. L.; van de Waterbeemd, M.; Boll, D.; Reinhardt-Szyba, M.; Belov, M. E.; Sasaki, E.; Zschoche, R.; Hilvert, D.; Makarov, A. A.; Heck, A. J. R., Expanding the structural analysis capabilities on an Orbitrap-based mass spectrometer for large macromolecular complexes. Analyst 143, 100-105 (2018).

16. Snijder, J.; Rose, R. J.; Veesler, D.; Johnson, J. E.; Heck, A. J. R., Studying 18 MDa Virus Assemblies with Native Mass Spectrometry. Angew. Chem. Int. Edit. 52, 4020-4023 (2013).

17. Keifer, D. Z.; Shinholt, D. L.; Jarrold, M. F., Charge Detection Mass Spectrometry with Almost Perfect Charge Accuracy. Anal. Chem. 87, 10330-10337 (2015).

18. Schultz, J. C.; Hack, C. A.; Benner, W. H., Mass Determination of Megadalton-DNA Electrospray Ions Using Charge Detection Mass Spectrometry. J. Am. Soc. Mass Spectrom. 9, 305-313 (1998).

19. McLuckey, S. A.; Goeringer, D. E., Ion/Molecule Reactions for Improved Effective Mass Resolution in Electrospray Mass Spectrometry. Anal. Chem. 67, 2493-2497 (1995).

20. Laszlo, K. J.; Bush, M. F., Analysis of Native-Like Proteins and Protein Complexes Using Cation to Anion Proton Transfer Reactions (CAPTR). J. Am. Soc. Mass Spectrom. 26, 2152-2161 (2015).

21. Abzalimov, R. R.; Kaltashov, I. A., Electrospray Ionization Mass Spectrometry of Highly Heterogeneous Protein Systems: Protein Ion Charge State Assignment via Incomplete Charge Reduction. Anal. Chem. 82, 7523-7526 (2010).

22. Zhao, Y.; Abzalimov, R.R.; Kaltashov, I.A. Interactions of Intact Unfractionated Heparin with Its Client Proteins Can Be Probed Directly Using Native Electrospray Ionization Mass Spectrometry. Anal. Chem. 88, 1711-1718 (2016).

23. Zhou, M.; Jones, C.M.; Wysocki, V.H., Dissecting the Large Noncovalent Protein Complex GroEL with Surface-Induced Dissociation and Ion Mobility-Mass Spectrometry. Anal. Chem. 85, 8262-8267 (2013).

24. van de Waterbeemd, M.; Fort, K. L.; Boll, D.; Reinhardt-Szyba, M.; Routh, A.; Makarov, A.; Heck, A. J. R., High-fidelity mass analysis unveils heterogeneity in intact ribosomal particles. Nat. Methods, 14 283-286 (2017).

25. Xia, Y.; Wu, J.; McLuckey, S. A.; Londry, F. A.; Hager, J. W., Mutual storage mode ion/ion reactions in a hybrid linear ion trap. J. Am. Soc. Mass Spectrom. 16, 71-81 (2005).

26. Liang, X.; Xia, Y.; McLuckey, S. A., Alternately Pulsed Nanoelectrospray Ionization/Atmospheric Pressure Chemical Ionization for Ion/Ion Reactions in an Electrodynamic Ion Trap. Anal. Chem. 78, 3208-3212 (2006).

27. McLuckey, S.A.; Goeringer, D.E.; Glish, G.L. Selective Ion Isolation/Rejection Over a Broad Mass Range in the Quadrupole Ion Trap. J. Am. Soc. Mass Spectrom. 2, 11-21 (1991).

28. Xia, Y.; Liang, X.; McLuckey, S.A. Pulsed dual electrospray ionization for ion/ion reactions. J. Am. Soc. Mass Spectrom. 16, 1750-1756 (2005).

29. Mann, M.; Meng, C.K.; Fenn, J.B. Interpreting Mass Spectra of Multiply Charge Ions. Anal. Chem. 61, 1702-1708 (1989).

30. McLuckey, S. A.; Huang, T.-Y., Ion/ion reactions: new chemistry for analytical MS. Anal. Chem. 81, 8669-8676 (2009).

31. Prentice, B. M.; McLuckey, S. A., Gas-phase ion/ion reactions of peptides and proteins: acid/base, redox, and covalent chemistries. Chem. Commun. 49, 947-965 (2013).

32. Wells, J. M.; Chrisman, P. A.; McLuckey, S. A., Formation and Characterization of Protein−Protein Complexes in Vacuo. J. Am. Chem. Soc. 125, 7238-7249 (2003).

33. McKay, A. R.; Ruotolo, B. T.; Ilag, L. L.; Robinson, C. V., Mass Measurements of Increased Accuracy Resolve Heterogeneous Populations of Intact Ribosomes. J. Am. Chem. Soc. 128, 11433-11442 (2006).

34. Freeke, J.; Robinson, C. V.; Ruotolo, B. T., Residual counter ions can stabilise a large protein complex in the gas phase. Int. J. Mass Spectrom. 298, 91-98 (2010).

35. Liepold, L.; Oltrogge, L. M.; Suci, P. A.; Young, M. J.; Douglas, T., Correct Charge State Assignment of Native Electrospray Spectra of Protein Complexes. J. Am. Soc. Mass Spectrom. 20, 435-442 (2009).

36. Chernushevich, I. V.; Thomson, B. A., Collisional Cooling of Large Ions in Electrospray Mass Spectrometry. Anal. Chem. 76, 1754-1760 (2004).

37. Gordiyenko, Y.; Deroo, S.; Zhou, M.; Videler, H.; Robinson, C.V. Acetylation of L12 Increases Interactions in the Escherichia Coli Ribosomal Stalk Complex. J. Mol. Biol. 380, 404-414 (2008).

38. Markus, C. W.; Wim, M., Structure and Function of the Acidic Ribosomal Stalk Proteins. Curr. Protein Pept. Sci. 3, 93-106 (2002).

39. Diaconu, M.; Kothe, U.; Schlunzen, F.; Fischer, N.; Harms, J.M.; Tonevitsky, A.G.; Stark, H.; Rodnina, M.V.; Wahl, M.C., Structural basis for the function of the ribosomal L7/12 stalk in factor binding and GTPase activation. Cell 121, 991–1004 (2005).

40. Ilag, L.L.; Videler, H.; McKay, A.R.; Sobott, F.; Ficini, P.; Nierhaus, K.H.; Robinson, C.V. Heptameric (L12)6/L10 rather than canonical pentameric complexes are found by tandem MS of intact ribosomes from thermophilic bacteria. Proc. Natl. Acad. Sci. USA 102, 8192-8197 (2005).

3.6 Figures

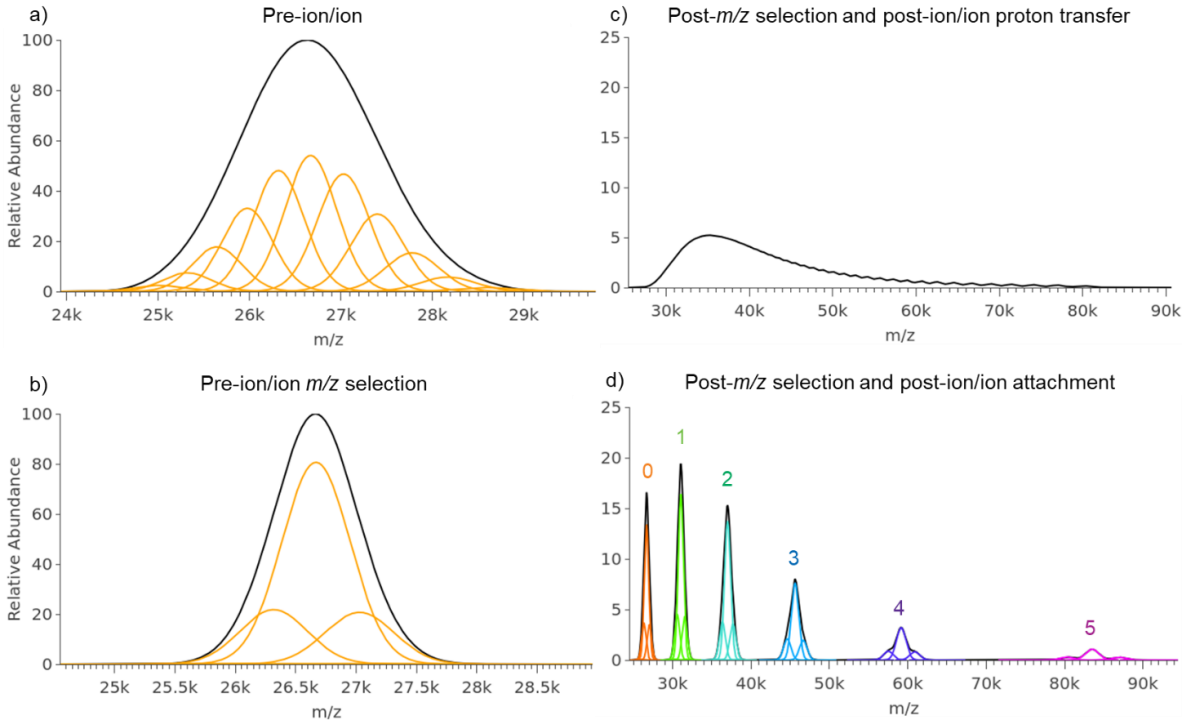

Figure 3.1. Simulated mass spectra of (a) a hypothetical 2 MDa (50 kDa FWHM) analyte particle with 70 to 80 charges, (b) selection (900 FHWM) of most abundant charge states, (c) up to 50 proton transfer reactions of the selected analyte charge states, and (d) up to 5 attachments (indicated by colored numbers) of the 10− charge states holomyoglobin (Δm = 17,557 Da) to the selected analyte charge states. Abundance scales in (c) and (d) are relative to (b).

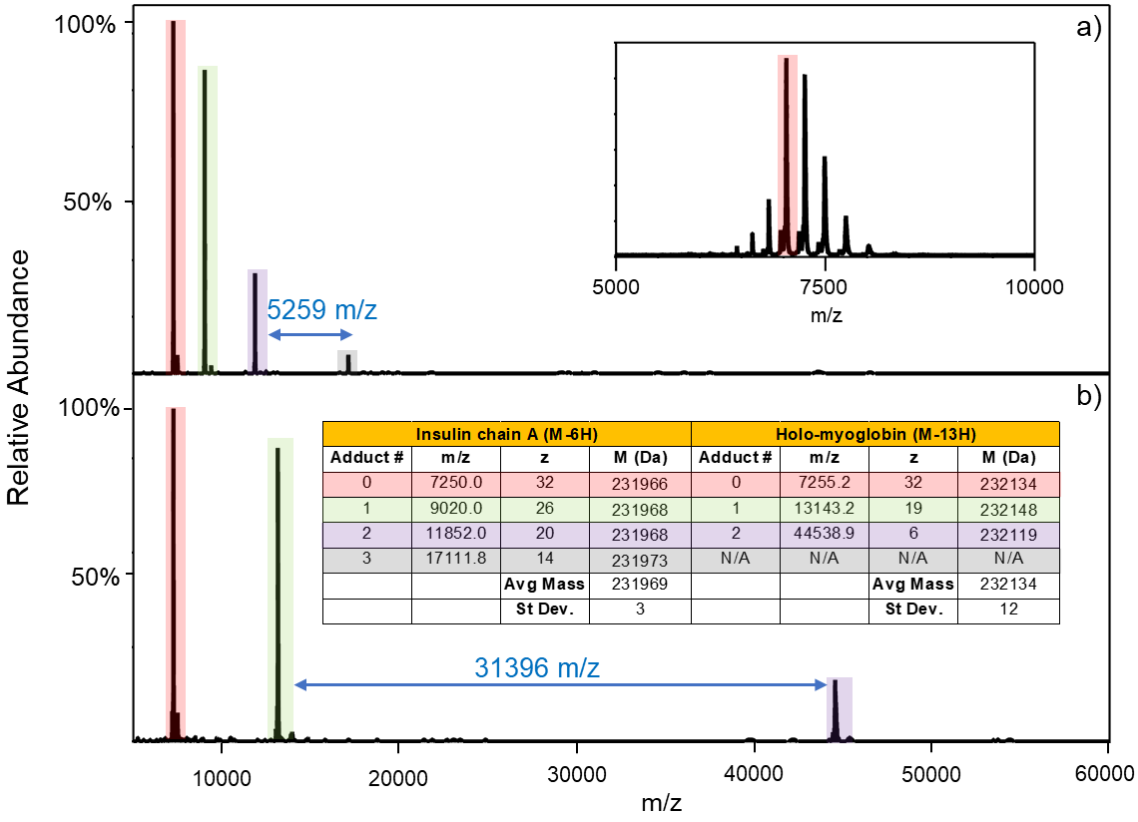

Insulin chain A (M-6H)				Holo-myoglobin (M-13H)			
Adduct #	m/z	z	M (Da)	Adduct #	m/z	z	M (Da)
0	7250.0	32	231966	0	7255.2	32	232134
1	9020.0	26	231968	1	13143.2	19	232148
2	11852.0	20	231968	2	44538.9	6	232119
3	17111.8	14	231973	N/A	N/A	N/A	N/A
		Avg Mass	231969			Avg Mass	232134
		St Dev.	3			St Dev.	12

Figure 1.2. Inset (upper right) Positive nESI mass spectrum of pyruvate kinase a) Post-ion/ion mass spectrum after reaction of the 32+ ions of pyruvate kinase with $[IcA-6H]^{6-}$ anions derived from nESI of IcA. b) Post-ion/ion mass spectrum after reaction of the 32+ ions of pyruvate kinase with the $[hMb-13H]^{13-}$ anions derived from nESI of holo-myoglobin.

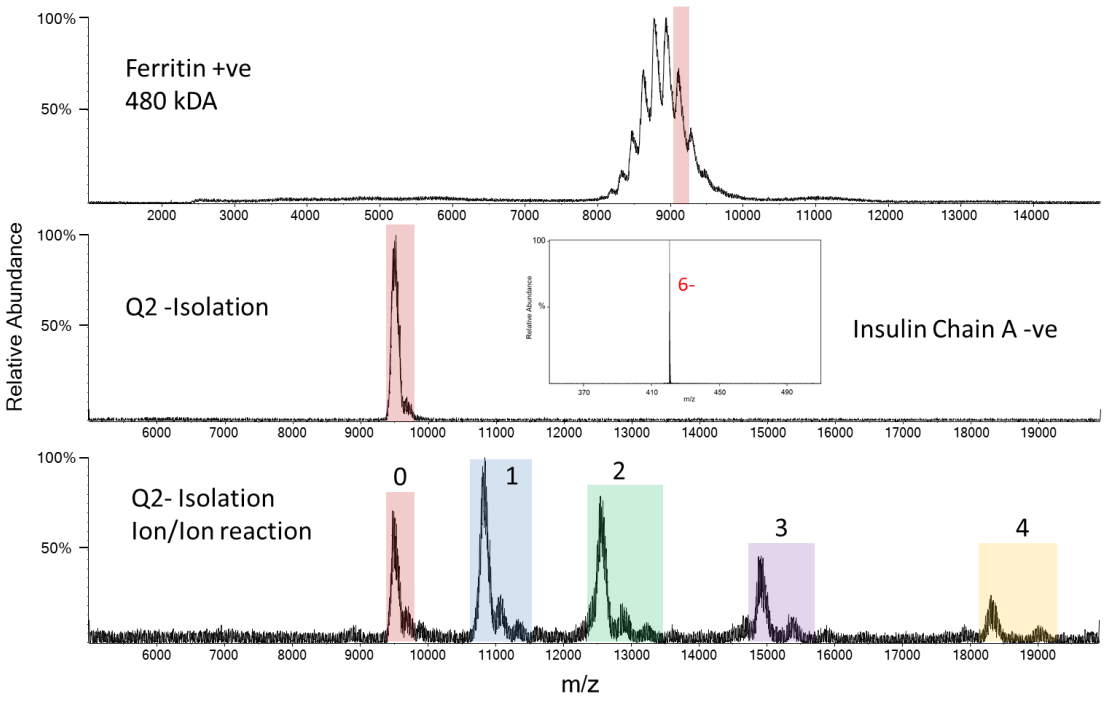

Figure 1.3. The spectra for Ferritin precursor (top), isolation (middle) and the ion/ion reaction with Insulin chain-A (bottom).

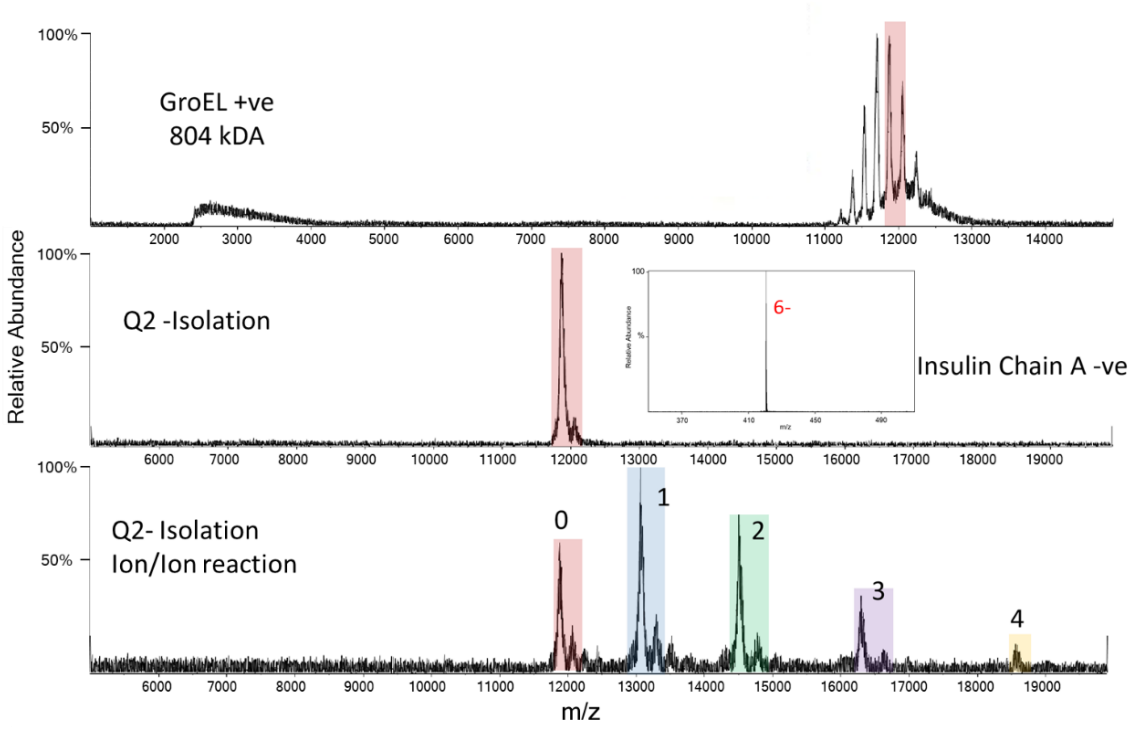

Figure 1.4. The spectra for GroEL precursor (top), isolation (middle) and the ion/ion reaction with Insulin chain-A (bottom).

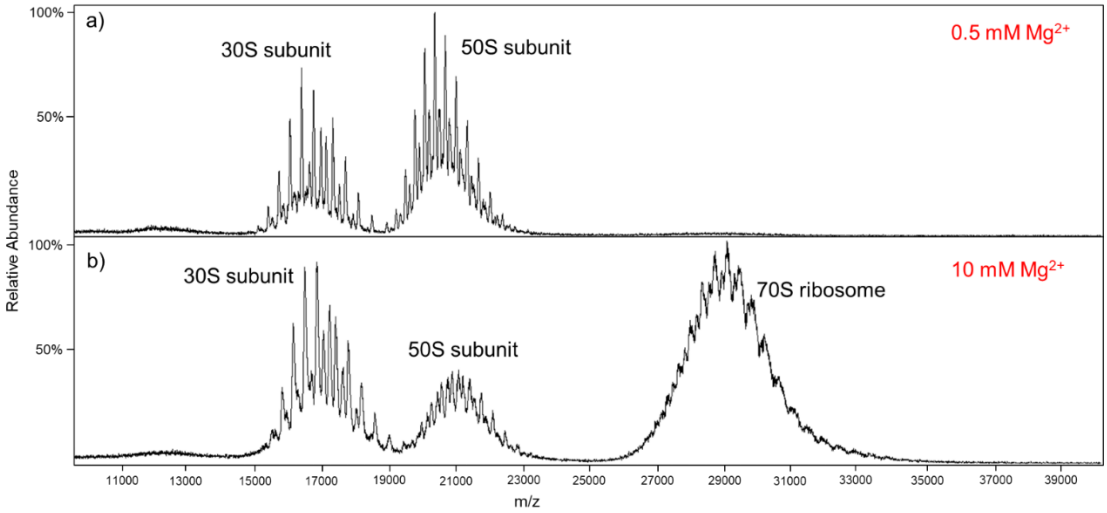

Figure 1.5. The mass spectra of the *E. coli* ribosome with (a) 0.5 mM and (b) 10 mM Mg^{2+} concentrations. The higher concentration preserves the 70S population centered around m/z 29,000.

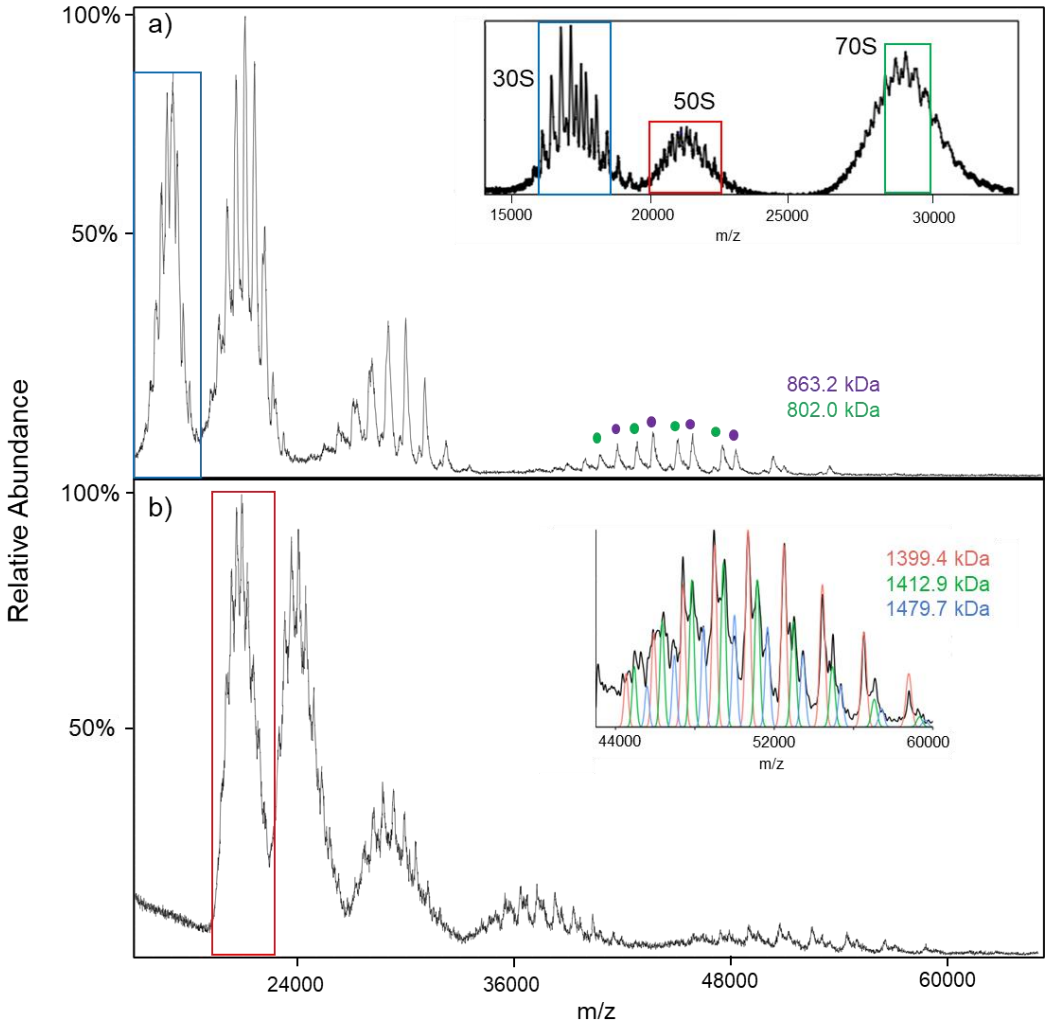

Figure 1.6. Post-ion attachment MS spectra of the *E. coli* ribosome subunits, (a) 30S and (b) 50S , reacting with with hMb. The concentrations of Mg^{2+} is 10 mM. The inset in panel (a) is the *E. coli* ribosome

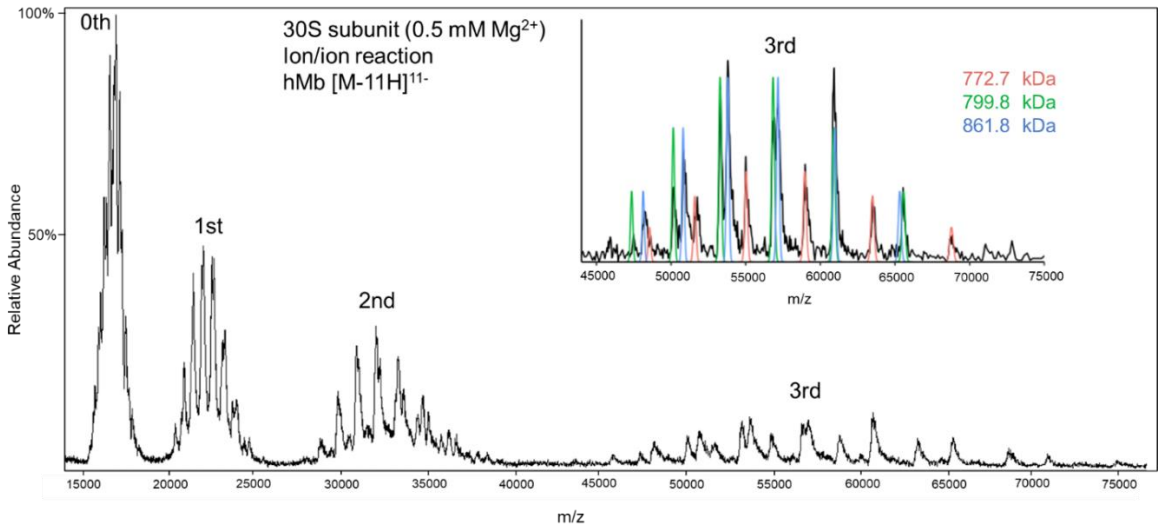

Figure 1.7. The post-ion attachment mass spectrum for the 30S ribosomal subunit reacting with $[hMb-11H]^{11-}$. The ribosomal ions were generated from a 0.5 mM Mg^{2+} solution of the *E. coli* ribosome. The inserted spectrum is the zoom-in of the 3rd adduction, which reveals a third population. The third population corresponds to the loss of both S1 and S2 ribosomal protein from the 30S subunit.

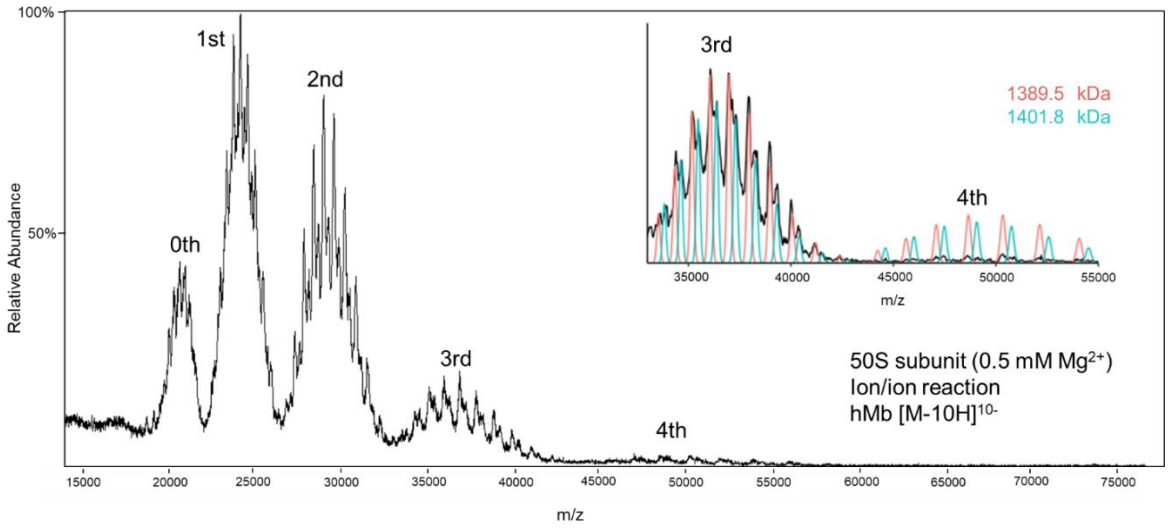

Figure 1.8. Post-ion attachment mass spectrum of the 50S ribosomal subunit reacting with[hMb-10H]$^{10-}$. The ribosomal ions were generated from a 0.5 mM Mg^{2+} solution of the *E. coli* ribosome.

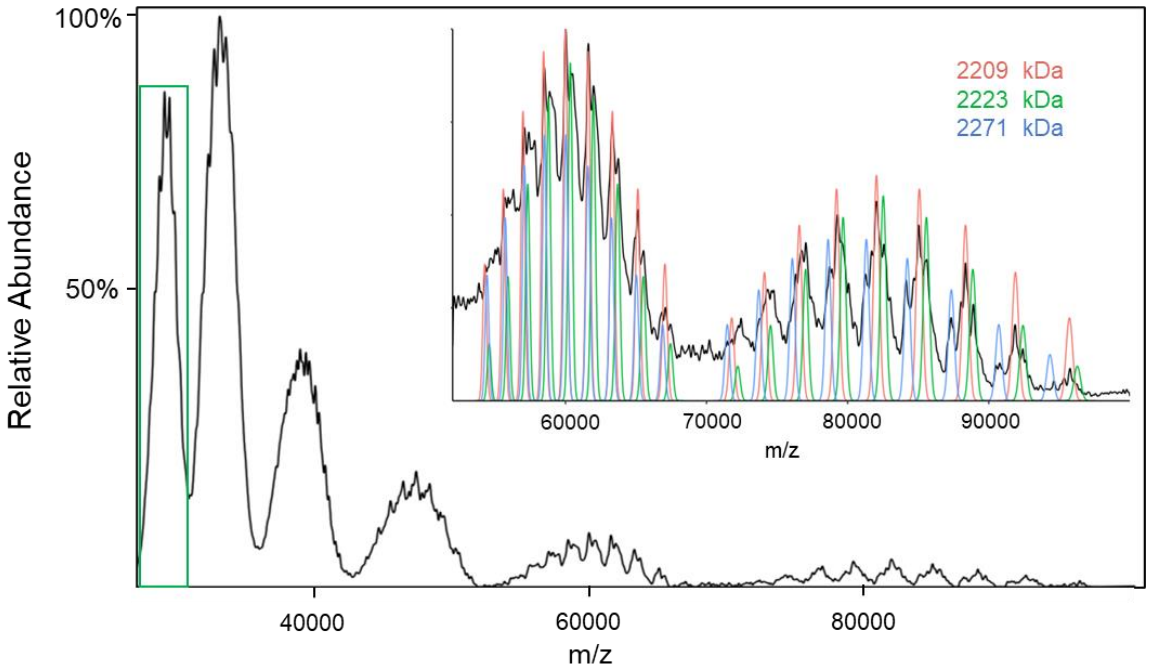

Figure 1.9. Post-ion attachment mass spectrum of 70S ribosome-related ions reacting with $[hMb-10H]^{10-}$. The 70S ribosome precursor population (green border) are shown in the insert to Figure 3.6a. The insert shows an expansion of the fourth and fifth anion attachment regions.

CHAPTER 4. DEVELOPMENT OF MS FOR LARGE (>200 kDa TO MDa) PROTEIN COMPLEXES

The mass measurement of viruses presents challenges due to the inherently large molecular weight, and the existence of heterogeneity from the assembly process. The introduction of electrospray ionization and native mass spectrometry have bridged the gap needed to study these systems. In a collaborative project with Merck Pharmaceuticals, we utilized our ion/ion reaction techniques to study the virus-like particles of the human papillomavirus.

4.1 Introduction

Electrospray ionization (ESI) is a soft ionization technique that allows for the preservation of non-covalently bound complexes (1,2). John Fenn described these ions as flying elephants, because prior to its advent, only small molecules were amenable to MS analysis. Large complex analysis typically couples ESI with native MS (nMS) - a technique that utilizes solvent conditions that are non-denaturing to allow for the study of intact proteins and non-covalent protein-protein complexes (3,4). Despite its many advantages as a complementary biophysical method to crystallography and NMR, there are short-comings. For example, nMS yields a relatively narrow charge state distribution (CSD) of ions relative to when denaturing conditions are employed. It is important to note that more independent mass measurements will yield a higher accuracy for the mass assignment (5,6). Moreover, with nMS the narrower CSD is comprised of broad and overlapping peaks due to extensive adduction of salts. The salt adduction broadens each *m/z* peak, and in certain cases, the adjacent ions become indistinguishable, leading to what is commonly referred to as a "blob". The problem is exacerbated when the analytes are heterogeneous, and the ions of each component appear in the same *m/z* space. To solve this problem, we utilize gas-phase ion/ion chemistry (7). In short, we isolate a segment of the "blob" and react it with an oppositely charged reagents. The resulting spectrum will yield new product peaks that are different by a specific Δm and Δz, which will allow for mass determination of the initial precursor.

4.2 Experimental

4.2.1 Sample preparation for native mass spectrometry of bio-complexes

The HPV virus-like particle was purchased from Creative Diagnostics. The sample was prepared in two separate ways: denatured sample preparation and native-like sample preparation, for the proton transfer reaction and the multiply-charged ion attachment experiments, respectively. The denatured sample preparation was done by washing the sample with water (using a 3 kDa MWCO spin column) to remove excess salts, and then adding acetonitrile and acetic acid. The native-like sample preparation was done by buffer exchange into 150 mM ammonium acetate using a spin column with a 300 kDa MWCO filter.

4.2.2 Sample preparation for the reagent anions

Perflouoro-1-octonol was used as the reagent for the proton transfer experiments. Oxidized insulin chain A (IcA) from bovine pancreas (average mass, free acid = 2531.66 Da) was purchased from Sigma Aldrich. The lyophilized solid was reconstituted in water. The working solution was a 50:50 mixture of aqueous ammonium hydroxide (pH 11) and HPLC grade methanol (Sigma Aldrich) to give a final concentration of 25 µM. The most abundant charge states were $[IcA\text{-}5H]^{5-}$ and $[IcA\text{-}6H]^{6-}$. The sample preparation for the pepsin and myoglobin reagents were similar to IcA.

4.2.3 Ion-ion reactions in the mass spectrometer.

All experiments were performed using a QTOF 5600 (SCIEX), which was previously modified to allow for ion/ion reactions (8). The positive and negative ions were generated by utilizing an alternately pulsed nano-electrospray ionization source (nESI) (9). Mutual ion polarity trapping was enabled by applying a supplemental AC to the end plates of the linear ion trap reaction cell, q2. Multiply protonated protein cations and reagent anions were sequentially isolated before being stored in q2 to react over times of 50-100 ms. The reagent anions were isolated during Q1 transmission by conventional RF-DC apex isolation. The protein cations were too high in *m/z* to be isolated via conventional RF-DC apex isolation. Therefore, sequential resonance ejection ramps in q2 were used to eject ions of lower and higher *m/z* ratios that bordered the population of interest (10).

4.2.4 Native MS

Both analyte and reagent ions were generated via nESI from separately pulsed borosilicate glass emitters (11). The large bio-complexes were sprayed in positive mode with approximately +1500 V applied to a platinum wire, which was in contact with the solution. The reagent anions were sprayed in negative mode with an applied voltage of approximately -1400 V. The large complex ions were initially injected into the instrument and isolated (see above) and stored in q2. Subsequently, the reagent anions were injected and isolated during Q1 transmission before being accumulated and stored in q2. The mutual storage time can be controlled to determine the number of sequential adductions. Nitrogen gas was used in q2 at pressures ranging from 6-8 mtorr. Due to the size of the viral particles, the difference in DC offsets of Q0 and q2 were increased to as high as 50-70 V to collisionally activate the ions upon injection into q2 to drive off weakly-bound adduct species. A Q0-q2 voltage difference of 5-15 V was used for the reagent anions as minimal salt adduction was observed for these species. Mass calibration over a wide range was done in two stages, using primary and secondary calibrants. Cesium iodide, the primary calibrant, was used to calibrate the instrument over the range of *m/z* 1,000-10,000. This allowed for an accurate mass determination of the pyruvate kinase tetramer, the secondary calibrant, from the mass spectrum derived under native conditions. Finally, the population of pyruvate kinase charge states was reacted with the oxidized insulin chain A, $[IcA\text{-}6H]^{6-}$ anion ($[IcA\text{-}6H]^{-}$; Δm = 2526 Da) resulting in a series of peaks extending beyond m/z 100,000. This experiment allowed for the mass scale to be calibrated over the range of m/z 6,500-100,000 (**see chapter 3**).

4.3 Results and Discussion

4.3.1 Measuring oligomers

In our initial experiments, the goal was to demonstrate a charge state reduction method for the L1 protein. The aggregation of L1 monomers to form pentamers (capsomers) is depicted in **Figure 4.1a**. L1 forms this capsomere which self-aggregates to form the virus-like particle (VLP). The final structure consists of 72 capsomers. The L1 protein Type 11 (from *E. coli*) was purchased from Creative Diagnostic (CD). The CD sample underwent an LC/MS workflow, which yielded monomer, dimer, trimer and "other" (**Figure 4.1b**). The assignment for the monomer, dimer and trimer came from the zero-charge deconvolution of the mass spectrum. However, the charge states

were not clearly resolved for the "other" population. The mass spectrum of the CD sample without any prior purification/separation can be seen in **Figure 4.1c**. The blob seen is an combination of the monomer, dimer, trimer and the "other" population.

The proposed solution was to explore the utility of gas-phase ion/ion strategies. Specifically, proton transfer reaction (PTR) and multiply-charged ion attachment (**Figure 4.2**). The former involves a reagent that is oppositely charged that either removes a proton (if the analyte is a cation) or donates a proton (if the analyte is an anion). This works well for smaller analytes, and samples with relatively simple mixtures. When faced with more challenging samples, we developed a methodology where the reagent ion collides with the analyte and forms a long-lived complex that survives detection. The difference in mass and charge can be selected at the user's discretion. This method was previously demonstrated with the *E. coli* ribosome as the model system. Most of the data for specific aim 1 was done by utilizing the PTR method.

The first specific aim was to demonstrate a charge state reduction of the CD sample and reveal the monomer, dimer and trimer (**Figure 4.3**). The pre-ion/ion mass spectrum of the CD sample can be seen in the top panel. In this spectrum, there are no clearly resolved peaks. The next step involved selection of a segment of the mass spectrum (blue box), in this case a region centered around *m/z* 1200 and reacting it with the de-protonated perfluoro-1-octanol dimer (PFO). The isolation was done by applying the appropriate RF and DC voltages to Q1. The bottom panel is the resulting ion/ion PTR. The spectrum shows the monomer, dimer (centered between each monomer), and trimer (satellite peaks on each side of the dimer peaks). The results were consistent with the LC/MS data in **Figure 4.1**. However, the peaks identified as "other" in the LC trace were not see in this data set.

In hopes of identifying the unknown "other" peaks, we moved the isolated precursor peaks to a higher *m/z* value. It is well known in the native MS (nMS) community that larger complexes tend to appear at higher *m/z* values, which is partly due to the relatively smaller solvent-accessible surface area present in large non-covalently bound complexes. We moved the isolated segment to *m/z* 2000 (**Figure 4.4**). The resulting spectrum from the ion/ion PTR showed similar peaks attributable to the monomer, dimer and trimer. However, there are low level components that are above the noise threshold. The zero-charge deconvolution of this spectrum indicates that the tetramer and pentamer are responsible for the low-level components. This result was promising as

it clearly showed the presence of larger oligomers, which was suggested by the LC/MS method used for the analysis of the CD sample, but not unambiguously demonstrated.

An interesting observation was made when comparing an older sample against a freshly prepared sample (**Figure 4.5**). The older sample was left in the fridge for about 2 months. The typical monomer, dimer and trimer peaks were present in both spectra, along with the tetramer and pentamer. In the old sample, however, there were other peaks present at higher *m/z*. These peaks are evidence of higher order oligomers, as they do not correspond to the oligomers mentioned above. This could indicate L1 assembly process over a slow time period.

4.3.2 Measuring VLP

A separate approach to studying this VLP system would be from the top-down, wherein the final assembled system would be measured initially. However, to achieve a mass measurement, we need to utilize a different sample preparation methodology. The sample contained polysorbate 80 (PS-80), which is used as a stabilizer (12) for the storage of the HPV VLP sample. The sample preparation methodology consists of utilizing a spin column with a MWCO filter that is high enough to remove the excess salts. The high concentration of the PS-80 creates micelles that are large enough to be retained in the 100 kDa MWCO filter. In this case, we used a Vivaspin 300 kDa MWCO spin column to aid in the removal of these large PS-80 micelles. The resulting spectrum can be seen in **Figure 4.6**, where there is a population of peaks in the *m/z* 35000 – 55000 region. Based on the anticipated charge-state of the ~19 MDa VLP using the Rayleigh limit, the peaks should appear around a similar *m/z* area (13). There are multiple populations (shoulders) in this region, indicating heterogeneity. The isolation of those peaks was done by utilizing stored waveform isolation Fourier transform (SWIFT) in q2. Our QTOF platforms Q1 RF/DC isolations function up to *m/z* 3000. Consequently, these ions required the SWIFT isolation, which allowed for a higher *m/z* isolation limit. The isolation of ions at this high of an *m/z* is difficult. The severe loss of signal when removing the border ions, and the lower well-depth for these ions present challenges in generating a tight isolation window.

Due to these difficulties in isolating high *m/z* ions, the resulting width of the isolated region was about *m/z* 10000. The ion/ion reaction of the precursor spectrum and apo-myoglobin can be seen in **Figure 4.7**. The result of this reaction did not achieve discernable and separate peaks. A tighter isolation window (*m/z* 5000 window) and higher charged reagent, pepsin (z = 38-)

generated similar results. If the tops of the smoothed peaks were selected, the calculated mass measurement of VLP would be ~21 MDa. To achieve better results, we need to either have a tighter isolation, or use a reagent with a much higher charge state. The search for a higher charged reagent and the optimization of a tighter VLP isolation are currently under way.

4.4 Conclusions

The current results for this part of the study are promising. The ion/ion PTR worked well for the separation of the smaller oligomer ions in the mass spectrum. The LC/MS workflow is suitable for separating out and analyzing (through the MS zero-charge deconvolution) the monomer, dimer, and trimer. However, the "other" LC peaks are identified as such because the zero-charge deconvolution did not work, because the mass spectrum did not generate discernable peaks. These constraints of the LC/MS methods were successfully addressed by using this gas-phase strategy. Moving forward, our goal is controlling the assembly/disassembly of the L1 protein. Time has shown to be a factor in the assembly process, as there were higher ordered oligomers in the older sample. The ultimate goal is measuring the fully-formed VLP (~19 MDa) – which will most likely require the use of the multiply-charged ion attachment methodology.

4.5 References

1. Katta, V.; Chait, B. T., Observation of the heme-globin complex in native myoglobin by electrospray-ionization mass spectrometry. J. Am. Chem. Soc. 113, 8534-8535 (1991).

2. Rostom, A. A.; Robinson, C. V., Detection of the Intact GroEL Chaperonin Assembly by Mass Spectrometry. J. Am. Chem. Soc. 121, 4718-4719 (1999).

3. Hernandez, H.; Robinson, C.V., Determining the stoichiometry and interactions of macromolecular assemblies from mass spectrometry. Nat. Protoc. 2, 715 (2007).

4. Leney, A. C.; Heck, A. J. R., Native Mass Spectrometry: What is in the Name? J. Am. Soc. Mass Spectrom. 28, 5-13 (2017).

5. Laszlo, K. J.; Bush, M. F., Analysis of Native-Like Proteins and Protein Complexes Using Cation to Anion Proton Transfer Reactions (CAPTR). J. Am. Soc. Mass Spectrom. 26, 2152-2161 (2015).

6. Liepold, L.; Oltrogge, L. M.; Suci, P. A.; Young, M. J.; Douglas, T., Correct Charge State Assignment of Native Electrospray Spectra of Protein Complexes. J. Am. Soc. Mass Spectrom. 20, 435-442 (2009).

7. Abdillahi, A.M.; Lee, K. W.; McLuckey, S. A. Mass Analysis of Macro-Molecular Analytes via Multiply-Charged Ion Attachment. Anal. Chem. 92(24), 16301–16306 (2020).

8. Xia, Y.; Wu, J.; McLuckey, S. A.; Londry, F. A.; Hager, J. W., Mutual storage mode ion/ion reactions in a hybrid linear ion trap. J. Am. Soc. Mass Spectrom. 16, 71-81 (2005).

9. Liang, X.; Xia, Y.; McLuckey, S. A., Alternately Pulsed Nanoelectrospray Ionization/Atmospheric Pressure Chemical Ionization for Ion/Ion Reactions in an Electrodynamic Ion Trap. Anal. Chem. 78, 3208-3212 (2006).

10. McLuckey, S.A.; Goeringer, D.E.; Glish, G.L. Selective Ion Isolation/Rejection Over a Broad Mass Range in the Quadrupole Ion Trap. J. Am. Soc. Mass Spectrom. 2, 11-21 (1991).

11. Xia, Y.; Liang, X.; McLuckey, S.A. Pulsed dual electrospray ionization for ion/ion reactions. J. Am. Soc. Mass Spectrom. 16, 1750-1756 (2005).

12. Shi, L.; Sanyal, G.; Ni, A.; Luo, Z.; Doshna, S.; Wang. B.; Graham, TL.; Wang, N.; Volkin, DB., Stabilization of human papillomavirus virus-like particles by non-ionic surfactants J. Pharm. Sci. 94(7), 1538-51 (2005).

13. Snijder J. et al.: Studying 18 MDa Virus Assemblies with Native Mass Spectrometry.: Angew. Chem. Int. Ed. 52. 4020–4023 (2013).

4.6 Figures

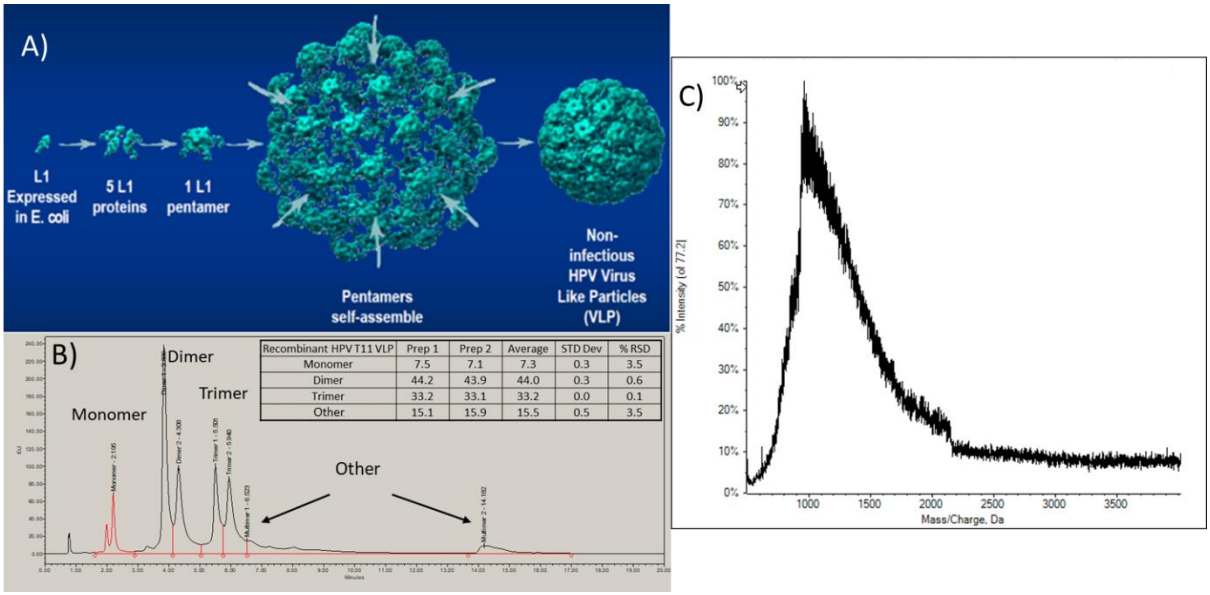

Figure 4.1. L1 protein analysis. A) The self-assembly process of the L1 monomer to form the intact VLP. B) The LC/MS of the CD sample, indicating unknown peaks defined as other. C) The mass spectrum of the CD sample without any prior purification. Panel A is reproduced from Creative Diagnostics website <https://www.creative-diagnostics.com/news-recombinant-hpv-l1-vlp-68.htm>

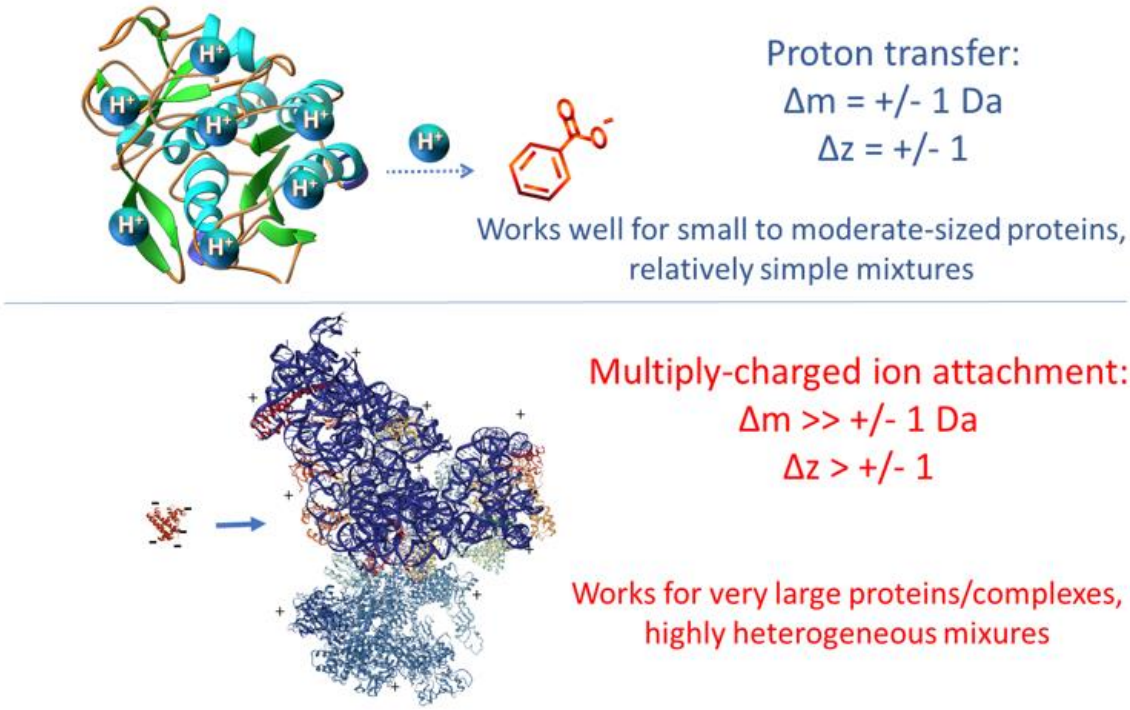

Figure 4.2. Ion/ion reaction strategies. Proton transfer occurs when a reagent removes a proton from the analyte. Multiply-charged ion attachment is formed by long-lived complexes where the reagent collides to the analyte.

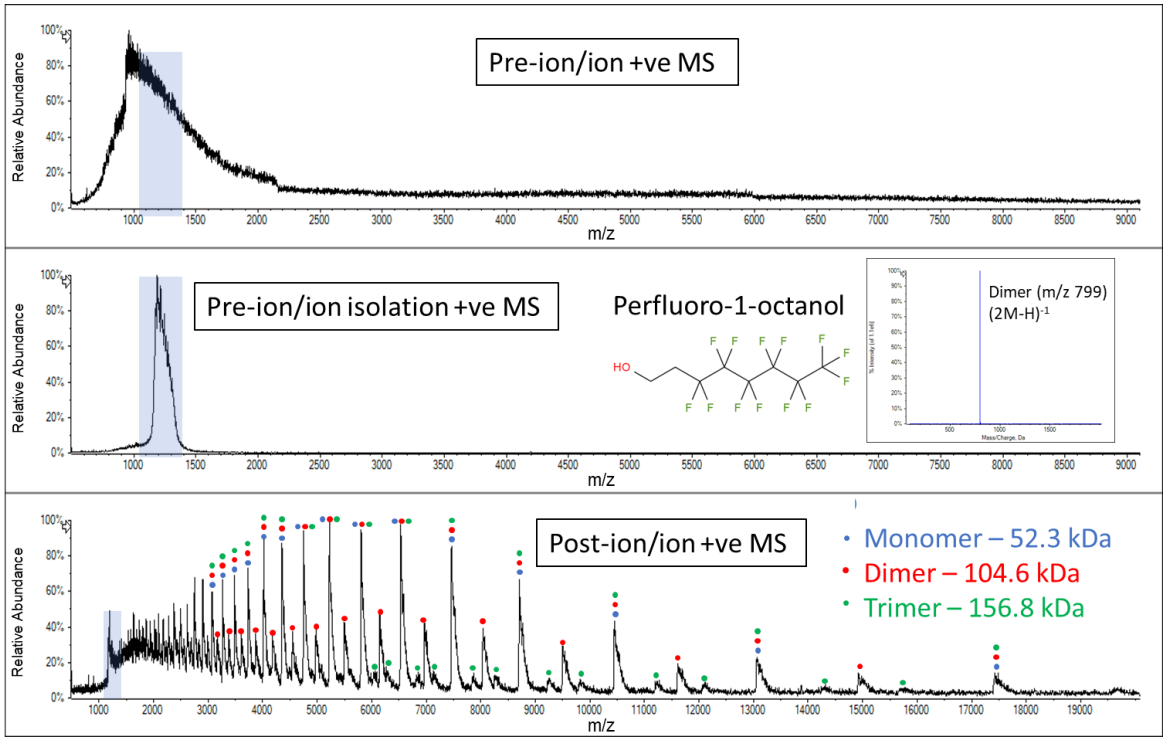

Figure 4.3. Ion/Ion reaction of the CD sample. Top: Mass spectrum of the CD sample without prior LC purification. Middle: The isolated segment of the precursor and the reagent ion PFO. Bottom: The ion/ion reaction of the precursor analyte and the PTR reagent.

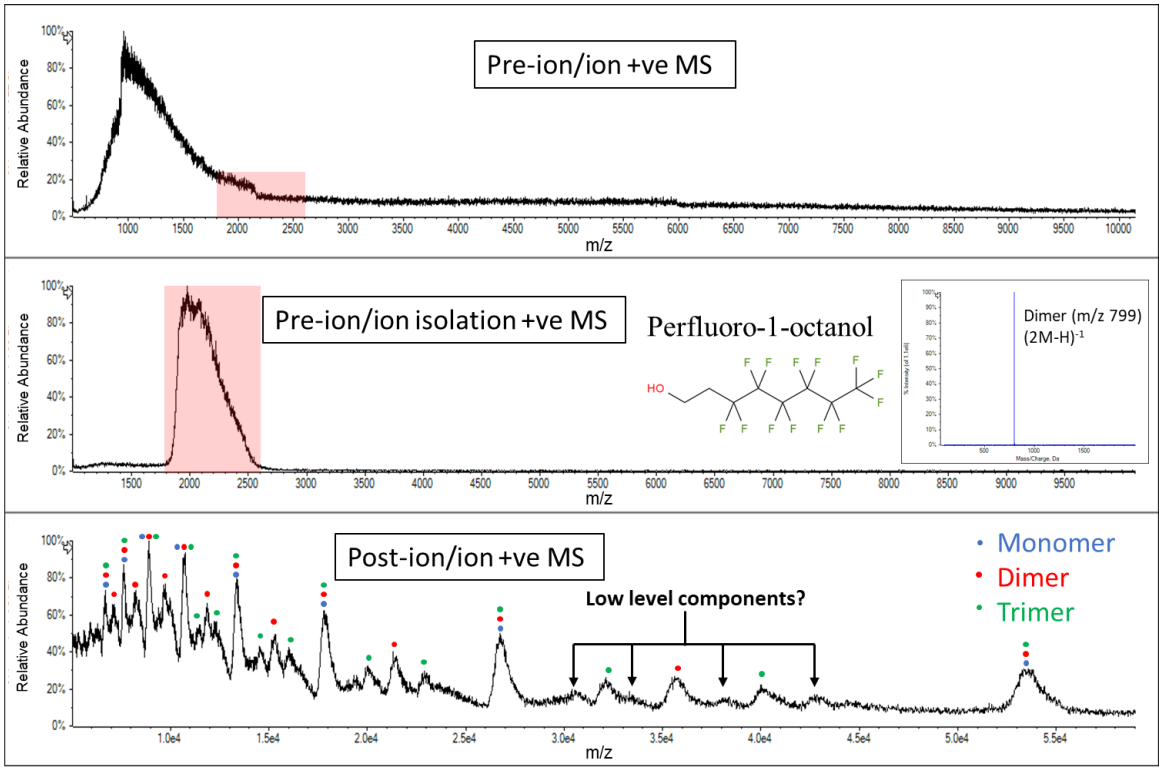

Figure 4.4. Ion/Ion reaction of the CD sample with higher isolation. Top: Mass spectrum of the CD sample without prior LC purification. Middle: The isolated segment of the precursor and the reagent ion PFO. Bottom: The ion/ion reaction of the precursor analyte and the PTR reagent. The low level components did not appear in Figure 3.3.

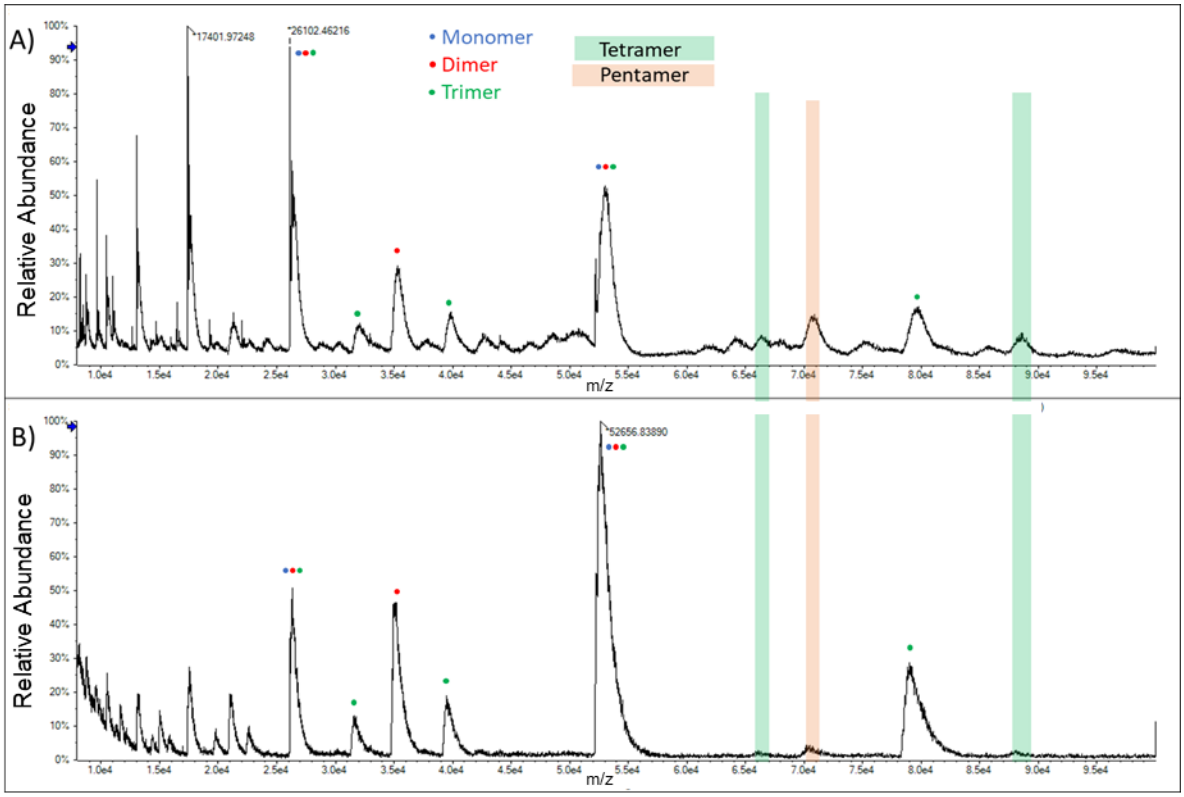

Figure 4.5. Ion/Ion reaction of the old vs new CD sample with higher isolation. A) The mass spectrum of the old CD sample reacting with PFO. Sample was prepared on 2020-12-08. B) The mass spectrum of the new CD sample reacting with PFO. Sample was prepared on 2021-02-08.

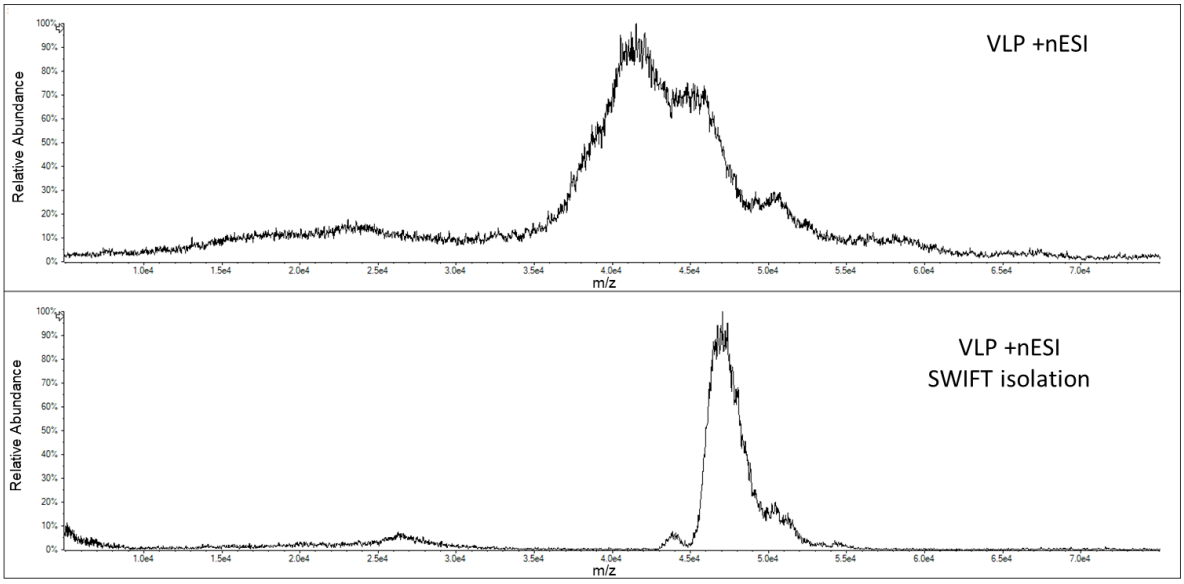

Figure 4.6. Precursor spectrum of the VLP under native conditions (top panel). The isolated region of the population centered around m/z 47k using SWIFT isolation (bottom panel).

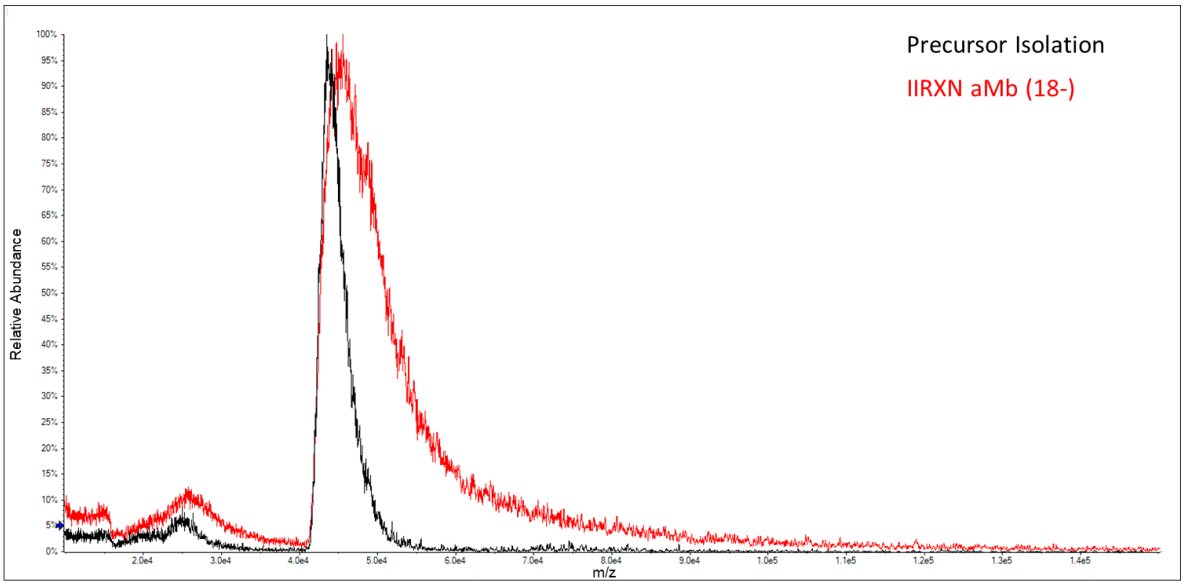

Figure 4.7. Ion/ion reaction of the isolated region of the VLP precursor spectrum and apo-myoglobin 18-.

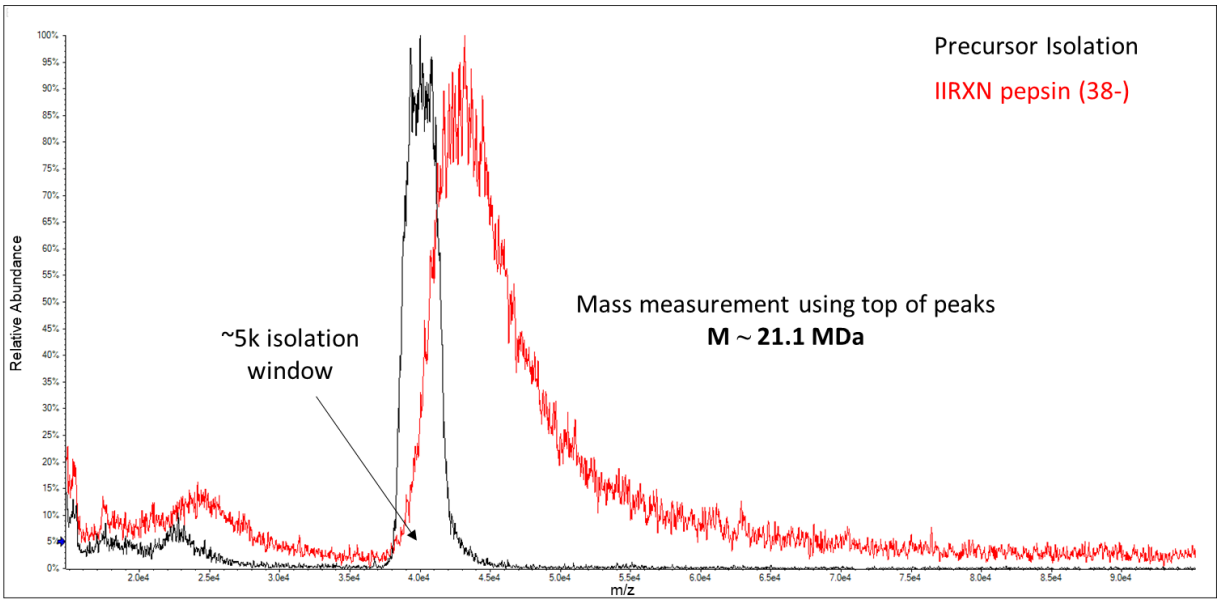

Figure 4.8. Ion/ion reaction of the isolated region of the VLP precursor spectrum and pepsin 38-.

CHAPTER 5. ACTIVATION AND FRAGMENTATION OF NATIVE MS IONS

Mass spectrometry (MS) is a useful tool for structural elucidation. An approach to uncover structural information about the analyte via MS involves the activation of ions via collisions with a separate entity, which can be a neutral gas molecule or a large surface. Fragmentation with respect to large native MS ions will be described in this chapter, along with mention of the introduction of a larger bath gas in our collision chamber, which has allowed us to perform ion trap activation.

5.1 Introduction

For the last 30 years, initiated by the advent of electrospray ionization, researchers have studied ions comprised of non-covalently bound subunits (1). The development of native MS sample preparation methodology allowed for the study of these ions, enabling the mass measurement of these complexes after entering the gas-phase. Previous chapters have illustrated the difficulty with ascertaining the molecular weight of native MS ions. A separate but vital aspect of native MS experiments is the activation of ions to study the connectivity (2,3).

Tandem MS, also referred to as MS/MS or MS^n, is an experiment where a precursor is subjected to collisional activation to generate fragment ions that are then mass analyzed. For a protein complex, the most utilized fragmentation technique is referred to as collision-induced dissociation (CID). The typical CID fragmentation pattern of non-covalently bound complexes yields the loss of a monomer and an N-1mer that carries less charge (**Figure 5.1**). The monomers can be subsequently activated to yield the backbone sequence (4). The use of a surface, in place of bath gas, for the activation of ions has proven to generate impressive structural information. This method is referred to as surface induced dissociation (SID). Utilizing GroEL, a 14-mer that is commonly used native MS system, SID yielded fragments that corresponded to heptamers, while CID yielded the monomer and 13-mer (5). The recent rendition, generation 3, of the SID device have decreased in size enough to be used as the lenses surrounding the collision chamber, which has allowed for tandem SID (6). Our platform is capable of fragmenting by CID and other unique methodologies that will be discussed in detail below.

5.2 Experimental

5.2.1 Sample preparation for native mass spectrometry of bio-complexes

Rabbit pyruvate kinase and β-galactosidase were purchased from Sigma Aldrich. The lyophilized solid was reconstituted in water to create a stock solution at a concentration of 3 μM and 10 μM (calculated by using the mass of the tetramer), respectively. These samples underwent buffer exchange, via centrifugation, once with an ammonium acetate (Sigma Aldrich) buffer adjusted to pH 7 with ammonium hydroxide (Sigma Aldrich), using a 10 kilodalton (kDa) molecular weight cutoff (MWCO) Amicon Ultra 0.5 mL filter (Millipore Sigma). The recovered samples (15 μL) were diluted with the same buffer to achieve the same original concentration from the stock solutions.

GroEL (Sigma Aldrich) lyophilized powder preparation was described before in detail (5). Briefly, the sample was buffer exchanged and underwent acetone precipitation. The buffer exchange occurred via centrifugation with a 150 mM ammonium acetate (Sigma Aldrich) buffer adjusted to pH 7 with ammonium hydroxide (Sigma Aldrich), using a 10 kilodalton (kDa) molecular weight cutoff (MWCO) Amicon Ultra 0.5 mL filter (Millipore Sigma). The final recovered sample (~15 μL) was diluted with the same buffer to achieve 1 μM concentration from the stock solution.

E. coli 70S ribosome solution was purchased from New England Biolabs. The original sample, with an initial concentration of 13 μM, was constituted in a buffer containing 10 mM magnesium acetate, which is necessary for the 70S ribosome to be intact in the condensed phase. The sample preparation for the working solutions was described in detail previously (7) and modified accordingly. Briefly, the sample was buffer exchanged 8 times with 150 mM ammonium acetate and 10 mM magnesium acetate (Sigma Aldrich) with the same filter used in the GroEL preparation.

5.2.2 Native MS

The analyte ions were generated via nESI from separately pulsed borosilicate glass emitters. The large bio-complexes were sprayed in both positive and negative mode with approximately ±1200 V applied to a platinum wire, which was in contact with the solution. The reagent anions were sprayed in negative or positive mode, respectively, with an applied voltage of approximately

±1400 V. The large complex ions were initially injected into the instrument and isolated (see above) and stored in q2. Nitrogen, or sulfur hexafluoride (SF_6) gas was used in q2 at pressures ranging from 6-8 mtorr. Due to the salt adduction on the large *m/z* ions, the difference in DC offsets of Q0 and q2 were increased to as high as 50-70 V to collisionally activate the ions upon injection into q2 to drive off weakly-bound adduct species.

5.3 Results and Discussions

Our platform allows for collisional activation to be done by various means of ion acceleration. These include dipolar direct current (DDC), beam-type (high energy) collisional activation, and ion trap resonance excitation. Each of these will be explained in more detail below.

5.3.1 Dipolar Direct Current Ion Activation

DDC is a broadband activation technique that moves ions away from the center of the trap by applying a potential across opposing rods (8). This is demonstrated schematically in **Figure 5.2**. Under normal conditions, the rods all have the same DC potential. During DDC, an opposing pair of rods (B1 and B2), which normally have the same DC potential, have different DC voltages, which shifts the ions away from the center of the trap where the RF potential is at a minimum. The DDC voltage moves ions into regions of higher RF potentials where they can absorb power from the RF drive. As a result, the ion velocities increase leading to more energetic collisions with the background gas in the collision cell. This overall process is often referred to as 'RF-heating'. The effect of DDC in q2 can be seen in **Figure 5.3**, where the peaks associated with the charge states of pyruvate kinase sharpen with the use of higher DDC voltage. Moreover, ions at higher *m/z* are observed, which correspond to lower charge ions. This is a common phenomenon seen which is referred to as charge stripping, and normally appears before the ions has enough activation energy to fully fragment (9).

The DDC activation technique is a very useful tool for driving off salt adducts and fragmenting small molecules, but does not pair well with ions of high *m/z*. The upper *m/*z limit of DDC can be calculated by (8)

$$\left(\frac{m}{z}\right)_{high} = \frac{4e}{r_0^2\Omega^2}\ \frac{V_{RF}^2}{V_{DDC}} \qquad (1)$$

where e is the electron charge, r_0 is the radius of the rods, Ω is the drive angular frequency, V_{RF} is the 0-p amplitude of the drive RF voltage and V_{DDC} is the magnitude of the applied dipolar DC voltage. There is an inverse relationship between the *m/z* and the DDC voltage, and ions with high *m/z* are displaced further from the center of the trap, with respect to lower *m/z* ions. The net result is that there is a "high *m/z*" cut-off associated with DDC and is a drawback for using DDC in the fragmentation of native MS ions.

5.3.2 Beam-type CID

The standard approach for tandem native MS is currently high energy CID, which our lab refers to as beam-type (BT) CID. This form of CID is a non-resonant dissociation technique, which relies on inducing energetic collisions via acceleration of the ions into a gas-filled collision cell. The kinetic energy of the accelerated ions leads to energetic collisions that impart enough energy for the ion to fragment. Consequently, this technique can fragment both weak and strong bonds. This method can also cause scattering, which leads to the loss of signal, or induce secondary fragmentation if the initial fragment products are not efficiently cooled. The fragmentation of ions of high *m/z* pairs well with BT-CID on our platform. The large complexes can fragment, and the fragment products are still large enough to have more interactions with the bath gas in q2 for effective collisional cooling.

Our lab can perform this experiment from Q0-q2 or Q1-q2 (**Figure 5.4**). The GroEL fragmentation spectra are comparable for the two BT-CID experiments. The fragment products are the monomer charge state distribution around *m/z* 2000, and the 13-mer charge state distribution around *m/z* 21000. Interestingly, the signal for the 13-mer fragment for the Q0-q2 BT-CID has less abundance than the Q1-q2 BT-CID. There is a large pressure difference between Q0 and Q1. Ion isolation using RF/DC voltages is done in Q1, which is why the pressure for the Q1 region is low. During Q0-q2 BT-CID, there may be some fragmentation towards the end of Q0, which is then loss due to the lack of collisional cooling in Q1. A separate experiment comparing the BT-CID of GroEL in the positive and negative mode from Q1-q2 can be seen in **Figure 5.5**. Similar fragmentation patterns are observed in the negative mode, as well. The average charge state for the 13-mer is shifted to the right. The negative mode of GroEL precursor is at a lower charge than the positive mode precursor (see chapter 7). Consequently, the lower average charge state of the 13-mer is due to the conservation of charge.

We have attempted the BT-CID of the 30S ribosome (**Figure 5.6**), which is not as efficient, but did produce RS6 protein in its 4 isomers at low *m/z* (7). Moreover, the charge states of the isolated 30S precursor sharpened, indicating the shedding of salt adducts from the collisional activation. The BT-CID of β-galactosidase can be seen in **Figure 5.7**. The main observations here is the loss of the octamer signal with BT-CID and the noticeable sharpening of the tetramer peaks. Many of our experiments have demonstrated that the β-galactosidase complex(s) are challenging to fragment utilizing BT-CID.

5.3.3 Ion Trap CID

Ion trap CID is a resonant dissociation technique that accelerates an ion based on its secular frequency, which when a voltage is applied at this frequency, will move away from the center of the trap. To reach the needed collision energy to induce fragments, ions are accelerated slowly, relative to BT-CID. Consequently, this technique is referred to as "slow-heating". The ions have many collisions with the bath gas during this excitation process. After the ion fragments, the secular frequency of those fragment ions become off-resonant. The fragment products continue colliding with the bath gas which then cools the products so that they may be effectively trapped. Thus, secondary fragments are less common in ion trap CID than it is in either beam-type CID or DDC CID.

The vast majority of native MS workflow takes advantage of the BT-CID methodology, especially with large *m/z* ions (7,10). This is because the ions need more imparted energy, with respect to smaller *m/z* ions, which is easier to attain via BT-CID. However, as can be seen, there are limitations with BT-CID. For example, β-galactosidase is a difficult system to fragment via BT-CID (**Figure 5.7**) due to its relatively high kinetic stability. All the experiments mentioned in this chapter employed the use of nitrogen as the bath/collision gas. We have not been able to fragment GroEL using ion-trap CID, even though we have the capabilities of applying the frequencies needed for that experiment and have not been able to fragment β-galactosidase with any of our activation techniques using nitrogen.

We have employed the use of SF_6, which has allowed us to fragment GroEL (**Figure 5.8**). The ion trap CID spectrum does not have any residual GroEL precursor. The average charge states for the 13-mer are lower in the ion trap CID spectrum, as well. The monomer charge states are correspondingly higher. This implies that the slow heating from the ion trap CID allows for the

unraveling of the monomer, which in turn abstracts more protons from the complex before dissociating. With SF6, we were also able to fragment β-galactosidase for the first time using both activation techniques (data not shown).

5.4 Conclusion

The advent of ESI and native MS has allowed for the study of large non-covalently bound complexes. The mass measurement difficulties of native MS ions have been explained in earlier chapters. However, the fragmentation of these complexes is important in understanding connectivity, which directly relate to the function of proteins. The activation techniques on our platform each have their respective benefits and shortcomings. The major benefit to ion trap CID is that the ions can remain in the collision cell. In contrast, BT-CID requires back transfer of ions (from q2 to Q1), which loses a percentage of analyte signal each time a back transfer is completed. Native MS ions tend to generate lower signal due to the difficulty in transmission of these ions. Consequently, ion trap CID with the use of SF_6 has shown great promise in allowing for MS^n experiments for native MS ions, without loss in signal, in our qTOF platform.

5.5 References

1. Fenn J.B. et al.: Electrospray ionization for mass spectrometry of large biomolecules.: Science 246. 64–71 (1989).

2. Leney A.C. and Heck A.J.R.: Native Mass Spectrometry: What is in the Name?: J. Am. Soc. Mass Spectrom. 28. 5–13 (2017).

3. Boeri Erba E. and Petosa, C.: The emerging role of native mass spectrometry in characterizing the structure and dynamics of macromolecular complexes.: Protein Sci. Publ. Protein Soc. 24. 1176–1192 (2015).

4. Zhou M. et al.: Higher-order structural characterisation of native proteins and complexes by top-down mass spectrometry.: Chem. Sci. 11. 12918–12936 (2020).

5. Zhou M. et al.: Dissecting the large noncovalent protein complex GroEL with surface-induced dissociation and ion mobility-mass spectrometry.: Anal. Chem. 85. 8262–8267 (2013).

6. Snyder D.T. et al.: Tandem surface-induced dissociation of protein complexes on an ultrahigh resolution platform.: Int. J. Mass Spectrom. 461. 116503 (2021).

7. van de Waterbeemd M. et al.: High-fidelity mass analysis unveils heterogeneity in intact ribosomal particles.: Nat. Methods 14. 283–286 (2017).

8. Webb I.K. et al.: Implementation of dipolar direct current (DDC) collision-induced dissociation in storage and transmission modes on a quadrupole/time-of-flight tandem mass spectrometer.: Rapid Commun. Mass Spectrom. 25. 2500–2510 (2011).

9. Lermyte F. et al.: Extensive Charge Reduction and Dissociation of Intact Protein Complexes Following Electron Transfer on a Quadrupole-Ion Mobility-Time-of-Flight MS.: J. Am. Soc. Mass Spectrom. 26. 1068–1076 (2015).

10. Rostom A.A. et al.: Detection and selective dissociation of intact ribosomes in a mass spectrometer.: Proc. Natl. Acad. Sci. U. S. A. 97. 5185–5190 (2000).

5.6 Figures

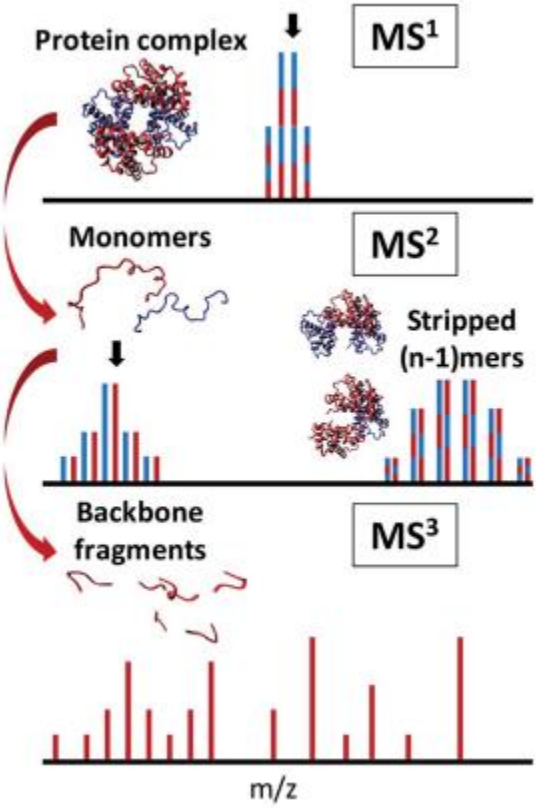

Figure 5.1. The mass spectrum of the protein complex (top), the fragmentation of the complex (middle) and the subsequent fragmentation of the monomers (bottom). Reproduced from Zhou M. et al., Chem. Sci. 11. 12918–12936 (2020).

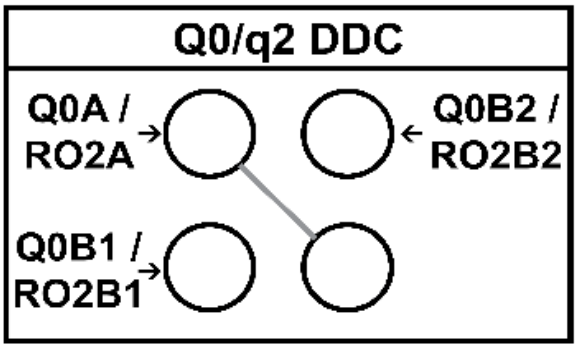

Figure 5.2. The rods of the quadrupole in Q0 and q2. Under normal conditions all DC voltages are the same. During DDC, the voltage differs between the B1 and B2 rods.

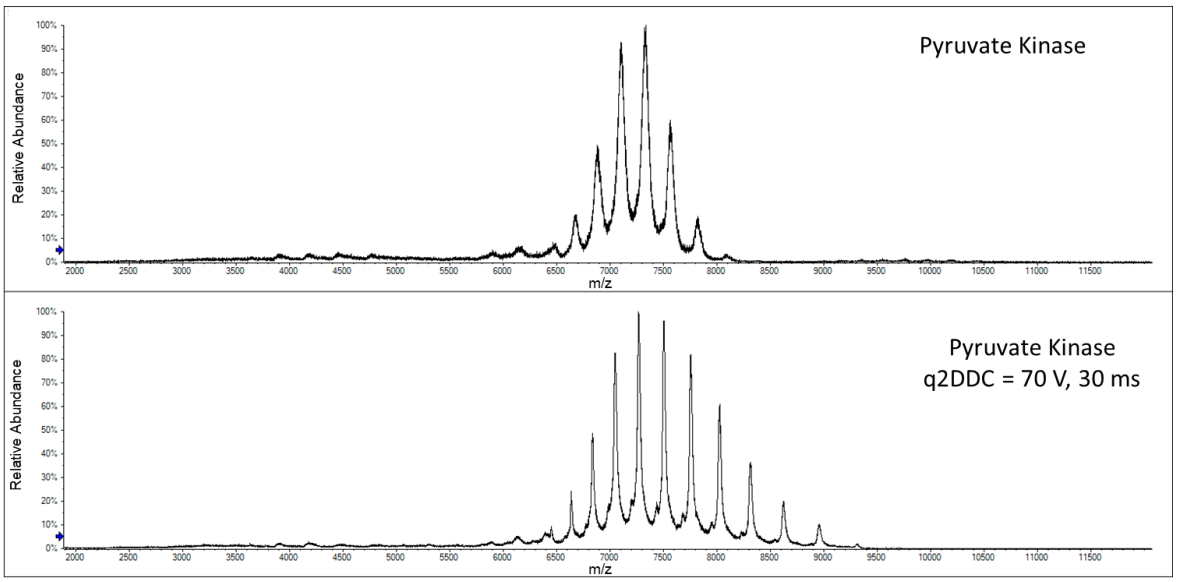

Figure 5.3. The nano-ESI mass spectrum of pyruvate kinase (top) and the application of q2-DDC on the precursor ions (bottom).

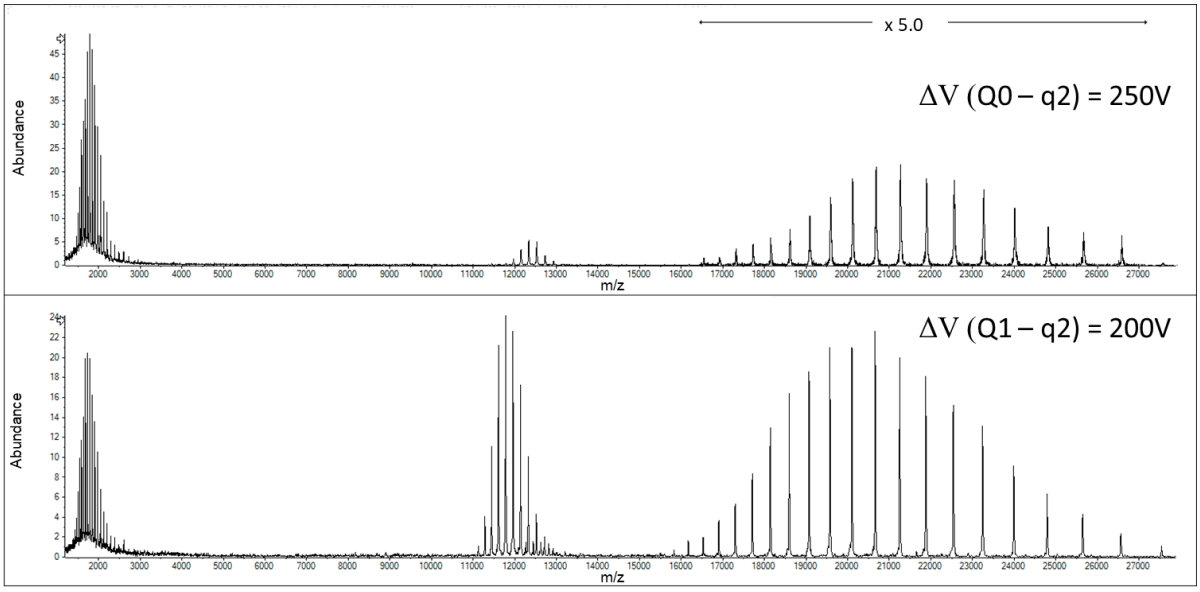

Figure 5.4. The BT-CID of GroEL with the gradient voltage between Q0-q2 (top), and Q1-q2 (bottom). The higher m/z 13-mer population for the top spectrum is multiplied by 5x.

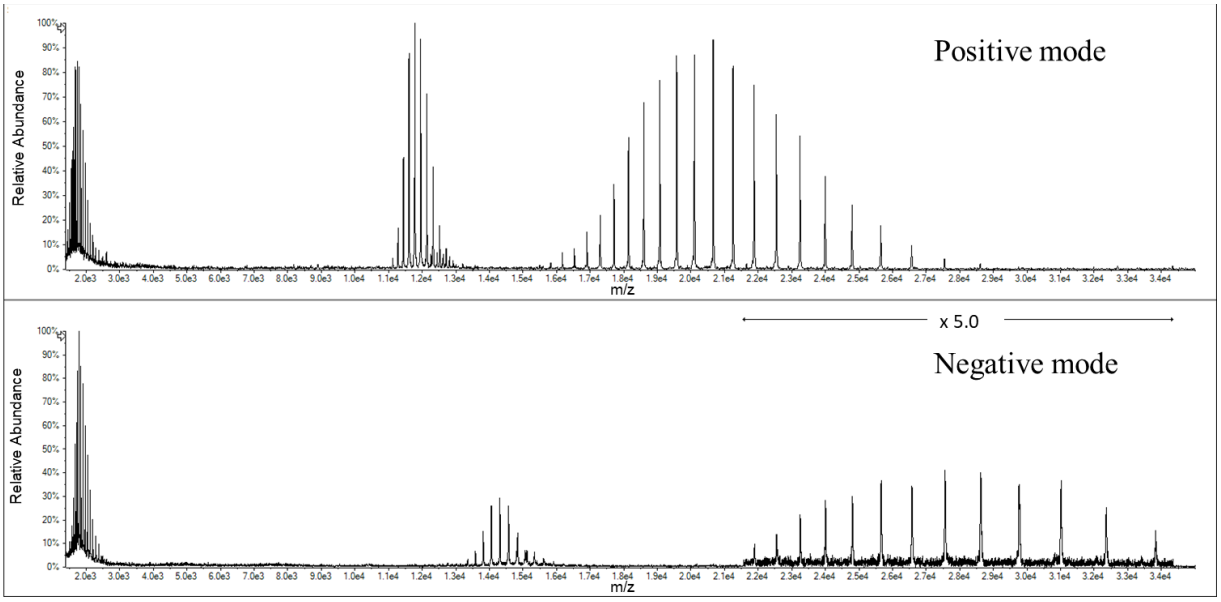

Figure 5.5. The BT-CID fragmentation of GroEL in the positive mode (top) and negative mode (bottom).

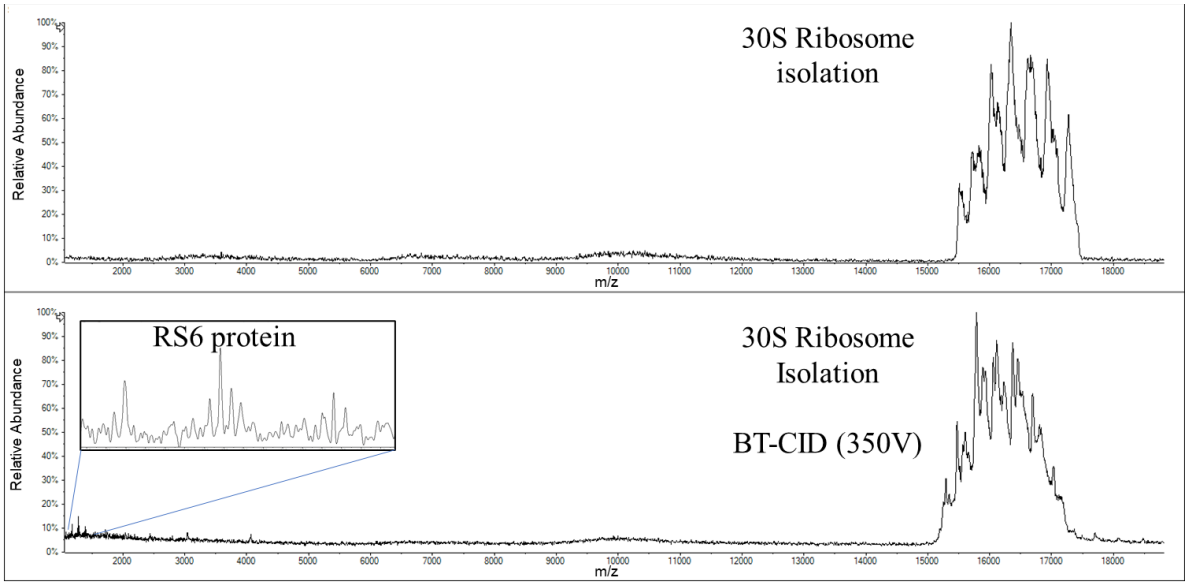

Figure 5.6. The mass spectrum of the isolated 30S precursor (top), and the BT-CID of that population (below).

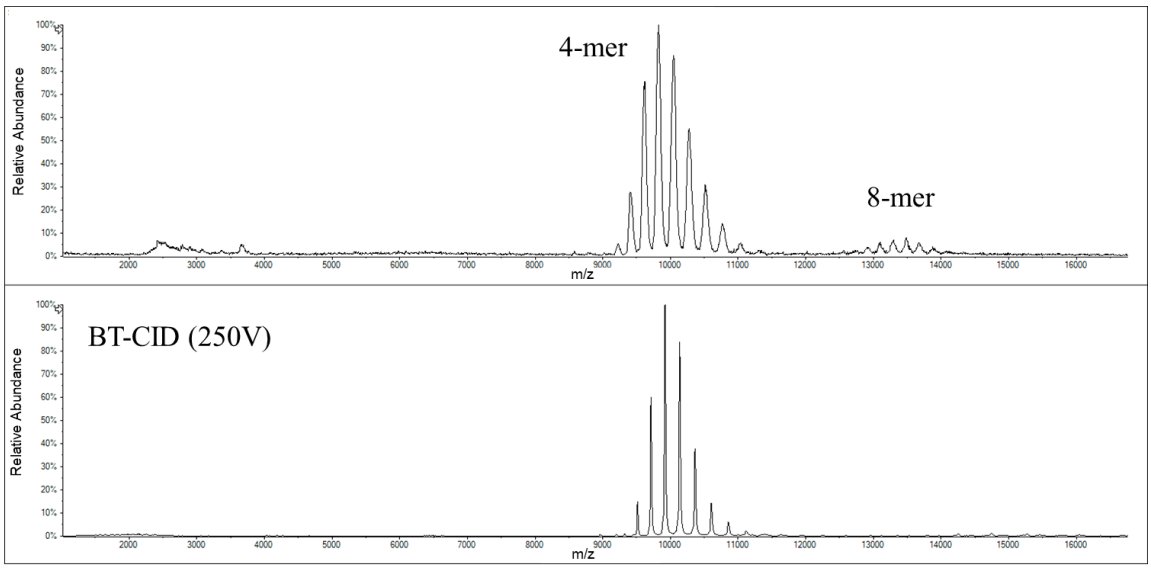

Figure 5.7. The mass spectrum of β-galactosidase (top), and the BT-CID of the precursor spectrum (below).

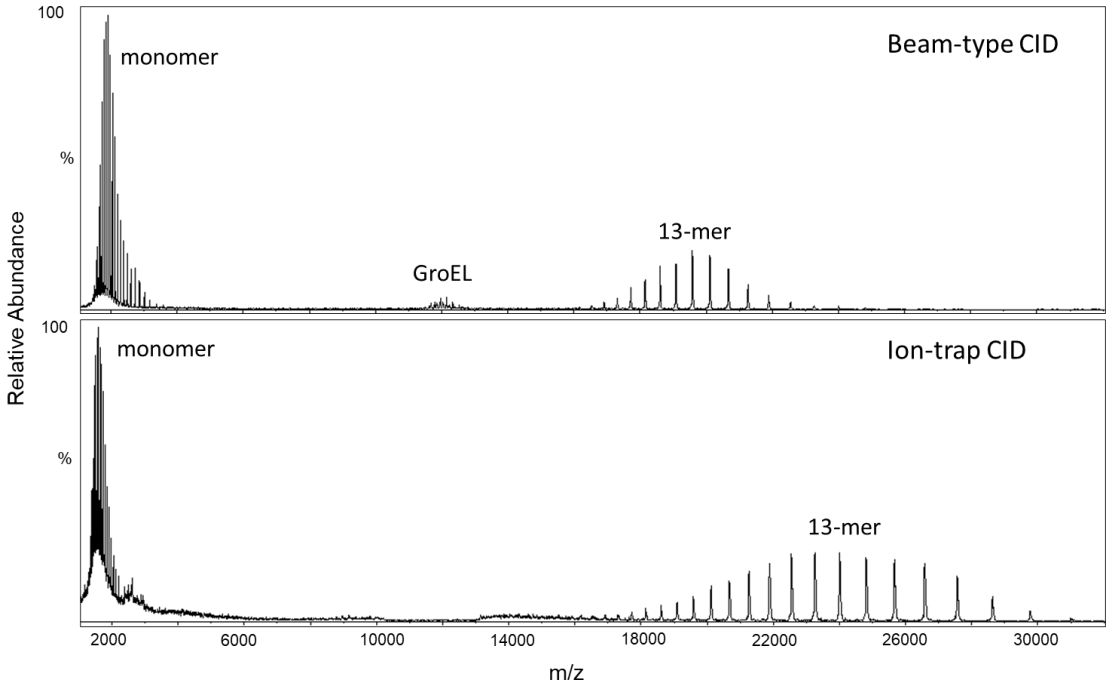

Figure 5.8. The mass spectra of BT-CID of GroEL (top) and the ion trap CID using SF_6 as the bath gas (bottom).

CHAPTER 6. PROTEIN COMPLEX SURFACE ANALYSIS USING MAMA-MIA AND CID

The improvements in the mass measurement and fragmentation efforts of large non-covalently bound systems have established native MS as an important complementary tool to other commonly used biophysical methods. However, there are certain difficulties with native MS ions, such as the potential overlap of charge states and the narrow charge state distributions that may preclude or prevent an accurate mass measurement. MAMA-MIA can address these problems by utilizing ion/ion reactions (see earlier chapters). A separate attempt at probing surface accessibility using MAMA-MIA will be the focus of this chapter.

6.1 Introduction

The ability for gas-phase analysis of proteins was demonstrated with electrospray ionization (ESI) (1). Shortly after this discovery, analyzing large systems such as viruses and ribosomes were attempted (2–4). This initiated a new field of MS, referred to as native MS, which corresponds to the native structure of ions in the condensed phase (5). Although native MS has shown great utility in structural characterization of large biomolecules, there are difficulties in the mass measurement because of narrow charge state distributions, which complicates the assignment of charge and, therefore, the mass (6). Moreover, when the charge states overlap because of severe salt adduction or heterogeneity, the assignment of charge and mass may be precluded altogether (7,8).

A separate aspect of native MS experiments, which extends beyond measuring the mass of the ions, is the ability to study the topology and the structural information of native ions. Utilizing ion mobility, in conjunction with native-ESI MS, to model the tertiary and quaternary structure of biomolecules has been previously demonstrated (9,10). In its simplest form, ion mobility works by separating ions across a drift tube, where the slowest ion has the most interactions with the bath gas, which prevents the forward momentum of the ions across a small potential gradient. Alternatively, another set of experiments uses deuterated-water as a reagent to study the surface of a protein. This approach relies on the rapid exchange of hydrogen to deuterium (HDX) at the amide site from a disordered region of a protein, such as one that is lacking hydrogen-bonding.

Tightly folded proteins are more protected from HDX, and therefore that exchange rate is abated (11,12).

The fragmentation of the complex has shown the ability to uncover the connectivity of the analyte. There are several different activation techniques such as photodissociation (13,14), surface induced dissociation (14,15) and electron transfer dissociation (17), but the gold standard is collision induced dissociation (3,18). Previous chapters of this dissertation have demonstrated the activation capabilities in our lab for native MS ions. After isolating and activating the MAMA-MIA product, we noticed an interesting observation. Depending on the reagent, the fragmentation of this product yielded a charge inverted reagent and charge reduced precursor, or the system fragmented, and the reagent was "sticky" enough to remain behind.

6.2 Experimental

6.2.1 Sample preparation for native mass spectrometry of bio-complexes

Hemoglobin and β-galactosidase were purchased from Sigma Aldrich. The lyophilized solid was reconstituted in water to create a stock solution at a concentration of 3 µM and 10 µM (calculated by using the mass of the tetramer), respectively. These samples underwent buffer exchange, via centrifugation, once with an ammonium acetate (Sigma Aldrich) buffer adjusted to pH 7 with ammonium hydroxide (Sigma Aldrich), using a 10 kilodalton (kDa) molecular weight cutoff (MWCO) Amicon Ultra 0.5 mL filter (Millipore Sigma). The recovered samples (15 µL) were diluted with the same buffer to achieve the same original concentration from the stock solutions.

GroEL (Sigma Aldrich) lyophilized powder preparation was described before in detail (19). Briefly, the sample was buffer exchanged and underwent acetone precipitation. The buffer exchange occurred via centrifugation with a 150 mM ammonium acetate (Sigma Aldrich) buffer adjusted to pH 7 with ammonium hydroxide (Sigma Aldrich), using a 10 kilodalton (kDa) molecular weight cutoff (MWCO) Amicon Ultra 0.5 mL filter (Millipore Sigma). The final recovered sample (~15 µL) was diluted with the same buffer to achieve 1 µM concentration from the stock solution.

6.2.2 Sample preparation for the reagent anions

Oxidized insulin chain A (IcA) from bovine pancreas (average mass, free acid = 2531.66 Da) was purchased from Sigma Aldrich. The lyophilized solid was reconstituted in water. The working solution was a 50:50 mixture of aqueous ammonium hydroxide (pH 11) and HPLC grade methanol (Sigma Aldrich) to give a final concentration of 25 µM. The most abundant charge states were $[IcA\text{-}5H]^{5-}$ and $[IcA\text{-}6H]^{6-}$. Bovine ubiquitin purchased from Sigma Aldrich was prepared in the similar manner. In experiments where a larger charge reduction was required, we utilized myoglobin from equine skeletal muscle (Sigma Aldrich). Holo-myoglobin (hMb) (average mass=17,567 Da), which retains the heme group, was prepared with piperidine (Sigma Aldrich). We isolated and used the two different charge states in the experiments shown in this manuscript. The final solution was 20 µM holo-myoglobin and 50 mM piperidine in water.

6.2.3 Ion-ion reactions in the mass spectrometer.

All experiments were performed using a QTOF 5600 (SCIEX), which was previously modified to allow for ion/ion reactions (20). The positive and negative ions were generated by utilizing an alternately pulsed nano-electrospray ionization source (nESI) (21). Mutual ion polarity trapping was enabled by applying a supplemental AC to the end plates of the linear ion trap reaction cell, q2. Multiply protonated protein cations and reagent anions were sequentially isolated before being stored in q2 to react over times of 50-100 ms. The reagent anions were isolated during Q1 transmission by conventional RF-DC apex isolation. The protein cations were too high in *m/z* to be isolated via conventional RF-DC apex isolation. Therefore, sequential resonance ejection ramps in q2 were used to eject ions of lower and higher *m/z* ratios that bordered the population of interest (22).

6.2.4 Native MS

The analyte ions were generated via nESI from separately pulsed borosilicate glass emitters. The large bio-complexes were sprayed in both positive and negative mode with approximately ±1200 V applied to a platinum wire, which was in contact with the solution. The reagent anions were sprayed in negative or positive mode, respectively, with an applied voltage of approximately ±1400 V. The large complex ions were initially injected into the instrument and isolated (see above)

and stored in q2. Nitrogen was used in q2 at pressures ranging from 6-8 mtorr. Due to the salt adduction on the large *m/z* ions, the difference in DC offsets of Q0 and q2 were increased to as high as 50-70 V to collisionally activate the ions upon injection into q2 to drive off weakly-bound adduct species.

6.3 Results and Discussions

6.3.1 Observation of a sticky reagent

The ability for MAMA-MIA to create space between adjacent states is paramount in its ability in ascertain mass information under non-favorable conditions, i.e. overlapping charge states from severe salt adduction and/or inherent heterogeneity. Our lab was interested in understanding more about the strength of the non-covalent bonding between the analyte and reagent, which forms a complex that survives detection. The general experimental workflow using GroEL as the native MS ion system can be seen in **Figure 6.1**, for insulin chain A as the reagent, and **Figure 6.2**, for holo-myoglobin as the reagent. The main features of this experiment involve the ion/ion reaction of the native MS ions with the oppositely charged reagent, and the subsequent isolation of the first attachment population. Our isolation technique has been mentioned previously, but in short, we performed isolation utilizing a fixed frequency and the sweeping of q2 RF to the *m/z* borders of the peaks of interest.

After isolating this 1st attachment population, we performed a back transfer of those ions to Q1, and then accelerated them back into our collision cell (q2) to effect beam-type CID. This is a high-energy technique that is described in an earlier chapter. In short, the ions undergo acceleration via a steep gradient of the ion optics, and once the ion reaches q2 multiple energetic collisions occur that induces fragmentation of the population if enough energy is imparted. The result of the fragmentation of the population of ions is dependent on the reagent used in the preceding ion/ion reaction. For the holo-myoglobin reagent, the BT-CID yields the loss of the reagent (at lower *m/z*) and the recovery of the precursor, albeit a charge reduced version (**Figure 6.3**, top). The most abundant charge state of the charge inverted reagent was 10+, which indicates a change in charge of 20 for the initial holo-myoglobin ion. The results for the insulin chain A reagent differed, as insulin chain A was not released upon excitation of the 1st attachment population (**Figure 6.3**, bottom). The insulin chain A remained on the 13-mer complex. The

increase in mass can be seen when comparing the zero-charge deconvolution of the 13-mer, from the GroEL precursor, and the 13-mer from the 1st attachment of GroEL/insulin chain A (**Figure 6.4**). The molecular weight difference is approximately 2700 Da which agrees with the mass of the insulin chain A (~2500 Da). The extra mass may be from extra salt adducts on the 13-mer complex.

To confirm that this phenomenon was reagent specific, we utilized two different reagents and performed the same experiments. The fragmentation result from using ubiquitin as the reagent was similar to the holo-myoglobin experiment (**Figure 6.5**). Spraying a negative GroEL analyte and using lysozyme as the charge reducing reagent, the fragmentation result was also similar to the holo-myoglobin experiment (data not shown). Moreover, we utilized a different analyte, β-galactosidase which, depending on the spray conditions, can form oligomers at various abundances (**Figure 6.6**). The 1st attachment population fragmentation results from the 4-mer and 8-mer of β-galactosidase with holo-myoglobin can be seen in **Figure 6.7** and **Figure 6.8**, respectively. The holo-myoglobin dissociates from the β-galactosidase after activating the 1st attachment population. The experiment with β-galactosidase, and insulin chain A as the reagent, did not yield any fragments, even upon our harshest conditions (data not shown).

Consequently, insulin chain A appeared to be the only reagent we have used that did not break apart from the protein complex after activation. The insulin chain A sample is the fully oxidized version with four sulfonic acids. Conversely, the other reagents utilized were deprotonated at the carboxylic acid sites. The difference in the interaction strength (23) between carboxylates and sulfonates can be seen in **Figure 6.9**. This implies that the sulfonates are "stickier" than the carboxylates, and thus, possibly, opens a new direction of research, such as studying the surface accessibility of a hetero-complex using MAMA-MIA.

6.3.2 Hemoglobin

Hemoglobin is a hetero-tetramer that is responsible for oxygen transport in red blood cells (24). This protein consists of two separate components, the α and β that form clusters around a heme group (25). The mass spectrum of hemoglobin consists of a dimer and tetramer, where the latter has 4 heme groups associated with the complex. The CID fragmentation of the entire population of peaks, the dimer and tetramer, yield a convoluted spectrum with monomer, dimer, trimer and residual tetramer overlapping (**Figure 6.10**). Isolating out a single tetramer charge state

simplifies the mass spectrum interpretation, and the typical monomer and N-1mer is observed (**Figure 6.11**). The MAMA-MIA reaction with that isolated hemoglobin peak and insulin chain A with the subsequent isolation of the 1st attachment can be seen in **Figure 6.12**. The fragmentation of that population yields a distribution of monomers and trimers **Figure 6.13**. The zero-charge deconvolution indicates the presences of both α and β monomers along with the addition of an insulin chain A attached to each subunit. The percentage of holo-α (with insulin chain A) and apo-α is ~15% and the percentage of holo-β and apo-β is ~23%. This is calculated by utilizing the abundances of the zero-charge deconvolution for each population. The β-subunit is larger in mass, and presumably surface area, than the α-subunit. Consequently, there may be more accessibility for the insulin chain A to preferentially attach to the β-subunit. This work is at an early stage, but this technique shows promise in being able to probe surface area of hetero-complexes.

6.4 Conclusion

The utility of MAMA-MIA extends beyond the mass measurement of native MS ions. The use of a reagent, such as insulin chain A, that can survive subsequent activation can be useful in understand surface accessibility of hetero-complexes. The future direction of this project is ideally utilizing a system that has a buried component that differs from the surface proteins. The expected result would be that the insulin chain A would not attach to that buried component upon complex fragmentation. This would give the proof of concept for this surface analysis methodology.

6.5 References

1. Fenn J.B. et al.: Electrospray ionization for mass spectrometry of large biomolecules.: Science 246. 64–71 (1989).

2. Rostom A.A. and Robinson C.V.: Detection of the Intact GroEL Chaperonin Assembly by Mass Spectrometry.: J. Am. Chem. Soc. 121. 4718–4719 (1999).

3. Rostom A.A. et al.: Detection and selective dissociation of intact ribosomes in a mass spectrometer.: Proc. Natl. Acad. Sci. U. S. A. 97. 5185–5190 (2000).

4. Tito M.A. et al.: Electrospray Time-of-Flight Mass Spectrometry of the Intact MS2 Virus Capsid.: J. Am. Chem. Soc. 122. 3550–3551 (2000).

5. Leney A.C. and Heck, A.J.R.: Native Mass Spectrometry: What is in the Name?: J. Am. Soc. Mass Spectrom. 28. 5–13 (2017).

6. Liepold L. et al.: Correct Charge State Assignment of Native Electrospray Spectra of Protein Complexes.: J. Am. Soc. Mass Spectrom. 20. 435–442 (2009).

7. Snijder J. et al.: Studying 18 MDa Virus Assemblies with Native Mass Spectrometry.: Angew. Chem. Int. Ed. 52. 4020–4023 (2013).

8. Abdillahi A.M. et al.: Mass Analysis of Macro-molecular Analytes via Multiply-Charged Ion Attachment.: Anal. Chem. 92. 16301–16306 (2020).

9. Politis A. et al.: Integrating Ion Mobility Mass Spectrometry with Molecular Modelling to Determine the Architecture of Multiprotein Complexes.: PLOS ONE 5. e12080 (2010).

10. Hall Z. et al.: Structural Modeling of Heteromeric Protein Complexes from Disassembly Pathways and Ion Mobility-Mass Spectrometry.: Structure 20. 1596–1609 (2012).

11. Konermann L. et al.: Hydrogen exchange mass spectrometry for studying protein structure and dynamics.: Chem. Soc. Rev. 40. 1224–1234 (2011).

12. Engen J.R.: Analysis of Protein Conformation and Dynamics by Hydrogen/Deuterium Exchange MS.: Anal. Chem. 81. 7870–7875 (2009).

13. Greisch J.-F. et al.: Expanding the mass range for UVPD-based native top-down mass spectrometry.: Chem. Sci. 10. 7163–7171 (2019).

14. Lee K.W. et al.: Digital ion trap mass analysis of high mass protein complexes using IR activation coupled with ion/ion reactions.: Int. J. Mass Spectrom. 458. 116437 (2020).

15. Panczyk E.M. et al.: Surface-Induced Dissociation of Protein Complexes Selected by Trapped Ion Mobility Spectrometry.: Anal. Chem. 93. 5513–5520 (2021).

16. Snyder D.T. et al.: Tandem surface-induced dissociation of protein complexes on an ultrahigh resolution platform.: Int. J. Mass Spectrom. 461. 116503 (2021).

17. Lermyte F. et al.: ETD Allows for Native Surface Mapping of a 150 kDa Noncovalent Complex on a Commercial Q-TWIMS-TOF Instrument.: J. Am. Soc. Mass Spectrom. 25. 343–350 (2014).

18. van de Waterbeemd M. et al.: High-fidelity mass analysis unveils heterogeneity in intact ribosomal particles.: Nat. Methods 14. 283–286 (2017).

19. Zhou M. et al.: Dissecting the large noncovalent protein complex GroEL with surface-induced dissociation and ion mobility-mass spectrometry.: Anal. Chem. 85. 8262–8267 (2013).

20. Xia Y. et al.: Mutual storage mode ion/ion reactions in a hybrid linear ion trap.: J. Am. Soc. Mass Spectrom. 16. 71–81 (2005).

21. Liang X. et al.: Alternately Pulsed Nanoelectrospray Ionization/Atmospheric Pressure Chemical Ionization for Ion/Ion Reactions in an Electrodynamic Ion Trap.: Anal. Chem. 78. 3208–3212 (2006).

22. McLuckey S.A. et al.: Selective ion isolation/rejection over a broad mass range in the quadrupole ion trap.: J. Am. Soc. Mass Spectrom. 2. 11–21 (1991).

23. Shih M. and McLuckey S.A.: Ion/ion charge inversion/attachment in conjunction with dipolar DC collisional activation as a selective screen for sulfo- and phosphopeptides.: Int. J. Mass Spectrom. 444. 116181 (2019).

24. Schechter A.N.: Hemoglobin research and the origins of molecular medicine.: Blood 112. 3927–3938 (2008).

25. Zhang J. et al.: Native Top-Down Mass Spectrometry for the Structural Characterization of Human Hemoglobin.: Eur. J. Mass Spectrom. Chichester Engl. 21. 221–231 (2015).

6.6 Figures

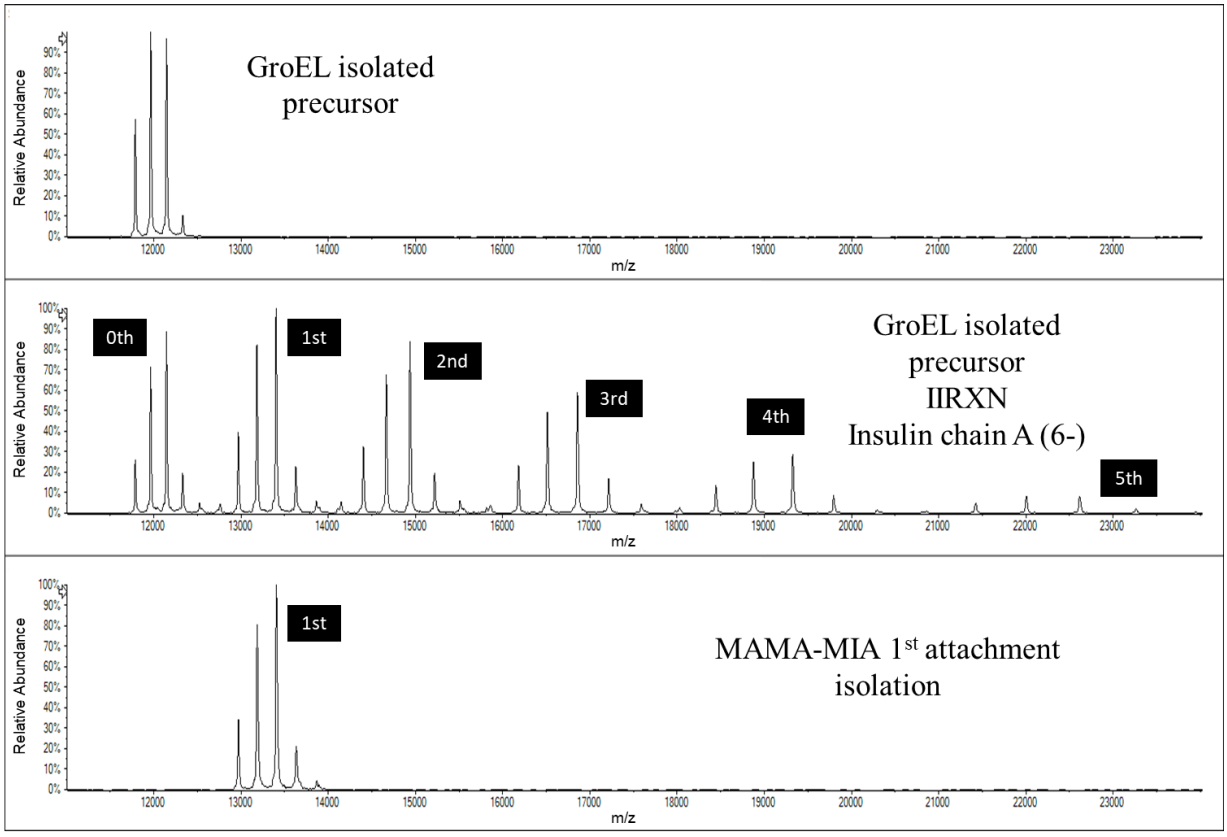

Figure 6.1. The mass spectra of a slightly isolated population of GroEL (top), an ion/ion reaction of that precursor and insulin chain A (middle) and the isolated 1st attachment population (bottom).

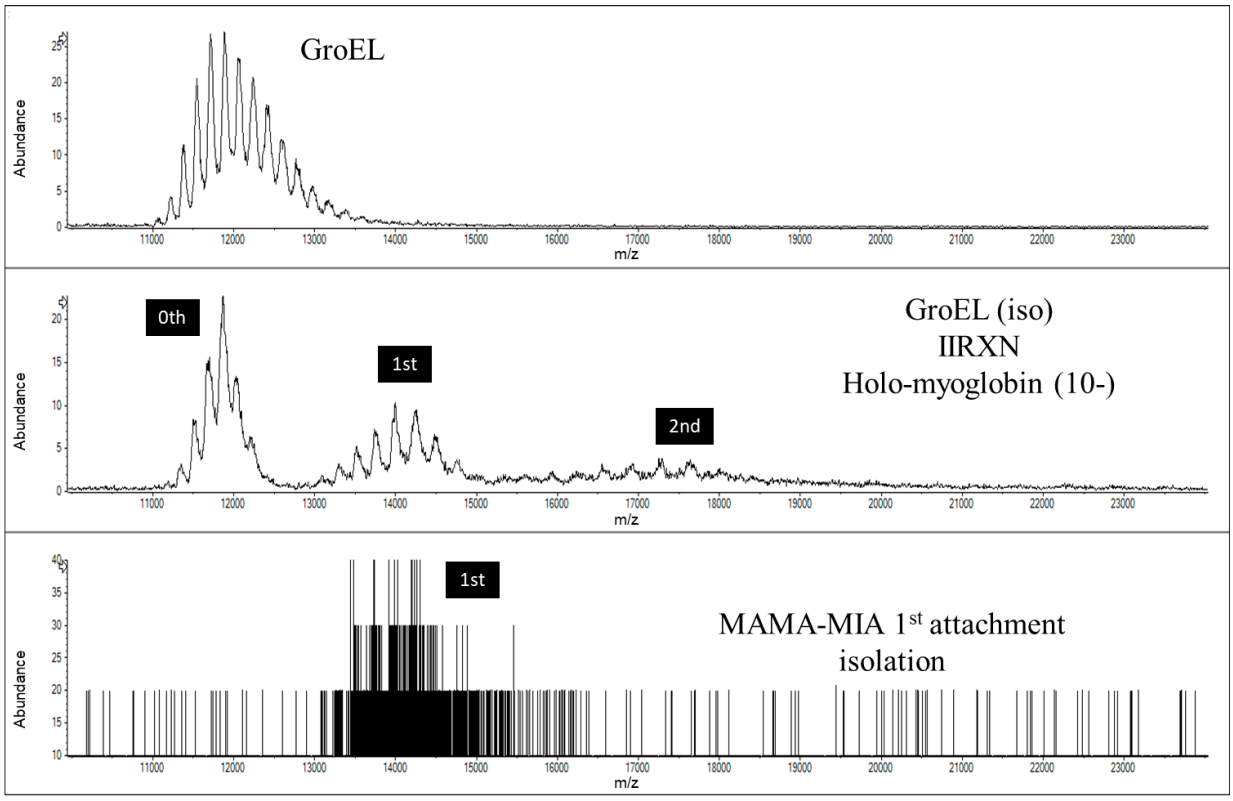

Figure 6.2. The mass spectra of GroEL (top), an ion/ion reaction of a slightly isolated population of GroEL precursor and holo-myoglobin (middle) and the isolated 1st attachment population which did not have enough signal to smooth (bottom).

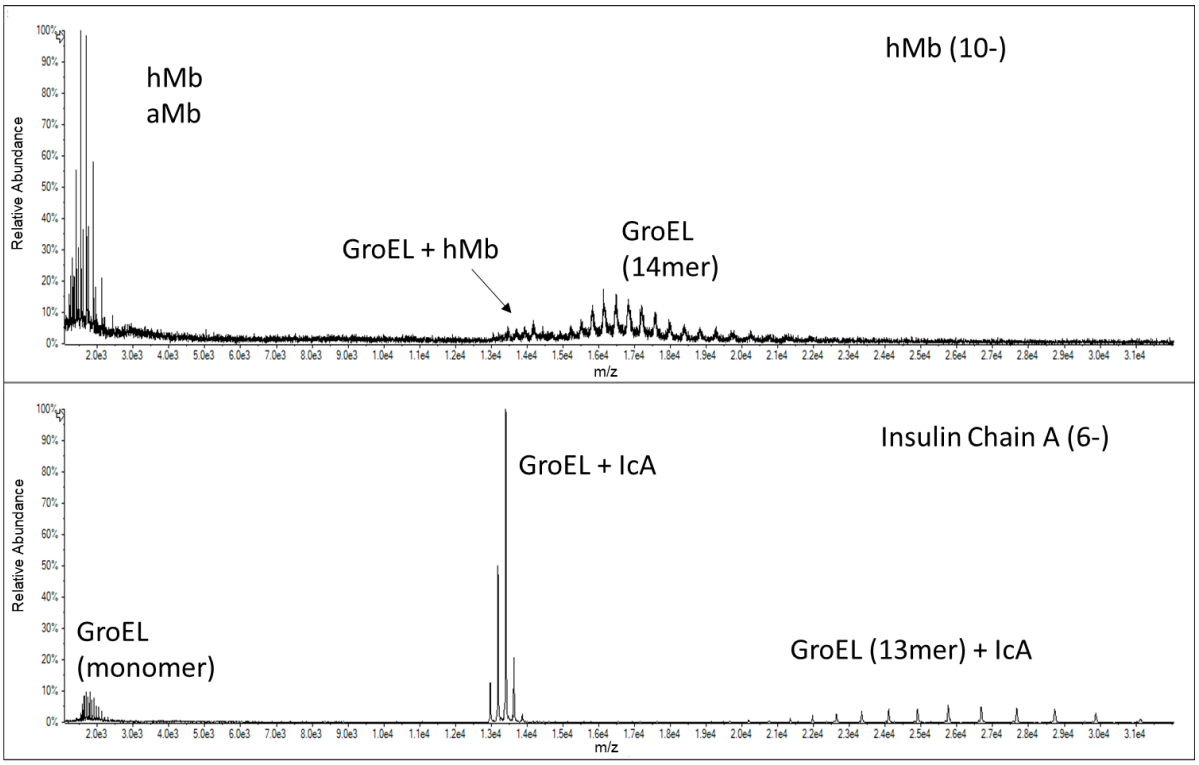

Figure 6.3. The fragmentation spectra of the 1st attachment population using holo-myoglobin (top) and insulin chain A (bottom) as the MAMA-MIA reagents.

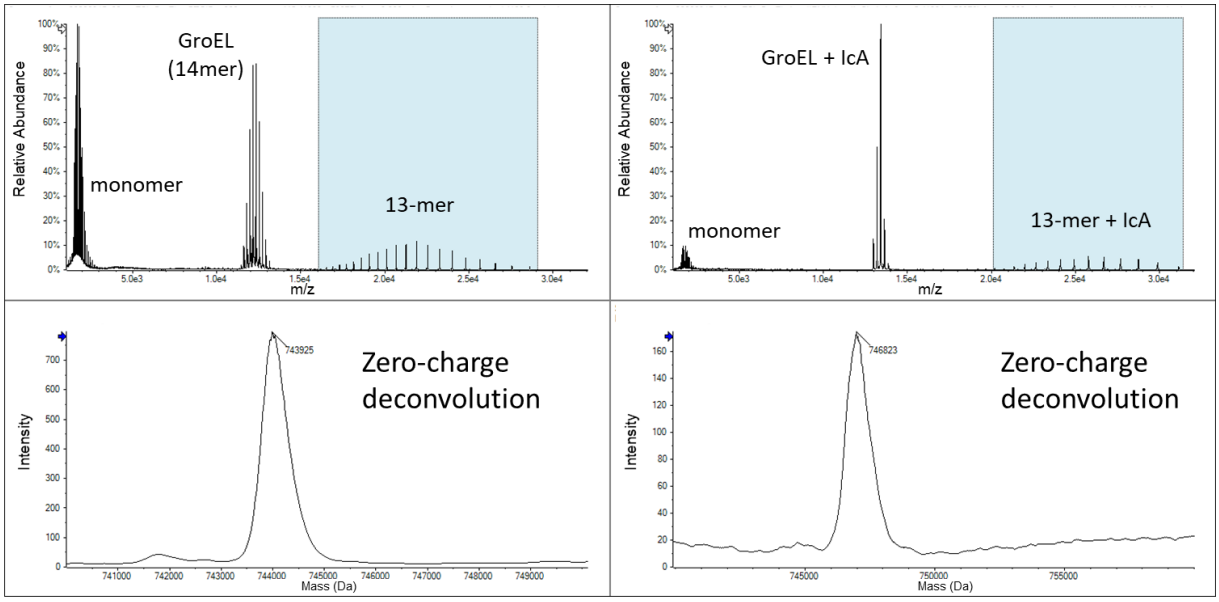

Figure 6.4. The MS/MS spectra, and the respective zero-charge deconvolution of the 13-mer, for GroEL precursor (left column), and the 1st attachment MAMA-MIA population using insulin chain A as the reagent (right column).

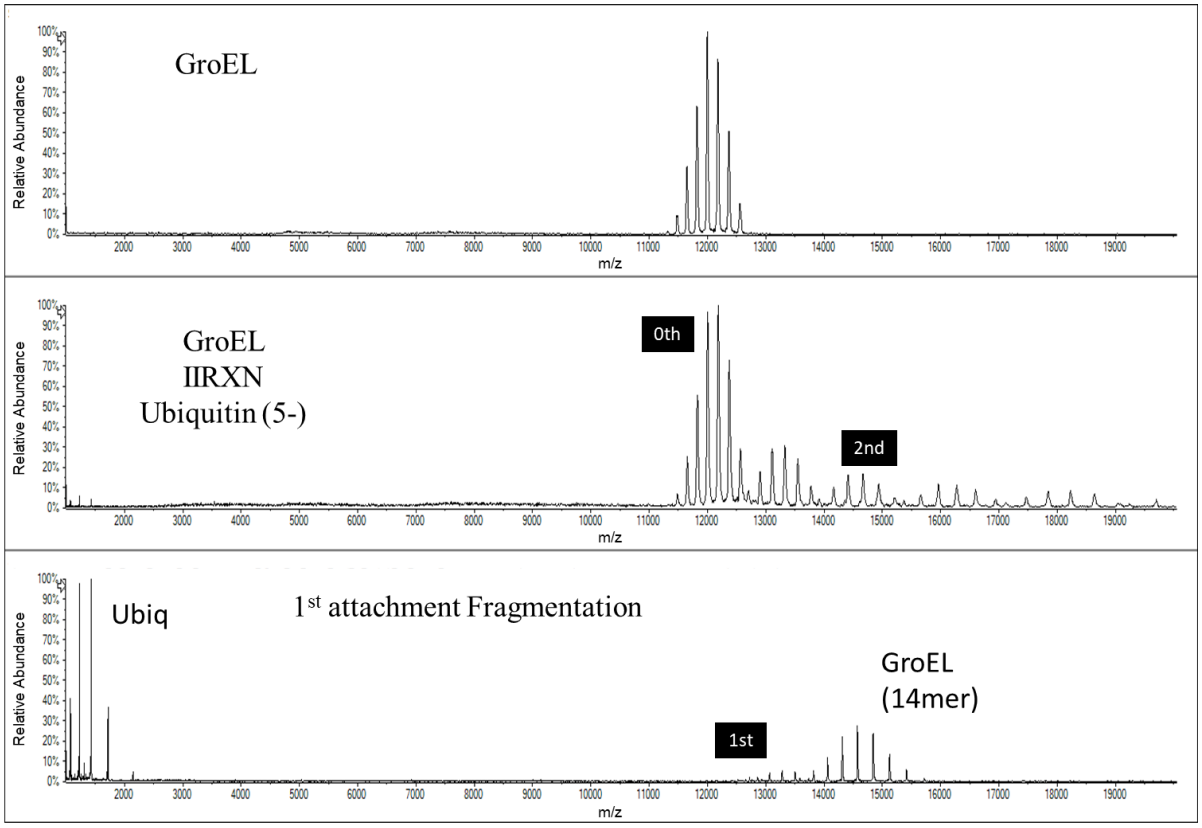

Figure 6.5. The mass spectra of GroEL (top), an ion/ion reaction of GroEL precursor and ubiquitin (middle) and the BT-CID fragmentation of the isolated 1st attachment population (bottom).

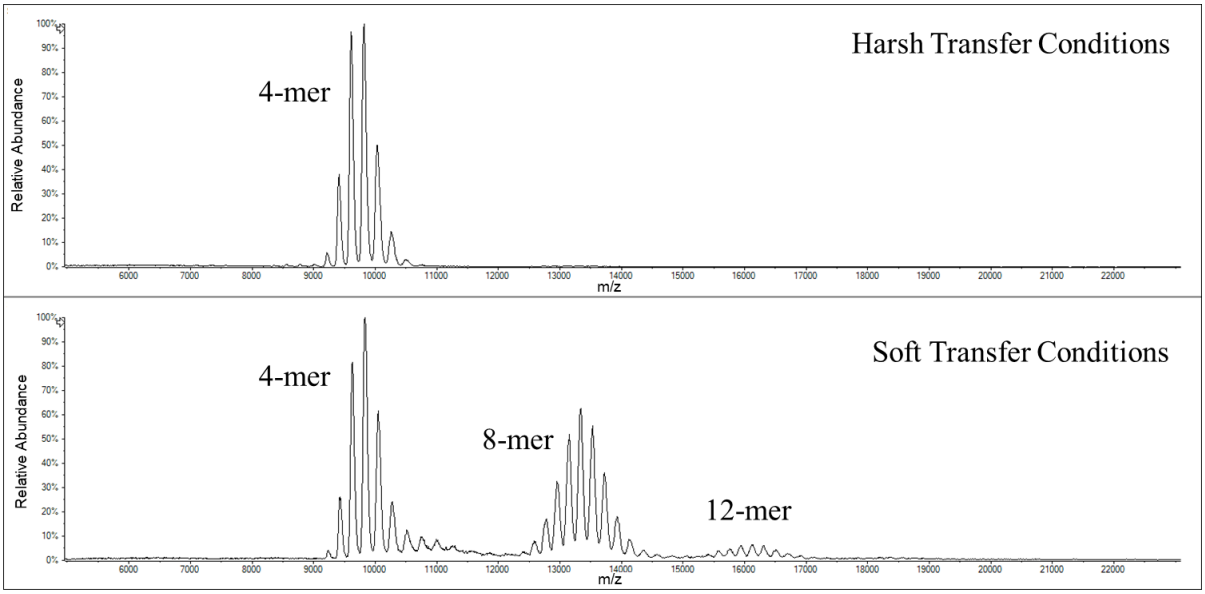

Figure 6.6. The mass spectra and effects of harsh (top) and soft (bottom) transfer conditions for β-galactosidase.

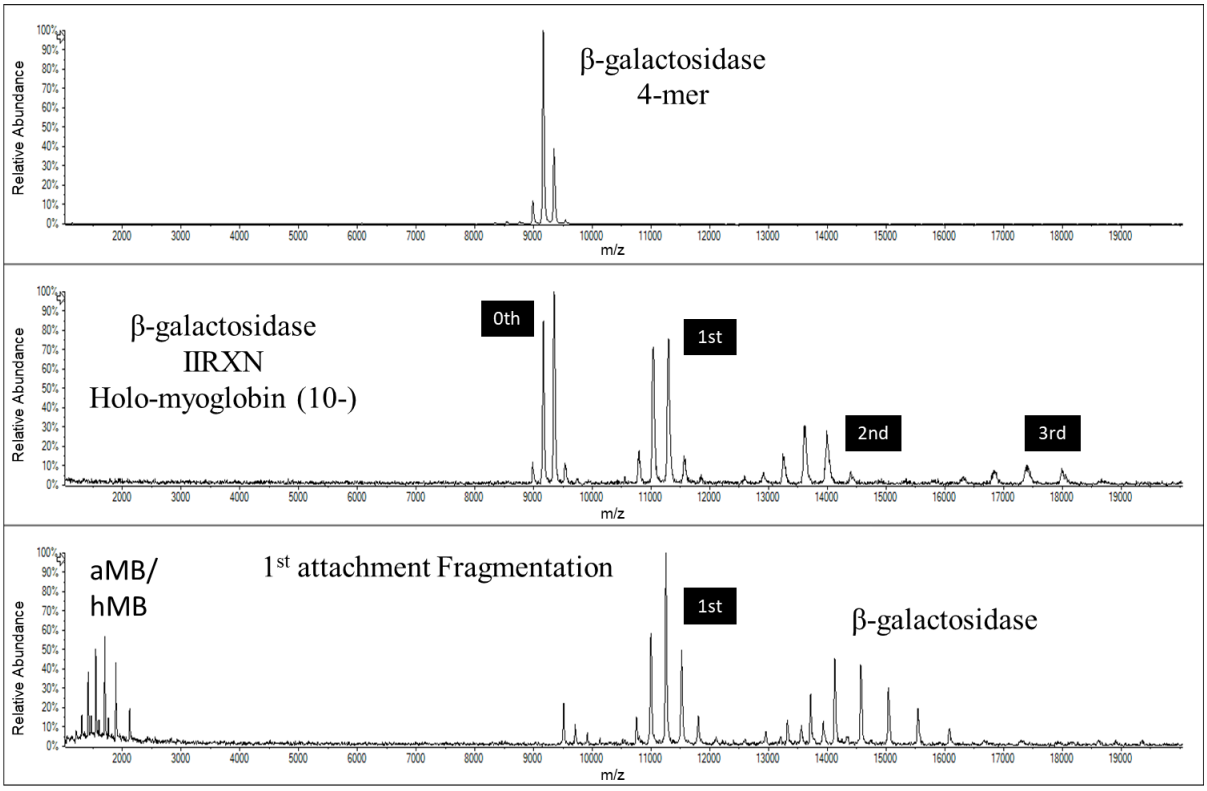

Figure 6.7. The mass spectra of β-galactosidase 4-mer (top), an ion/ion reaction of β-galactosidase 4-mer precursor and holo-myoglobin (middle) and the BT-CID fragmentation of the isolated 1st attachment population (bottom).

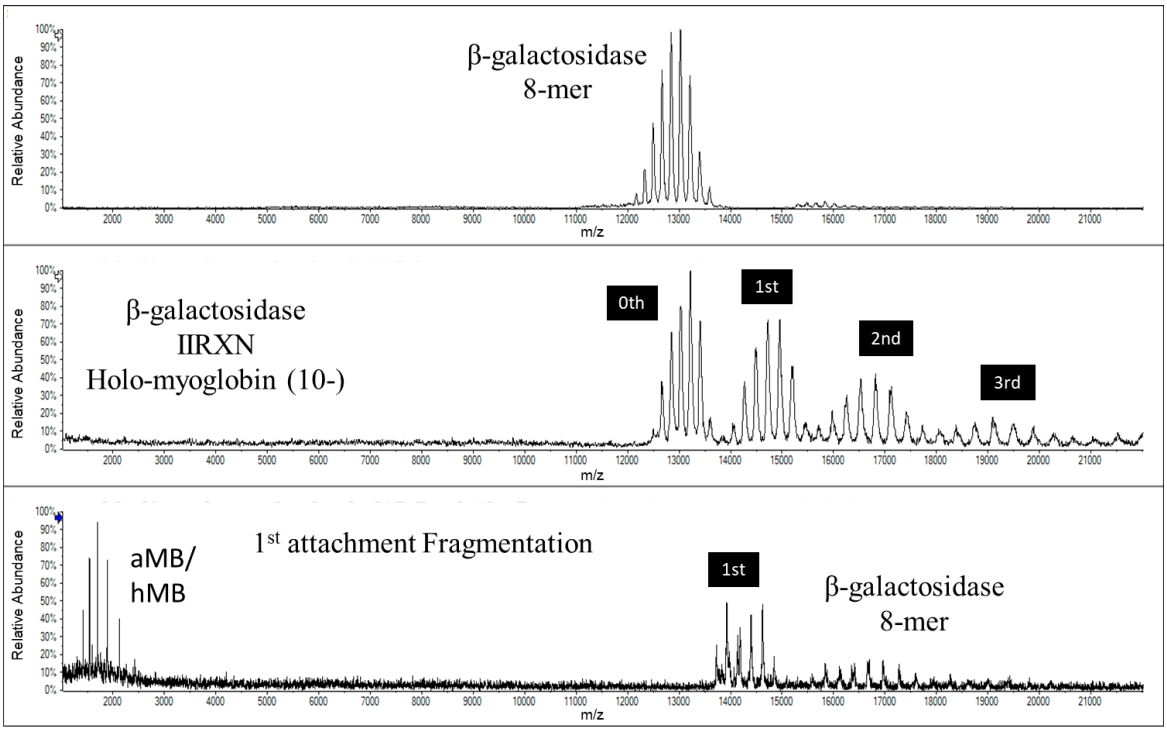

Figure 6.8. The mass spectra of β-galactosidase 8-mer (top), an ion/ion reaction of β-galactosidase 8-mer isolated precursor and holo-myoglobin (middle) and the BT-CID fragmentation of the isolated 1st attachment population (bottom).

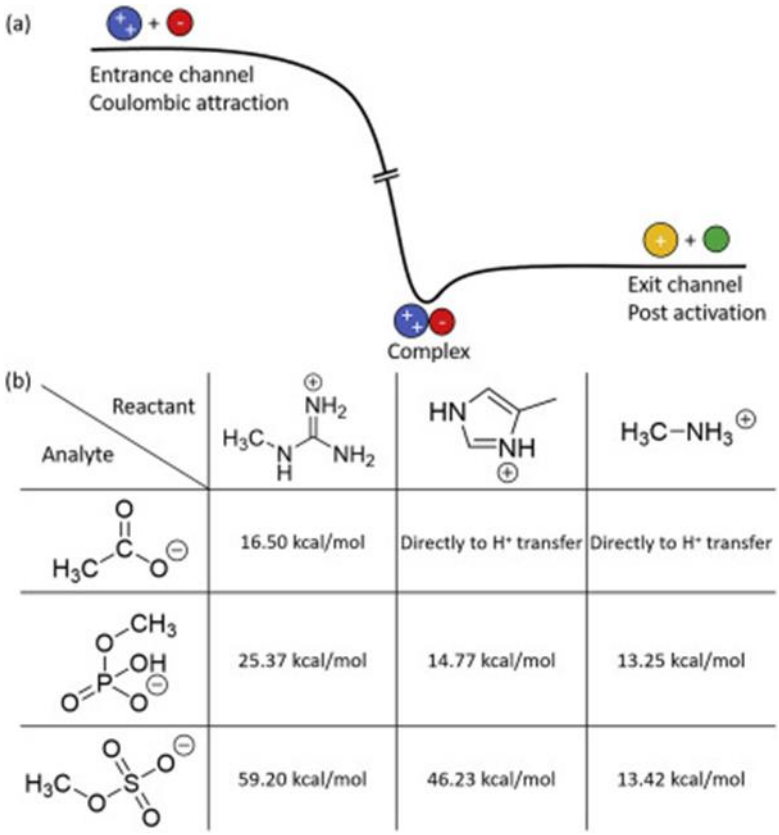

Figure 6.9. A generic energy diagram for proton transfer reaction (a), and the interaction strength between three basic groups and 3 reactant groups (b). Reproduced from Shih M. and McLuckey, S.A., Int. J. Mass Spectrom. 444. 116181 (2019).

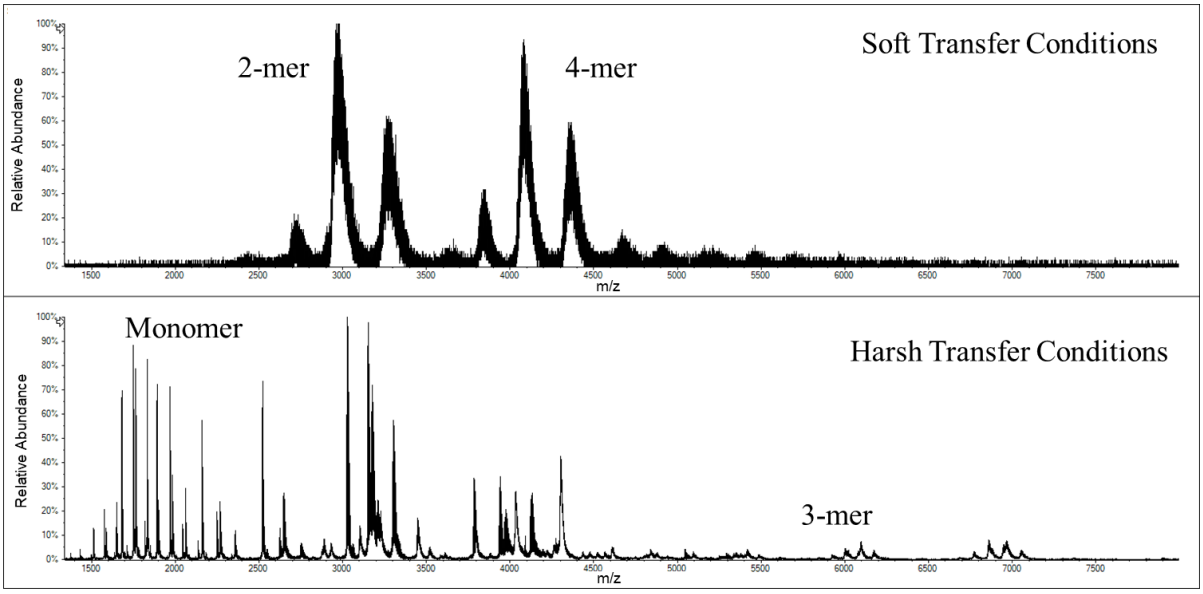

Figure 6.10. The mass spectrum of hemoglobin with soft conditions (top) and harsh transfer conditions (bottom).

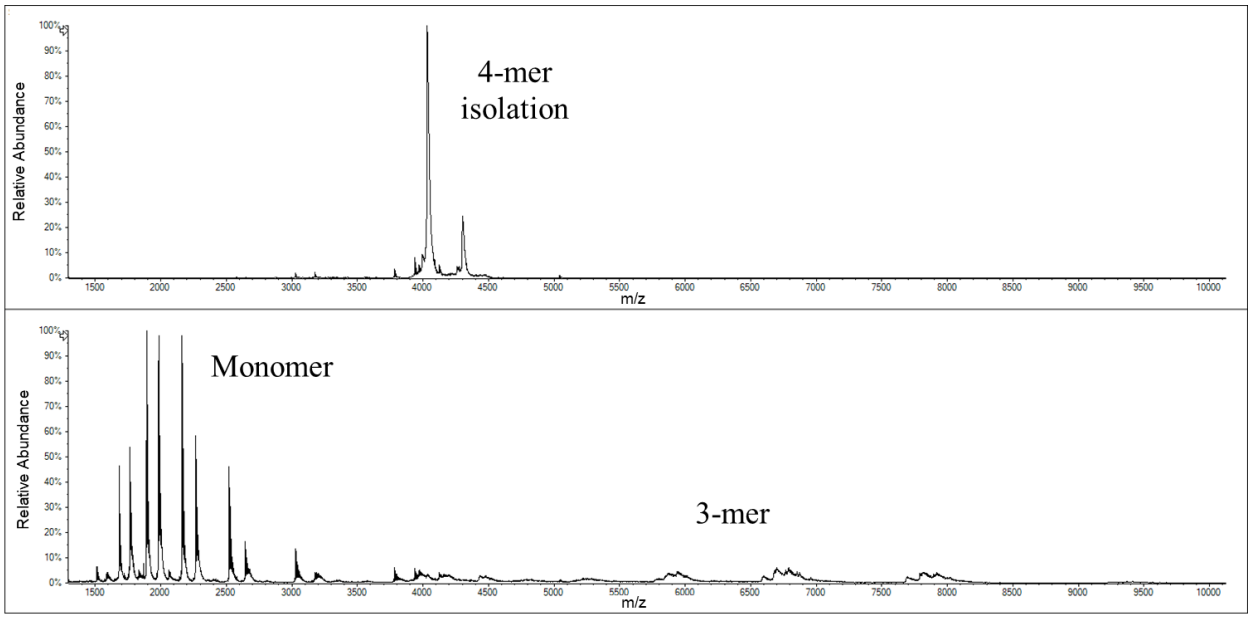

Figure 6.11. The mass spectrum of hemoglobin with tetramer isolation (top) and the BT-CID of that precursor (bottom).

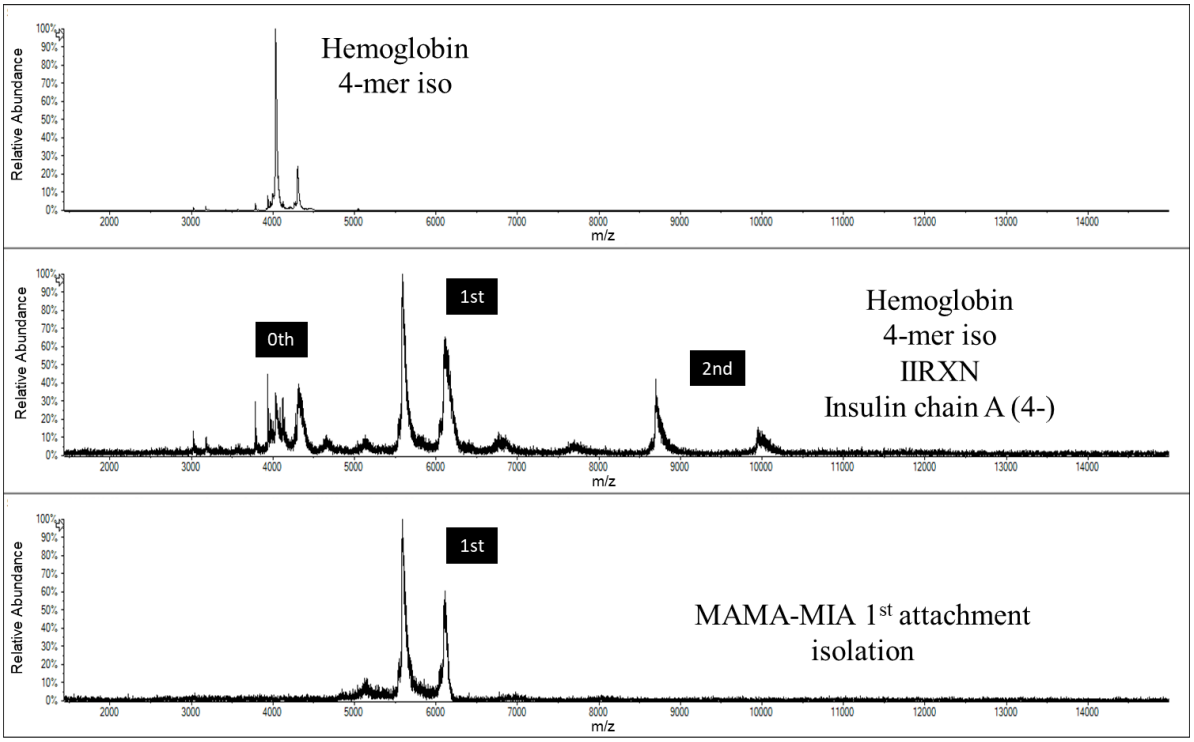

Figure 6.12. The mass spectra of hemoglobin 4-mer isolation (top), an ion/ion reaction of that precursor and insulin chain A (middle) and the isolated 1st attachment population (bottom).

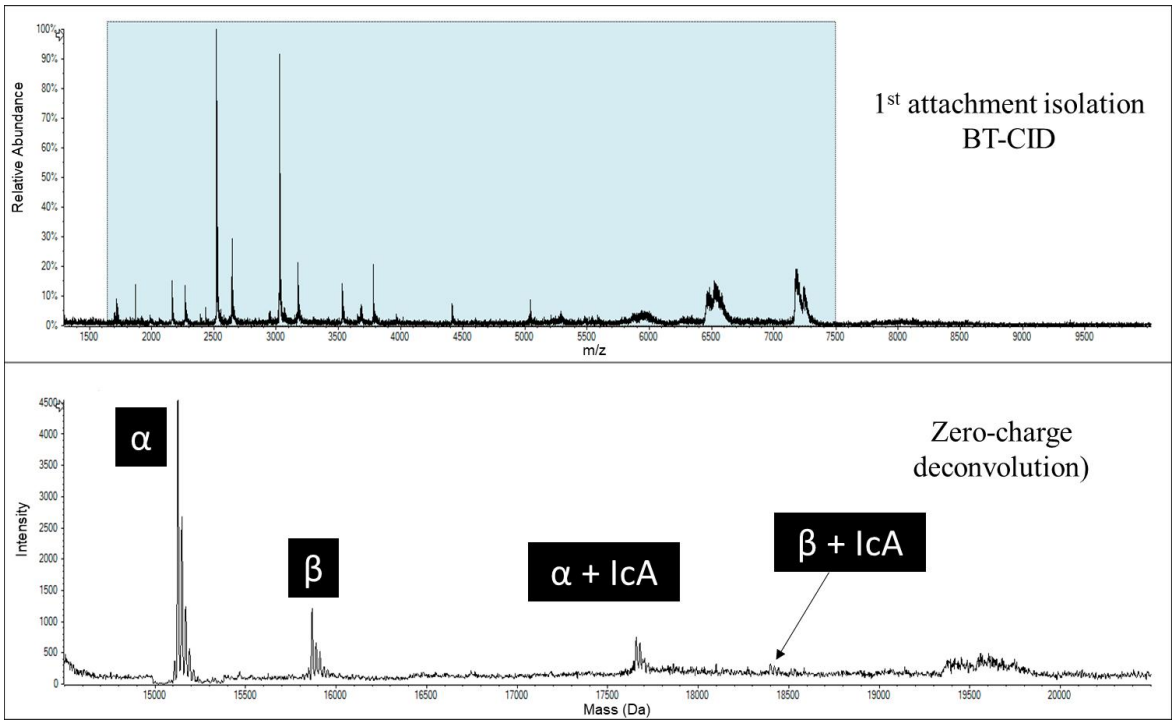

Figure 6.13. The BT-CID of the isolated 1st MAMA-MIA attachment of hemoglobin/insulin chain A (top) and the zero-charge deconvolution (bottom) of the shaded region.

CHAPTER 7. DEVELOPMENT OF NEGATIVE MODE MAMA-MIA

This chapter is a continuation of our MAMA-MIA development that focuses on the use of negative mode electrospray ionization (ESI) of the analyte. Consequently, we can access higher charge states with the use of a cationic reagent. With the employment of this negative mode strategy of MAMA-MIA, we have uncovered several populations of the *E. coli* ribosome that have not previously been mentioned in literature.

7.1 Introduction

Native MS, an approach intended to preserve large non-covalently bound complexes, pushed the capabilities of ESI to analyze large systems. Typically, nMS utilizes positive mode ionization with charge-reducing reagents, which can form adducts to broaden each peak. Previous studies have noted that negative mode ionization is more suitable for some nMS studies (1,2). However, the possibility of very broad peaks (i.e., the notorious blob), due to extensive salt adduction, heterogeneity and incomplete desolvation, may still preclude the resolution needed to assign charge states in the negative mode. Several approaches to the mass measurement of native MS ions have been described in earlier chapters (see chapter 3 introduction).

We have an approach, described in chapter 3, which uses ion/ion reaction chemistry to separate adjacent peaks wide enough to ascertain a mass measurement. In short, a population of the cationic analytes are isolated and reacted with an anionic reagent to form long-lived products that span across a wide *m/z*, while creating sufficient spacing between adjacent peaks to measure an accurate charge assignment of the precursor. This chapter presents negative MAMA-MIA, which has some advantages, such as the lowering of the average charge state, which is certainly noticeable for protein complexes. For example, the charge state distribution of GroEL varies depend on the ionization polarity (**Figure 7.1**). The most abundant charge state of GroEL lowers by 8 charges when employing negative mode ESI, which is already an improvement in facilitating resolution of neighboring charge states. However, this is not true for all analytes. For example, the charge state distribution of *E. coli* ribosome subunits, which consists of proteins and ribonucleic acids, are slightly higher charged in the negative mode spectrum (**Figure 7.2**).

7.2 Experimental

7.2.1 Sample preparation for native mass spectrometry of bio-complexes

GroEL (Sigma Aldrich) lyophilized powder preparation was described before in detail (3). Briefly, the sample was buffer exchanged and underwent acetone precipitation. The buffer exchange occurred via centrifugation with a 150 mM ammonium acetate (Sigma Aldrich) buffer adjusted to pH 7 with ammonium hydroxide (Sigma Aldrich), using a 10 kilodalton (kDa) molecular weight cutoff (MWCO) Amicon Ultra 0.5 mL filter (Millipore Sigma). The final recovered sample (~15 µL) was diluted with the same buffer to achieve 1 µM concentration from the stock solution.

E. coli 70S ribosome solution was purchased from New England Biolabs. The original sample, with an initial concentration of 13 µM, was constituted in a buffer containing 10 mM magnesium acetate, which is necessary for the 70S ribosome to be intact in the condensed phase. The sample preparation for the working solutions was described in detail previously (4) and modified accordingly. Briefly, the stock solution was buffer exchanged 8 times with 150 mM ammonium acetate and 10 mM magnesium acetate (Sigma Aldrich) at pH 7.4 with the same filter mentioned above. The sample was then diluted with 150mM ammonium acetate buffer at pH 7.4 to obtain a final concentration of 0.5 mM Mg^{2+} for the working solution.

7.2.2 Sample preparation for the reagent anions

The reagents ubiquitin and carbonic anhydrase were purchased from Sigma Aldrich. The lyophilized solid of each reagent was reconstituted in equal parts of H_2O:Methanol with 1% glacial acetic acid at 10 µM concentrations. Denaturing conditions were used to ensure higher charge state formation.

7.2.3 Ion-ion reactions in the mass spectrometer.

All experiments were performed using a QTOF 5600 (SCIEX), which was previously modified to allow for ion/ion reactions (5). The positive and negative ions were generated by utilizing an alternately pulsed nano-electrospray ionization source (nESI) (6). Mutual ion polarity trapping was enabled by applying a supplemental AC to the end plates of the linear ion trap reaction cell, q2. Multiply deprotonated protein anions and reagent cations were sequentially

isolated before being stored in q2 to react over times of 50-100 ms. The reagent anions were isolated during Q1 transmission by conventional RF-DC apex isolation. The protein cations were too high in *m/z* to be isolated via conventional RF-DC apex isolation. Therefore, sequential resonance ejection ramps in q2 were used to eject ions of lower and higher *m/z* ratios that bordered the population of interest (7).

7.2.4 Native MS

The analyte ions were generated via nESI from separately pulsed borosilicate glass emitters. The large bio-complexes were sprayed in negative mode with approximately -1200 V applied to a platinum wire, which was in contact with the solution. The reagent cations were sprayed in positive mode with an applied voltage of approximately +1400 V. The large complex ions were initially injected into the instrument and isolated (see above) and stored in q2. Nitrogen was used in q2 at pressures ranging from 6-8 mtorr. Due to the salt adduction on the large *m/z* ions, steep gradients ranging from 50-70 V to collisionally activate the ions upon injection into q2 to drive off weakly-bound adduct species.

7.3 Results and Discussions

The *E. coli* ribosome is molecular machine that consist of two subunits, the 30S and the 50S. Previous results from positive mode MAMA-MIA for the ribosome can be seen in chapter 3. For the 30S and 50S ribosome, we measured extra populations that were in low abundance for the precursors (8). However, there was missing information from our 30S ribosome, such as the 5kDa stationary-phase protein that was attached to each population of the 30S subunit, albeit under low abundances, in previous studies using an orbitrap (4). Our set of experiments using the 30S ribosome in the negative mode has revealed the presence of this low-level population (**Figure 7.3**). This was possible because we were able to generate 4 attachments, whereas previous results in the positive mode generated 3 attachments. The ubiquitin reagent had far more signal in the isolated 10+ charge state than the previously used myoglobin (10-) charge state, which allowed for more attachments without unfavorably increasing the fill time of the reagent. Lower spray time for the reagent minimizes the probability of clogging the analyte tip, which is a common issue with native

MS experiments. This 4th attachment was increased by filling the trap with more ubiquitin cation reagent, to generate the inset in **Figure 7.3**.

The most impressive results were from the negative mode MAMA-MIA of the 50S subunit. Previously, we measured 2 populations under low magnesium concentrations (8). The results from the 50S ribosome anions can be seen in **Figure 7.4**. We were able to generate a 6th attachment population from the precursor, as opposed to the 4 attachments in our positive mode workflow (chapter 3). This is an extra 20 charges that were reduced in this set of experiments, which was enough to resolve 5 separate populations that were previously overlapped. We did not observe the mass of a fully intact 50S ribosome, so the mass configuration of the 5 populations is difficult. However, we set a provisional mass for the intact species which is approximately 3% higher in mass than the theoretical molecular weight of the 50S subunit, which is common in native MS experiments due to salt adducts. The assignments for the 30S and 50S populations can be seen in **Figure 7.5**. A negative mode MAMA-MIA experiment with the 70S ribosome shows the true strength of this technique. Prior to the reaction, the precursor charge states overlap, and no mass information can be attained from the spectrum. After isolating a segment from the 70S population and reacting with carbonic anhydrase (30+), we can space adjacent peaks by more than 60 charges after two attachments. An overlay of a simulated/calculated spectrum indicates that the mass measurement of the 70S ribosome is approximately 2.3 MDa (**Figure 7.6**).

7.4 Conclusion

We demonstrate that MAMA-MIA using a cationic reagent and a negatively charge complex under native conditions generates similar results to the positive mode MAMA-MIA. The major benefit to utilizing negative mode MAMA-MIA is the accessibility of higher charged cationic reagents, which can generate wider steps in the *m/z* axis. This has been demonstrated with the highly heterogenous *E. coli* ribosome system. We were able to measure low-level populations for the 30/50S subunits by generating product peaks above *m/*z 100k. Moreover, a mass measurement of the 70S under conditions of severe overlap was done with two attachments of a 30+ carbonic anhydrase.

7.5 References

1. Harvey S.R. et al.: Surface-Induced Dissociation of Anionic vs Cationic Native-Like Protein Complexes.: J. Am. Chem. Soc. 143. 7698–7706 (2021).

2. Liko I. et al.: Negative Ions Enhance Survival of Membrane Protein Complexes.: J. Am. Soc. Mass Spectrom. 27. 1099–1104 (2016).

3. Zhou M. et al.: Dissecting the large noncovalent protein complex GroEL with surface-induced dissociation and ion mobility-mass spectrometry.: Anal. Chem. 85. 8262–8267 (2013).

4. van de Waterbeemd M. et al.: High-fidelity mass analysis unveils heterogeneity in intact ribosomal particles.: Nat. Methods 14. 283–286 (2017).

5. Xia Y. et al.: Mutual storage mode ion/ion reactions in a hybrid linear ion trap.: J. Am. Soc. Mass Spectrom. 16. 71–81 (2005).

6. Liang X. et al.: Alternately Pulsed Nanoelectrospray Ionization/Atmospheric Pressure Chemical Ionization for Ion/Ion Reactions in an Electrodynamic Ion Trap.: Anal. Chem. 78. 3208–3212 (2006).

7. McLuckey S.A. et al.: Selective ion isolation/rejection over a broad mass range in the quadrupole ion trap.: J. Am. Soc. Mass Spectrom. 2. 11–21 (1991).

8. Abdillahi A.M. et al.: Mass Analysis of Macro-molecular Analytes via Multiply-Charged Ion Attachment.: Anal. Chem. 92. 16301–16306 (2020)

7.6 Figures

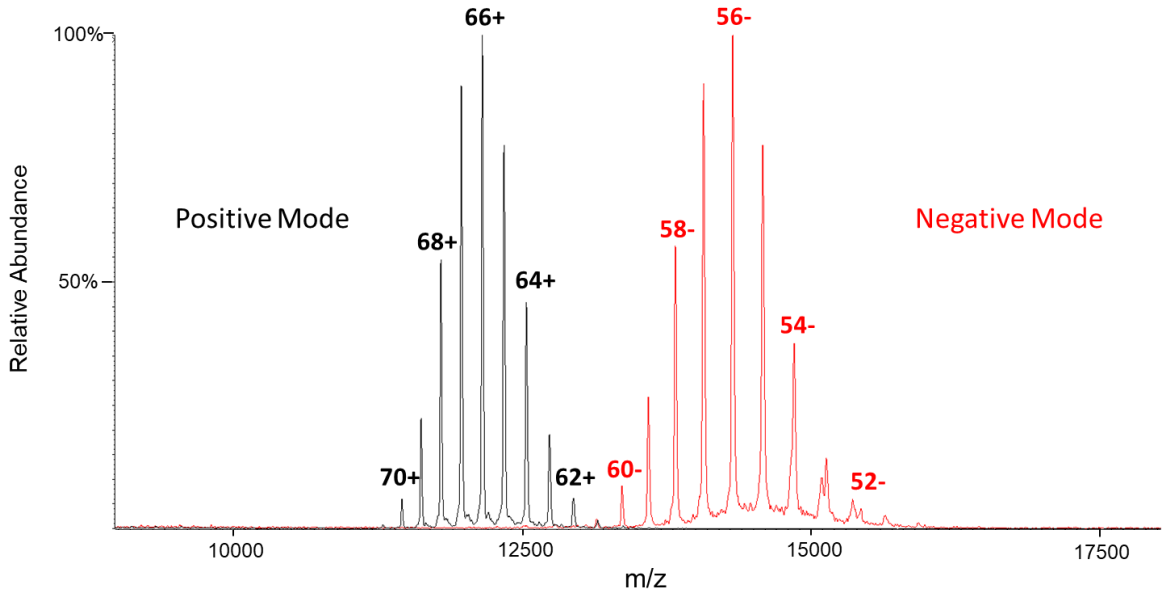

Figure 7.1. A mass spectrum overlay of GroEL in the positive mode (black trace) and negative mode (red trace).

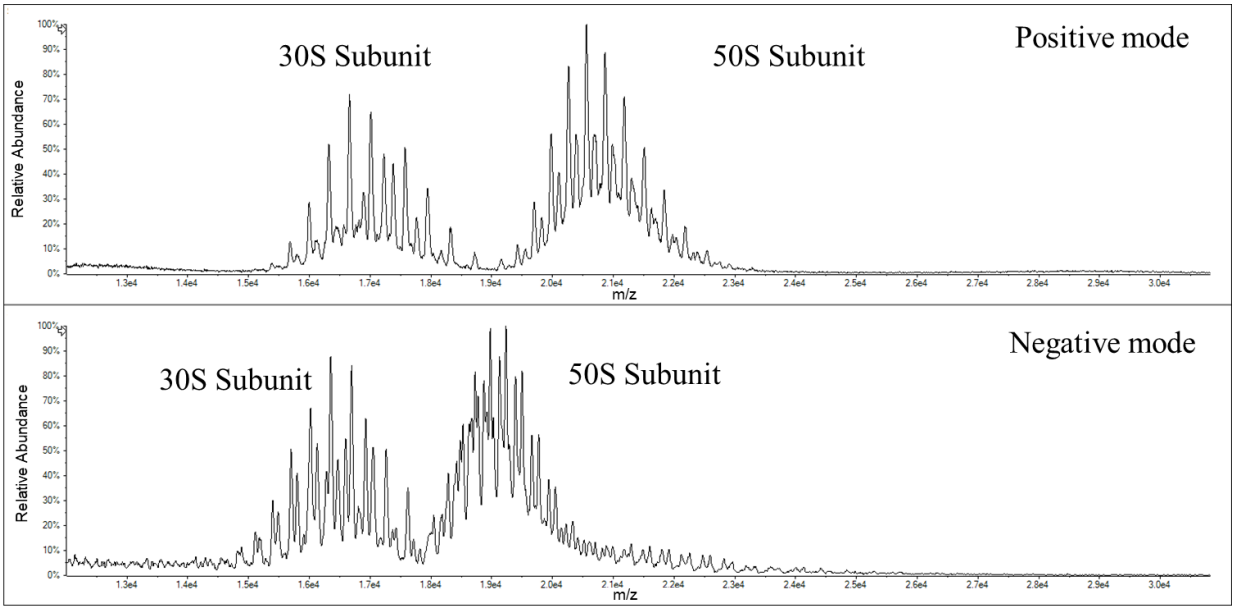

Figure 7.2. Mass spectra of *E. coli* ribosome under low Mg^{2+} conditions in the positive (top) and negative mode (bottom).

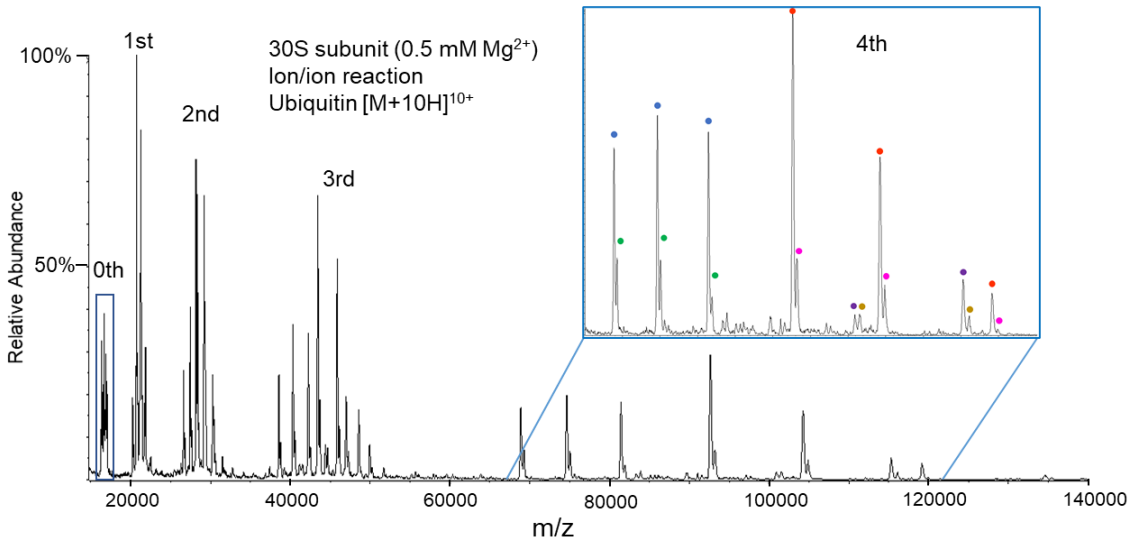

Figure 7.3. The post-ion/ion reaction mass spectrum of an isolated 30S precursor and ubiquitin. The inset is a zoom-in of the 4th attachment. The colored circle masses correspond with the mass measurements found in Figure 7.5.

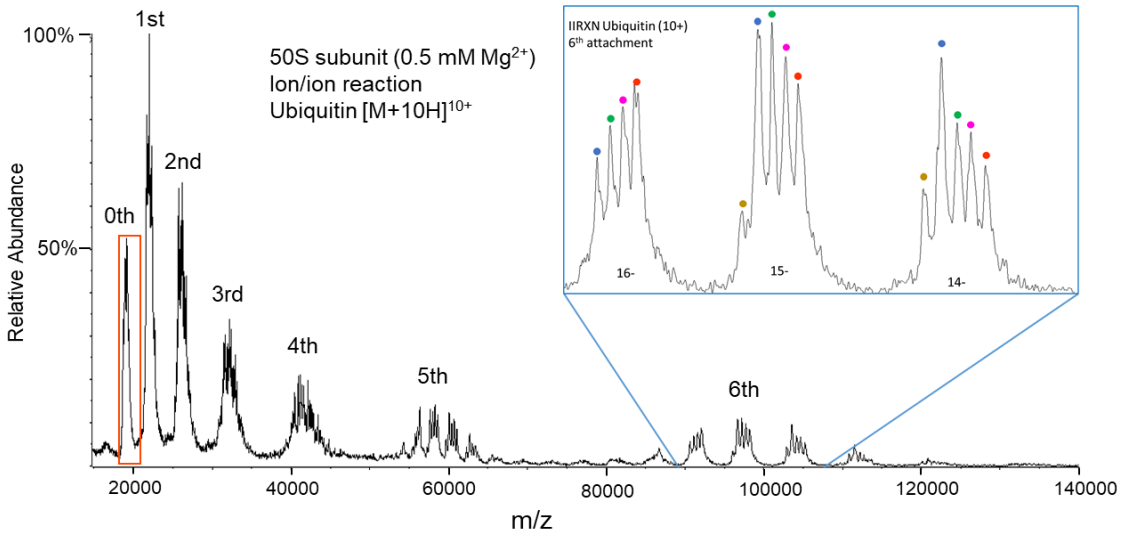

Figure 7.4. The post-ion/ion reaction mass spectrum of an isolated 50S precursor and ubiquitin. The inset is a zoom-in of the 6th attachment. The colored circle masses correspond with the mass measurements found in Figure 7.5.

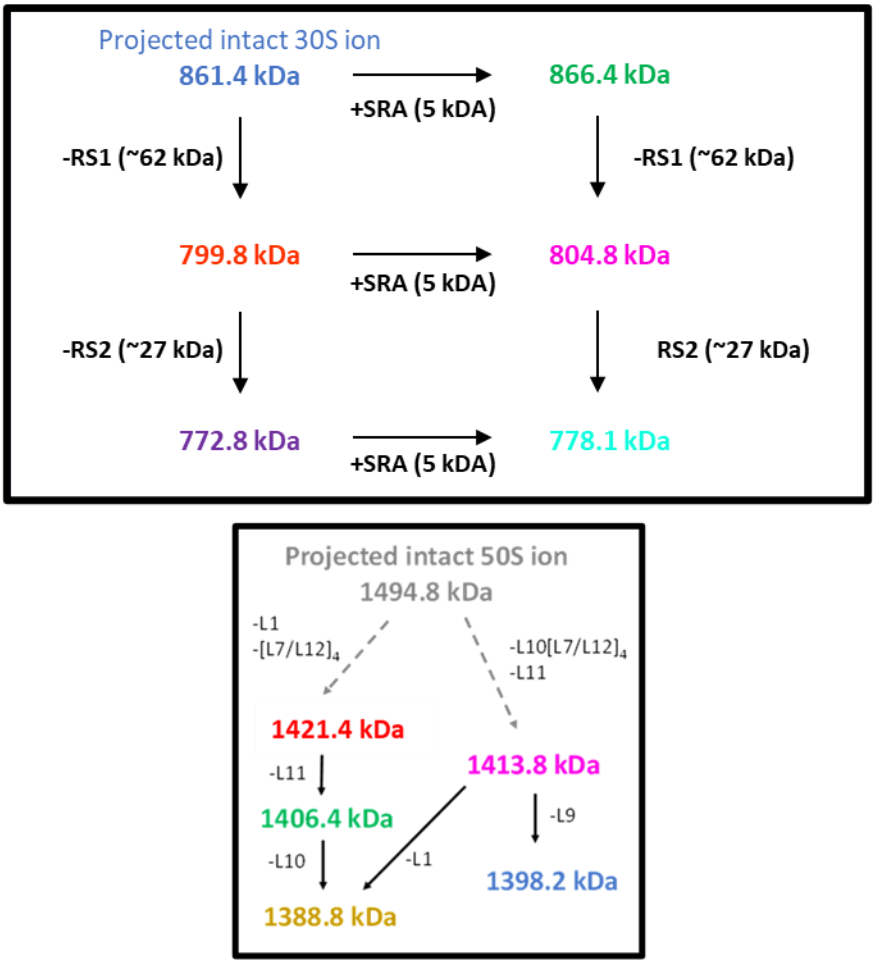

Figure 7.5. The mass measurements from the 30S subunit (top) and the 50S subunit (bottom).

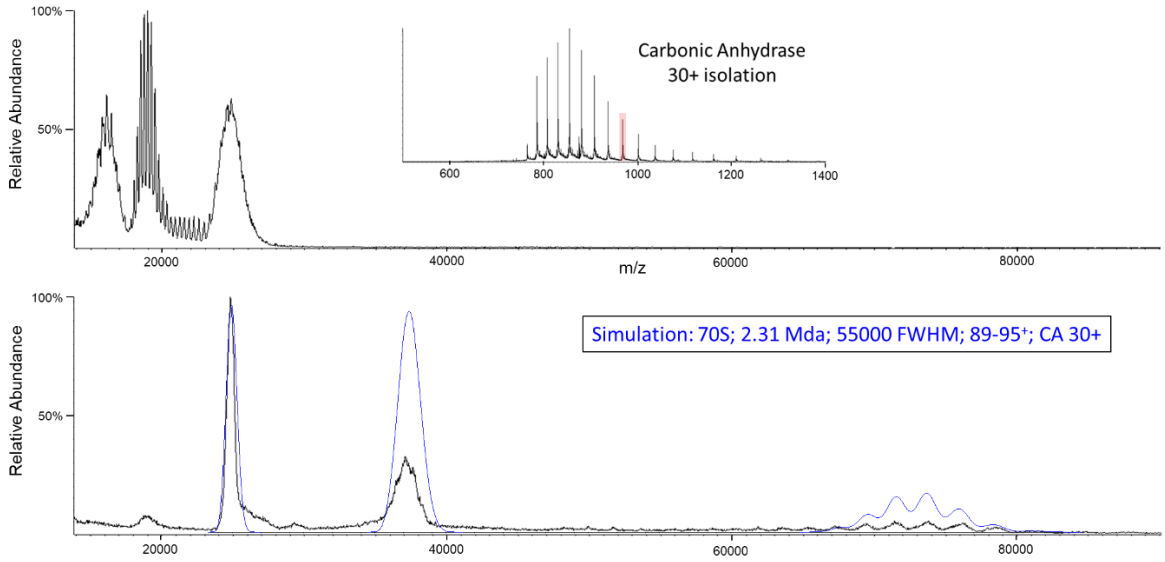

Figure 7.6. The mass spectrum of *E. coli* ribosome with 10 mM Mg^{2+} and carbonic anhydrase (top) and the ion/ion reaction of an isolated 70S precursor and carbonic anhydrase (black trace) 30+ overlaid with a simulated spectrum (blue trace).

LIST OF PUBLICATIONS

Abdillahi, A.M.; Lee, K. W.; McLuckey, S. A. Mass Analysis of Macro-Molecular Analytes via Multiply-Charged Ion Attachment. Anal. Chem. 92(24), 16301–16306 (2020).

Pitts-McCoy, Anthony; Abdillahi, A.M.; Lee, K. W.; McLuckey, S. A. Multiply-Charged Cation Attachment to Facilitate Mass Measurement in Negative Mode Native Mass Spectrometry. *Submitted*. (2021).

VITA

Education

Purdue University — West Lafayette, IN
Doctor of Philosophy (PhD) in Chemistry — 2017 – Present
Thesis: *Study of large biomolecules using native MS and ion/ion reactions*
Advisor: Scott McLuckey (mcluckey@purdue.edu)

Drexel University — Philadelphia, PA
Master of Science (MS) in Analytical Chemistry — 2013 – 2015
Thesis: *Investigating the effects of ESD upon sample morphology and MALDI-TOF signal*
Advisor: Kevin Owens (kevin.owens@drexel.edu)

Denison University — Granville, OH
Bachelor of Science (BS) in Biochemistry — 2007 - 2011

Summary

Detail oriented analytical chemist with industrial experience and a background in biochemistry. Proven ability to deliver results from research projects under time constraints. Adept at learning new skills, method development, and providing technical solutions. Assumed the responsibility of a safety officer to advocate safe lab practices.

Skills

Proficiency in mass spectrometry*, infrared spectroscopy, chromatography (GC, HPLC, SEC) and atomic force microscopy. Highly capable in handling protein (sub-kilodalton to megadalton) analytes – protein purification, MS interface conditions and ion optic steering.

Software: Maple, XCalibur, Mass Hunter, Analyst, Electronic Lab Notebook and MATLAB programming.
Languages: Fluent in Somali.

*Expertise in SCIEX mass spectrometers, including custom modifications and system maintenance. Experienced with Bruker MALDI-TOF instrumentation – including mass spec imaging.

Employment History

Researcher July 2017 – Present

Purdue University, West Lafayette IN

- Developed an alternate method to detect the mass of large biomolecules (MDa) using ion-ion reactions.
- Studied a new coding language to create a program needed for data analysis, not commercially available.
- Collaborated with Merck on large biomolecule studies.
- Mentored and trained younger students on our instrumentation.

Chemist February 2016 – July 2017

Monroe Energy LLC, Marcus Hook PA

- Performed routine testing of distillate samples to ensure customer specification compliance.
- Reviewed and revised SOPs to comply with the newly rewarded ISO 17025 certification.
- Trained coworkers on the revised SOPs**.**
- Maintained laboratory instrumentation and developed an aromatic content method for distillate samples using an Agilent GC-MS.
- Communicated production issues to upper level management and refinery leads.

Analytical Chemist August 2015 – February 2016

Dow Chemical Company, Collegeville PA

- Joined the Formulation Systems Analysis group to troubleshoot product development complaints from customers.
- Directed complex projects that required multiple subject matter experts to completion.
- Analyzed samples primarily using FTIR and Pyrolysis GC-MS.
- Generated data, maintained electronic databases, and sent progress/final reports to the customers.

Researcher September 2014 – June 2015

*Drexel University**, Philadelphia, PA***

- Investigated the sample morphology of electrospray deposition (ESD) using AFM instrument.

- Created an MS imaging program to measure surface pattern reproducibility.
- Established a link between the morphology and the MS sample signal by optimizing the ESD method.

Lab Analyst November 2011–August 2013

Twin Rivers Technologies, Quincy, MA

- Operated and calibrated the following analytical equipment: GCs, Autotitrator, Spectrophotometer, PH Meters, Karl Fisher Titrator etc.
- Performed routine analysis of fatty acids/glycerin, which included: Iodine Value, Acid Value, GC, Moisture, Color, Free Fatty Acid, Insolubles, Heat Stability, and Fatty Acid Methyl Esters.
- Trained new analyst on analytical techniques to assist them in transitioning to their position.

Publications

Pitts-Mccoy A, **Abdillahi A**, Lee K, McLuckey S. Multiply-Charged Cation Attachment to Facilitate Mass Measurement in Negative Mode Native Mass Spectrometry. Submitted.

Abdillahi A, Lee K, McLuckey S. Mass Analysis of Macro-molecular Analytes via Multiply-charged Ion Attachment. *Analytical Chemistry*, 2020, 92(24): 16301–16306.

Jalisi S, Bearelly S, **Abdillahi A**, Truong MT. Outcomes in head and neck oncologic surgery at academic medical centers in the United States. *Laryngoscope*, 2013, 123(3): 689-98.

Presentations

69th ASMS Conference, Philadelphia, PA, November 2021, Oral "Development of Negative Mass Analysis of Macromolecular Analytes via Multiply-charged Ion Attachment (MAMA-MIA) for Mass Determination of Protein Complexes"

Merck – Purdue Center for Measurement Sciences Symposium, Virtual Seminar Series, January 2021, Oral "Development of MS for large (>200 kDa to MDa) protein complexes"

46th NOBCChE Conference, St. Louis, MO, November 2019, Oral "Extracting Mass Information of Large Complicated Systems Under Native Conditions"

67th ASMS Conference, Atlanta, GA, June 2019, Poster "Extracting Mass Information From Large Biomolecules via Ion-Ion Reaction Chemistry"

63rd ASMS Conference, St. Louis, MO, June 2015, Poster "Creating Reproducible Micropatterned Analyte Surfaces to Investigate the Effect of Sample Preparation Parameters in the MALDI Imaging Mass Spectrometry Process"

Professional Associations

American Society of Mass Spectrometry (ASMS)

Phi Lambda Upsilon (PLU) – National Honorary Chemical Society

National Organization for the Professional Advancement of Black Chemists and Chemical Engineers (NOBCChE)

Leadership Roles

Safety Officer January 2018 – Present

Purdue University, West Lafayette IN

- Maintained records regarding safety training and safety equipment testing.
- Trained incoming graduate students in my research group.
- Carried out safety audits and inspections.
- Disseminated new lab policies amongst my research group.

Social Chair/Recruiter (Chemistry Diversity Initiative) September 2018 – January 2021

Purdue University, West Lafayette IN

- Increased the Chemistry departments diversity and exposure to under-represented minorities (URM) by recruiting undergraduate seniors at targeted schools.
- Organized social events to foster camaraderie amongst the departments current URM students.
- Coordinated the Purdue Chemistry Black Lives Matter March following George Floyd's passing, which brought over 100 faculty, staff and students.

Outreach Coordinator (PLU) June 2018 – September 2019

Purdue University, West Lafayette IN

- Organized scientific demonstrations and activities with neighboring elementary schools.

- Led demonstrations for the graduate students and wrote detailed methods for each experiment.
- Trained incoming outreach coordinator to ensure proper succession.